ISSN 1408-7073

RMZ – MATERIALS AND GEOENVIRONMENT

PERIODICAL FOR MINING, METALLURGY AND GEOLOGY

RMZ – MATERIALI IN GEOOKOLJE

REVIJA ZA RUDARSTVO, METALURGIJO IN GEOLOGIJO

RMZ-M&G, Vol. 55, No. 4 pp. 408–523 (2008)

Ljubljana, December 2008

Historical Review

More than 80 years have passed since in 1919 the University Ljubljana in Slovenia was founded. Technical fields were joint in the School of Engineering that included the Geologic and Mining Division while the Metallurgy Division was established in 1939 only. Today the Departments of Geology, Mining and Geotechnology, Materials and Metallurgy are part of the Faculty of Natural Sciences and Engineering, University of Ljubljana.

Before War II the members of the Mining Section together with the Association of Yugoslav Mining and Metallurgy Engineers began to publish the summaries of their research and studies in their technical periodical Rudarski zbornik (Mining Proceedings). Three volumes of Rudarski zbornik (1937, 1938 and 1939) were published. The War interrupted the publication and not until 1952 the first number of the new journal Rudarsko-metalurški zbornik - RMZ (Mining and Metallurgy Quarterly) has been published by the Division of Mining and Metallurgy, University of Ljubljana. Later the journal has been regularly published quarterly by the Departments of Geology, Mining and Geotechnology, Materials and Metallurgy, and the Institute for Mining, Geotechnology and Environment.

On the meeting of the Advisory and the Editorial Board on May 22nd 1998 Rudarsko-metalurški zbornik has been renamed into "RMZ - Materials and Geoenvironment (RMZ -Materiali in Geookolje)" or shortly RMZ - M&G.

RMZ - M&G is managed by an international advisory and editorial board and is exchanged with other world-known periodicals. All the papers are reviewed by the corresponding professionals and experts.

RMZ - M&G is the only scientific and professional periodical in Slovenia, which is published in the same form nearly 50 years. It incorporates the scientific and professional topics in geology, mining, and geotechnology, in materials and in metallurgy.

The wide range of topics inside the geosciences are welcome to be published in the RMZ -Materials and Geoenvironment. Research results in geology, hydrogeology, mining, geotechnology, materials, metallurgy, natural and antropogenic pollution of environment, biogeochemistry are proposed fields of work which the journal will handle. RMZ - M&G is co-issued and co-financed by the Faculty of Natural Sciences and Engineering Ljubljana, and the Institute for Mining, Geotechnology and Environment Ljubljana. In addition it is financially supported also by the Ministry of Higher Education, Science and Technology of Republic of Slovenia.

Editor in chief

Table of Contents – Kazalo

Original Scientific Papers – Izvirni znanstveni članki

Review Papers – Pregledni članki

Passivation of welded AISI 316L stainless steel

Pasivacija varjenega nerjavnega jekla AISI 316L

Mirko Gojić[1], Dražen Marijan[2], Marijan Tudja[2], Stjepan Kožuh[1]

[1]University of Zagreb, Faculty of Metallurgy, Aleja narodnih heroja 3, 44103 Sisak, Croatia;
E-mail: kozuh@simet.hr; gojic@simet.hr
[2]PLIVA Croatia, Ltd, Quality, Prilaz baruna Filipovića 25, 10000 Zagreb, Croatia;
E-mail: drazen.marijan@pliva.hr

Received: September 15, 2008 **Accepted:** November 17, 2008

Abstract: The paper deals with the results of passivation of welded AISI 316L austenitic stainless steel. The effectiveness of passivation in a volume fraction 6.0 % HNO_3 solution containing the mass fraction of $CuSO_4 \cdot 5H_2O$ 2.0 % was tested by potentiodynamic polarization. Polarization was carried out in demineralized water before passivation and after it. At 80 °C demineralized water induced pitting corrosion and passivation was undertaken to protect the steel surface. As a result of passivation the pitting potential decreased. The satisfactory protective properties of the passive film on steel surface were found to agree with the high value of the pitting potential. After passivation, the presence of white dotty agglomerations of copper atoms was observed on the surface in the proximity of the melted zone.

Povzetek: Članek obravnava rezultate pasivacije varjenega nerjavnega jekla AISI 313L. Učinek pasivacije v volumenski 6-odstotni raztopini HNO_3, ki vsebuje še masni delež 2 % $CuSO_4 \cdot 5H_2O$ smo preizkušali s potenciodinamično polarizacijo. Polarizacija je potekala v demineriliziran vodi pred polarizacijo in po njej. Pri 80 °C demineriliziran voda povzroči točkasto korozijo, pasivacija pa zagotavlja zaščito površine jekla. Posledica pasivacije je zmanjšanje potenciala za točkasto korozijo. Zadostna zaščita pasivacijskega filma plasti na površini jekla je v skladu z velikim potencialom za točkasto korozijo. Po pasivaciji pa je značilna prisotnost točkastih aglomeratov bakrovih atomov v okolici vara.

Key words: stainless steel, passivation, pitting corrosion, morphology
Ključne besede: nerjavno jeklo, pasivacija, točkasta korozija, morfologija

Original scientific paper

Introduction

Austenitic stainless steels find important and manifold applications as construction materials in chemical and petrochemical industries, in oil and gas exploitation, shipbuilding, food and drug processing, and in water purification and distribution systems. Their chief characteristics are good resistance to corrosion and elevated temperatures, good cryogenic strength, and low magnetic permeability[1,2]. The AISI 304 and 316 austenitic stainless steels, with their low-carbon 304L and 316L grades, account for the largest fraction of the world's stainless steel production and exploitation. Welding of stainless steels causes formation of a very heterogeneous melted zone because of impurities segregated at delta ferrite/austenite interphases and because of possible presence of secondary precipitates (carbides, chi and sigma phases, etc.)[2].

Numerous investigations have shown the impairment of the corrosive and mechanical properties of the melted zone to be due in the first place to the dominant attack of corrosion at segregation sites, in dendrite nuclei, at the austenite/delta ferrite interphases, and at the interphases of the secondary precipitates present in the zone[3,4]. In certain environments and conditions, although belonging to a group of corrosion-resistant materials, austenitic stainless steels are prone to damage by corrosion, i.e. pitting corrosion.

Among various metals that are used to protect the surface of the water purification and distribution systems stainless steels come first. In real-life operating conditions corrosion causes dissolution of the surface layers of the construction material, enhances roughness and porosity of the surface, and accounts for uneven distribution of the alloying elements. To diminish those effects the passivation process must be carried out efficiently and on time[5]. In this work emphasis was placed on investigating the effectiveness of surface passivation of a welded joint (base metal, heat-affected zone, melted zone) because of its specific composition and microstructure.

Experimental

Investigation of corrosion behaviour was performed on a weld joint from AISI 316L austenitic stainless steel which formed part of a water purification and distribution system. The chemical composition of the steel is given in Table 1. The choice of measuring equipment, electrochemical reactor, and auxilliary and reference electrodes, and the preparation of the working electrode were made in conformity with ASTM standards[6,7]. The equipment for electrochemical measurements consisted of an EG&G PAR 273 A potentiostat/galvanostat, a Cole-Parmer 12700-55 thermostat, and an EG&G Corrosion Cell System, Model K47 electrochemical reactor. A standard three-electrode corrosion cell was used. A disc-shaped working electrode (A = 1 cm^2) was prepared from the AISI 316L weld joint. Welding was performed under a protective argon flow. The weld included the melted zone, the heat-affected zone, and the painted fraction of the base metal. An Ag/AgCl electrode served as the

reference electrode, and the counter electrode was a roller-shaped graphite electrode. Anodic potentiodynamic polarization curves were recorded in conformity with ASTM standards.

Table 1. Chemical composition of AISI 316L steel in mass fractions, *w*/%
Tabela 1. Kemična sestava jekla AISI 316L v masnih deležih, *w*/%

C	Si	Mn	P	S	Cr	Ni	Mo
0.023	0.35	0.71	0.033	0.007	17.49	11.27	2.09

Electrochemical measurements were carried out in a real medium (demineralized water, 80 °C) and the passivating in volume fraction 6.0 % HNO_3 solution containing the mass fraction of $CuSO_4 \cdot 5H_2O$ 2.0%.
In addition to electrochemical measurements, a comparative examination of the surface of welded and non-welded AISI 316L steel samples was performed with a Jeol JSM-5800 scanning electron microscope and an Oxford ISIS-302 chemical analyser. The welded sample was examined without prior mechanical treatment, whereas the non-welded one was polished with a 1000 grit abrasive paper in Al_2O_3 (0.5 μm) solution. The non-welded surface was machined to conform to ASTM criteria, to facilitate detection of defects due to passivation, and to make electrochemical measurements easier to conduct. For chemical cleaning the mass fraction 2 % of citric acid solution with 5 % the mass fraction of ammonia (1800 s, 80 °C) was used. Passivation was carried out at 60 °C in the volume fraction 6.0 % of HNO_3 solution containing the mass fraction of $CuSO_4 \cdot 5H_2O$ 2 % for 3400 s.

RESULTS AND DISCUSSION

Electrochemical measurements combined with surface analysis facilitated assessment of the surface condition of the AISI 316L steel weld. With the two methods the modifications produced by chemical cleaning and passivation could be followed simultaneously. In this way it was possible to establish a link between the corrosion parameters (R_p, E_{CORR}, $j_{CORR,}$ and E_p) and the morphological features of the surface.

Electrochemical measurements

Before testing the capability for passivation of the 6.0 % HNO_3 solution containing the mass fraction of $CuSO_4 \cdot 5H_2O$ 2 % with the help of a potentiodynamic polarization curve we first investigated how demineralized water (real medium), at 80 °C, affected the surface stability of the AISI 316L steel weld (Figure 1). We then determined the corrosive properties of the steel in demineralized water after passivation (Figure 2) and in the passivation solution (Figure 3). The general and pitting corrosion parameters as read from the potentiodynamic polarization curves are listed in Table 2. In practice, to be considered corrosion-resistant, steel is expected to have achieved the corrosion potential (E_{CORR}) before use. Defects on the steel surface due to long-term use will initiate porosity and roughness. A rough and porous structure will facilitate oxidation and dissolution of the surface layers, in other words it will become more susceptible to pitting corrosion. The instability of the steel surface will produce as a result a lower pitting potential (E_p). By undertaking a timely protective treatment i.e.

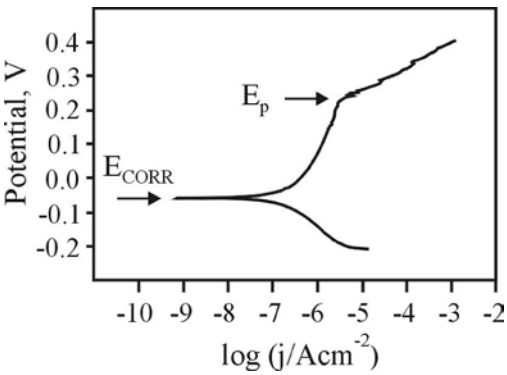

Figure 1. Anodic potentiodynamic polarization curve for AISI 316L steel weld in demineralized water before passivation, at the potential scan rate of 5 mV s^{-1}

Slika 1. Krivulja anodne potenciometrične polarizacije zvara jekla AISI 316L v demineriliziranivodi pred pasivacijo pri hitrosti menjave potenciala 5 mV s^{-1}

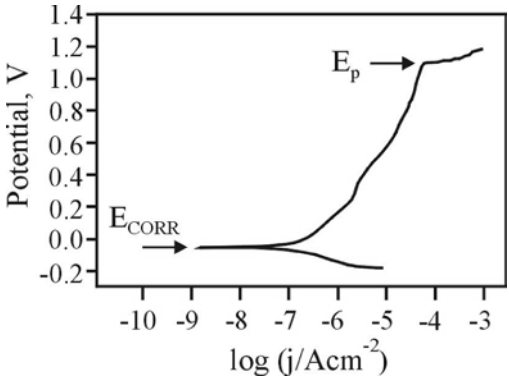

Figure 2. Anodic potentiodynamic polarization curve for AISI 316L steel weld in demineralized water after passivation, at the potential scan rate of 5 mV s^{-1}

Slika 2. Krivulja anodne potenciometrične polarizacije zvara jekla AISI 316L v demineriliziranivodi po pasivaciji pri hitrosti menjave potenciala 5 mV s^{-1}

passivation, the E_p potential will be shifted towards more positive values.

The values of general corrosion parameters measured in demineralized water demonstrated that general corrosion did not cause any major damage to the surface of the AISI 316L steel weld. The general corrosion rate of $4.530 \cdot 10^{-3}$ mm a^{-1} was taken to represent the average rate of deterioration of the weld surface. As well as from the rate, general corrosion could be assessed from the mass loss occurring over the period of steel exposure to demineralized water. Equivalent to the general corrosion rate of $4.530 \cdot 10^{-3}$ mm a^{-1} was a mass loss of 0.036 g dm^{-2} a^{-1}. It is well established that a medium having a general corrosion rate exceeding 0.127 mm a^{-1}, or a mass loss in excess of 10.087 g dm^{-2} a^{-1}, is not considered appropriate for use[8] he low values of general corrosion parameters were proof that general corrosion was not the reason why the surface of the welded AISI 316L steel needed to be passivated (Table 2). The chief reason for passivation was the onset of pitting corrosion. The pitting potential (E_p) at the steel surface was 0.228 V (Figure 1, Table 2). From Figure 1 it is evident that the E_p value was too low and the $E_p - E_{CORR}$ difference too small for the weld surface to resist pitting corrosion. The susceptibility to pitting corrosion of AISI 316L steel was the main reason why it was necessary to protect the steel surface by passivation.

The passivation effectiveness of the volume fraction 6.0 % HNO_3 solution containing the mass fraction of $CuSO_4 \cdot 5H_2O$ 2.0 % was evaluated using the parameters from the potentiodynamic polarization curve recorded in demineralized water after passivation (Figure 2, Table 2). The values of general corrosion parameters after passivation indicated that the corrosion

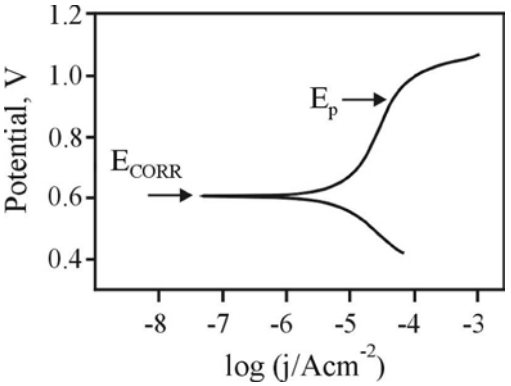

Figure 3. Anodic potentiodynamic polarization curve for AISI 316L steel weld in passivation solution, at the potential scan rate of 5 mV s^{-1}
Slika 3. Krivulja anodne potenciometrične polarizacije zvara jekla AISI 316L v raztopini za pasivacijo pri hitrosti menjave potenciala 5 mV s^{-1}

rate decreased (from $4.530 \cdot 10^{-3}$ mm a^{-1} to $1.204 \cdot 10^{-3}$ mm a^{-1}), i.e. that general corrosion resistance increased. The pitting potential at the passivated surface was higher (1.098 V) than the one at the nonpassivated surface (0.228 V). A rise in the E_p value led to a higher $E_p - E_{CORR}$ value (from 0.287 V to 1.063 V). The E_p and $E_p - E_{CORR}$ values indicated that the chosen passivation treatment provided effective protection against pitting corrosion to the AISI 316L steel surface exposed to demineralized water. However, unless the steel surface was thoroughly rinsed with demineralized water there was a risk of galvanic corrosion[9]. Galvanic corrosion occurs when two dissimilar metals, immersed in a corrosive medium, come in direct contact and form a galvanic couple. The greater the difference between standard electrode potentials (E^0) of individual metals in the couple the more pronounced galvanic corrosion. After passivation, the residual copper atoms (E^0 = 0.337 V) absorbed on the steel surface may have formed microcouples with the steel constituents, iron (E^0 = –0.037 V), nickel (E^0 = –0.250 V), and chromium (E^0 = –0.744 V), and thus may have induced galvanic corrosion. To prevent this from hapenning it was essential that the steel surface be thoroughly rinsed after passivation.

Taking the volume fraction 6.0 % HNO_3 solution with the mass fraction of $CuSO_4 \cdot 5H_2O$ 2.0 % to be an efficacious protective agent against pitting corrosion, it was important to determine general and pitting corrosion parameters for the situation where the steel was exposed solely to the passivation solution. Analysis

Table 2. General and pitting corrosion parameters of AISI 316L steel weld in demineralized water before and after passivation, and in passivation solution
Tabela 2. Parametri splošne in točkaste korozije zvara jekla AISI 316L v demineriliziran vodi pred pasivacijo in po njej ter v raztopini za pasivacijo

Solution	R_p/ kΩ	b_a/ dek^{-1}/V	$-b_c$/ dek^{-1}/V	E_{CORR}/ V	j_{CORR}/ (μA cm^2)	v_{CORR}/ mm a^{-1}	E_p/ V
Demineralized water	0.251	0.312	0.152	-0.059	0.430	$4.530 \cdot 10^{-3}$	0.228
Demineralized water after passivation	0.406	0.354	0.153	0.035	0.148	$1.204 \cdot 10^{-3}$	1.098
Passivation solution	0.010	0.387	0.296	0.643	4.74	0.049	0.900

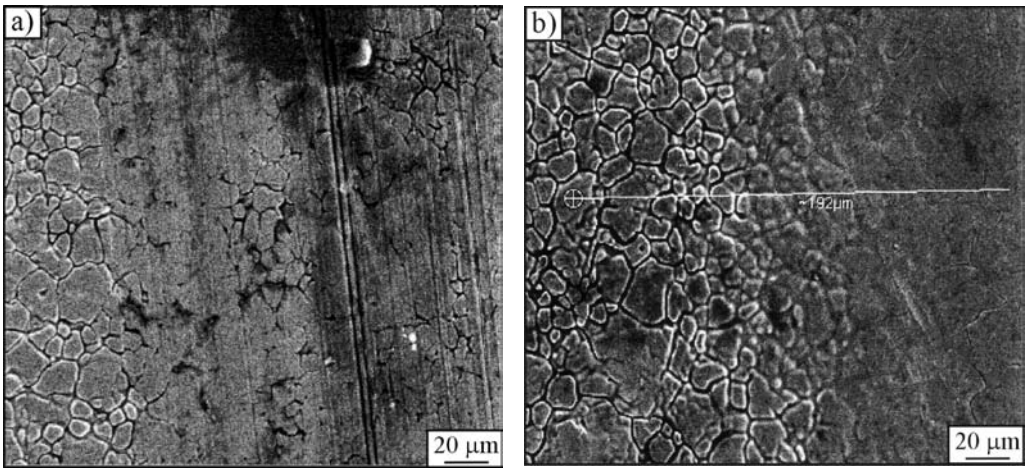

Figure 4. SEM micrograph of the initial surface of AISI 316L steel base metal (a) and weld joint (b)
Slika 4. Mikrografiji začetne površine jekla AISI 316L (osnovni material) (a) in zvarnega spoja (b)

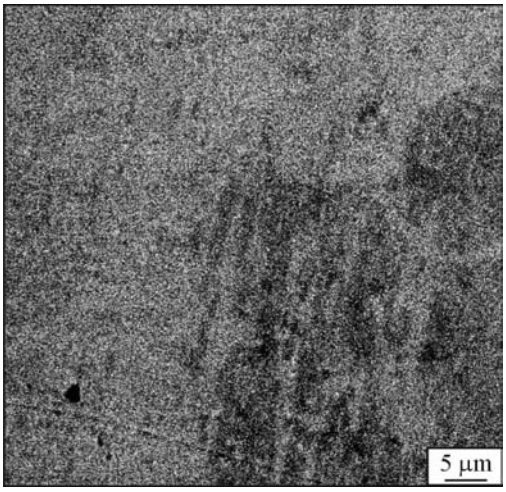

Figure 5. SEM micrograph of the surface of AISI 316L steel after polishing
Slika 5. Mikrografija polirane površine jekla AISI 316L; SEM

of the results obtained from the potentiodynamic polarization curve recorded in the passivation solution demonstrated that the passivation solution was more aggressive than demineralized water (Figure 3, Table 2). The aggressiveness of the passivation solution was as expected because, were it not so, the protection against pitting corrosion provided by the solution would not have been effective. However, the adverse effect of the passivation solution was still not strong enough to cause the steel surface to dissolve, i.e. to induce general corrosion (Table 2). A general corrosion rate of over 0.127 mm a^{-1} was considered to be hazardous to the steel surface[10]. The pitting potential value (0.900 V) was taken to prove that the passivation medium was well chosen.

Of the methods used for protecting the steel surface none has proved capable of completely stopping the process of corrosion. By efficient and timely protection of the steel surface only the rate of corrosion can be diminished. It is therefore essential to repeat the protective passivation treatment after a certain period. How often passivation needs repeating will depend on a number of fac-

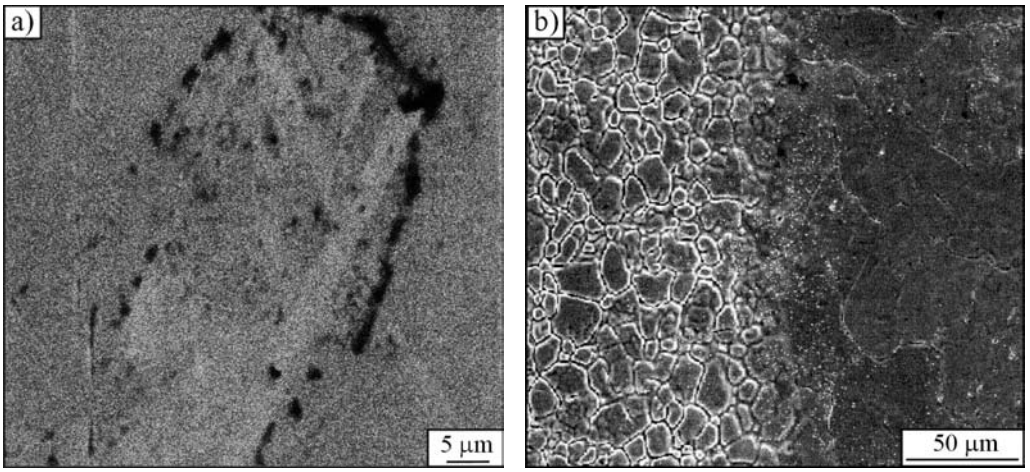

Figure 6. SEM micrograph of the surface of AISI 316L steel base metal (a) and weld joint (b) after passivation
Slika 6. Mikrografija pasiviranih površin jekla AISI 316L (osnovni material) (a) in zvarnega spoja (b); SEM

tors: operating conditions of the water purification and distribution system, type and frequency of welding, temperatures of the media present in the system, temperature stresses during exploitation, oxygen content in the system, reduced oxygen values, etc[11]. Assessment of the steel surface condition will therefore require not only laboratory studies but also real-life investigations in water distribution systems[12].

Surface analysis

Analysis of surface morphology of the AISI 316L base metal and weld joint was carried out before and after polishing, and also after passivation (Figures 4–6). Initially, the base metal surface showed the presence of grooves as well as of impurities, cracks, and dimples (Figure 4a). In the weld two zones could be distinguished: the melted zone and the zone adjacent to the melted zone (Figure 4b). The melted zone morphology was characterized by an even and compact structure (Figure 4b, right). The adjacent zone, contrariwise, exhibited cracks and grain boundaries (Figure 4b, left). Despite morphological differences, a quantitative linear analysis demonstrated equal proportions of individual elements in the two zones (Figure 7). Chemical cleaning helped reduce the cracks' width and achieve a more uniform structure of the welded surface.

The polished surface of AISI 316L steel was characterized by a smooth and uniform structure (Figure 5). After polishing there were no signs of cracks or impurities on the steel surface. The passivated surface of the base metal exhibited an irregular distribution of indentations (with a maximum diameter of up to 5μm) (Figure 6a). Quantitative linear analysis showed the chemical composition of the steel surface inside and outside indentations (dimples) to be identical (Figure 8). The appearance of dimples was the result of dissolution of unstable surface sulphur in the acidic me-

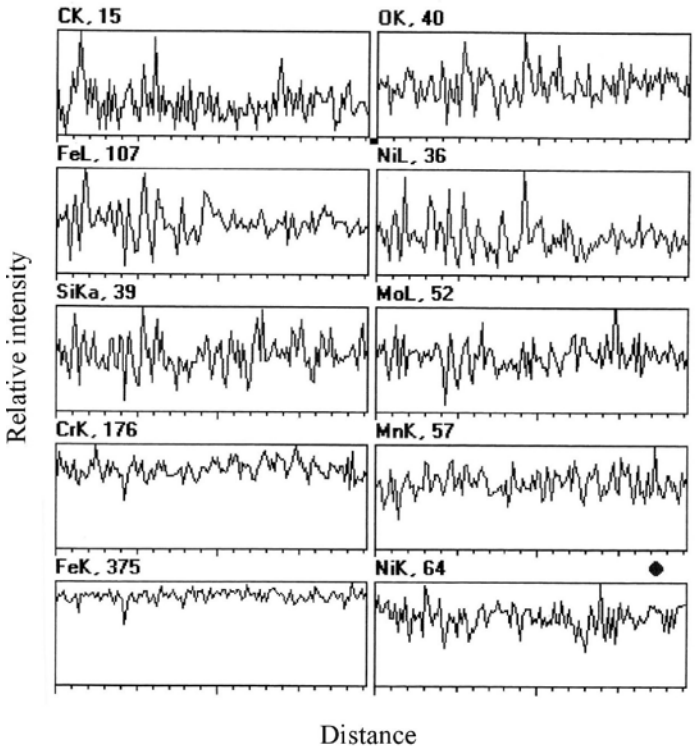

Figure 7. Quantitative linear analysis of the initial surface of AISI 316L steel weld joint
Slika 7. Kvantitativna kemična črtna analiza na začetni površini zvara jekla AISI 316L; EDXS

dium, i.e. in the passivation medium.

The passivation process is known to reduce not only localized sulphur concentration in AISI 316L steel but also its total concentration thus increasing steel resistance to pitting corrosion[10]. Increase in the pitting resistance of the weld following passivation was established by analysis of the parameters obtained by potentiodynamic measurements (Table 2). The passivated surface in the close proximity of the melted zone exhibited white dotty agglomerations and slightly less pronounced grain boundaries in comparison with the nonpassivated surface. The structure was granular, with grains having a smooth surface. Surface analysis showed the granular agglomerations to consist of copper atoms (Figure 9). Quantitative linear analysis of the steel surface following passivation failed to show a major difference in the content of individual elements between the melted zone and the adjacent zone (Figure 10). It may therefore be concluded that the passivation medium "attacked" the steel weld surface in a uniform manner. As a result of passivation all steel constituents formed oxides without prior dissolution. On the other hand, had

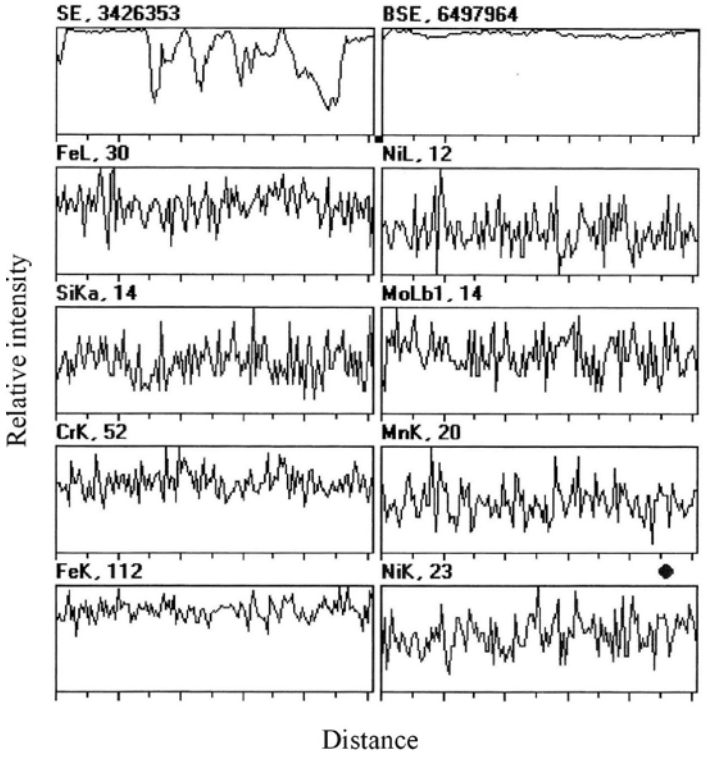

Figure 8. Quantitative linear analysis of the passivated surface of AISI 316L steel base metal
Slika 8. Kvantitativna kemična črtna analiza pasivirane površine jekla AISI 316L (osnovni material); EDXS

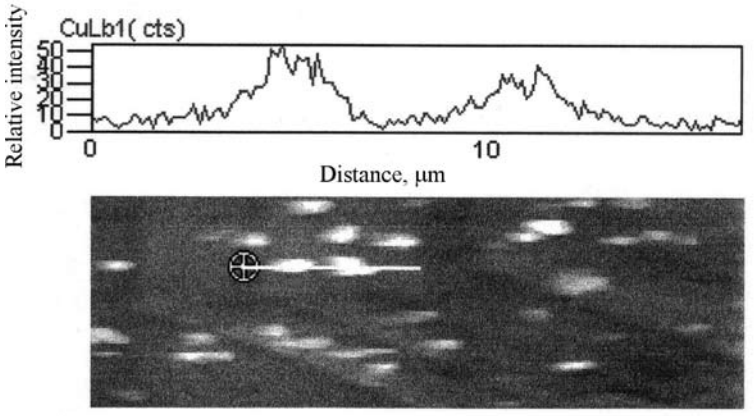

Figure 9. Quantitative linear analysis of small agglomerations on the surface of AISI 316L steel weld joint
Slika 9. Kvantitativna kemična črtna analiza drobnih aglomeratov na površini zvara jekla AISI 316L; EDXS

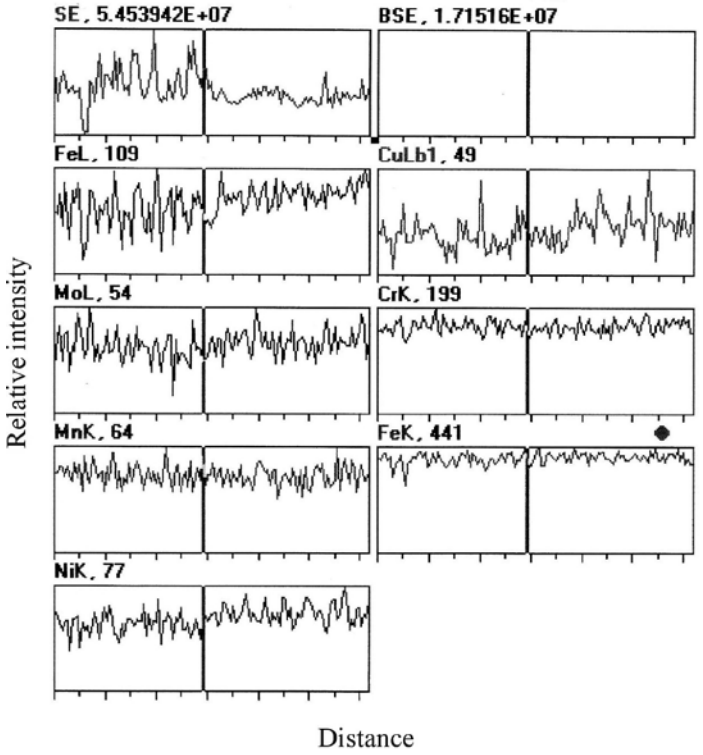

Figure 10. Quantitative linear analysis of the passivated surface of AISI 316L steel weld joint

Slika 10. Kvantitativna kemična črtna analiza pasivirane površine zvara jekla AISI 316L; EDXS

dissolution taken place before oxidation of surface atoms, quantitative analysis would have shown an uneven distribution of the alloying elements. The uniform surface composition of the steel weld, by warranting invariable ratios of chromium and iron mass fractions, proved to be a measure of effectiveness of passivation treatment[13,14].

Roughness measurements (R_a) are often used for testing the efficacity of passivation media. The postpassivation roughness values were 1.6 μm for the melted zone, 0.37 μm for the painted zone, and 0.25 μm for the base metal. The painted area of the passivated surface adjacent to the melted zone exhibited a highest level of roughness, being the site of highest exposure to the negative effect of heat input during welding. By failing to enhance surface roughness, passivation helped prevent a possible drop in surface stability of AISI 316L steel.

Conclusions

From the results of potentiodynamic measurements and surface analysis of the AISI 316L steel weld exposed to demineralized water it may be concluded that:

- General corrosion did not cause a major damage to the steel surface.
- At 80 °C demineralized water caused damage to the steel surface inducing pitting corrosion so that passivation treatment in the volume fraction 6.0 % HNO_3 solution containing the mass fraction of $CuSO_4 \cdot 5H_2O$ 2.0 % was undertaken.
- After passivation the general corrosion rate diminished (from $4.530 \cdot 10^{-3}$ mm a^{-1} to $1.204 \cdot 10^{-3}$ mm a^{-1}), and general corrosion resistance increased.
- The pitting potential at the passivated steel surface (1.098 V) was more positive than the one at the nonpassivated surface (0.228 V). A rise in the pitting potential was accompanied by increase in $E_p - E_{CORR}$ value (from 0.287 V to 1.063 V) indicating that the chosen passivation treatment provided efficacious protection against pitting corrosion.
- The passivation solution was more aggressive than demineralized water. The noted aggressivity was insufficient to cause dissolution of the steel surface.
- After passivation the steel surface needed to be thoroughly rinsed with demineralized water to prevent adsorption of copper atoms on the welded surface and possible occurrence of galvanic corrosion.
- After passivation the surface adjacent to the melted zone exhibited white dotty agglomerations. Analysis showed the agglomerations to consist of copper atoms.
- The painted portion of the passivated surface adjacent to the melting zone was characterized by the highest level of roughness, being the site of the most pronounced negative effect of heat input during welding.

REFERENCES

[1] LULA, R. A. (1986): Stainless Steel, American Society for Metals, Metals Park, Ohio.

[2] KOŽUH S., GOJIĆ M. (2006): Zavarivanje.; Vol. 49, No. 5, pp. 177–185.

[3] MUDALI U. K., DAYAL R. K. (2000): Materials Science and Technology.; Vol. 16, No. 4, pp. 392–398.

[4] ŠEVČIKOVÀ J., TULEJA S., KOCICH J. (1996): "Corrosion Resistance of Stainless Steel Welds", Proc. of the Int. Welding Conference Welding Science&Technology. Faculty of Metallurgy Technical University of Košice, Košice, pp. 279–282.

[5] EHEDG Update (2007): Trends in Food Science Technology. Vol 18, No. 1, pp. s112–s115.

[6] G5-94(1997):,*Standard Reference Test Method for Making Potentiostatic and Potentiodynamic Anodic Polarization Measurements*, 1997 Annual Book of ASTM Standards, ASTM, Easton, pp. 55.

[7] G 1-90 (1997): *Standard Practise for Preparing, Cleaning and Evaluating Corrosion Test Specimens,* 1997 Annual Book of ASTM Standards, ASTM, Easton, pp. str. 15.

[8] FONTANA M. G. (1986): Corrosion Engineering, Mc Grow-Hill, Singapur, pp. 172.

[9] KIRBY G. N. (1980): Selecting Materials for Process Equipment, Mc Grow-Hill, New York 1980, pp. 180.

[10] Coleman D. C., Evans R. W. (1990): Pharm. Engineering. Vol. 10, pp. 43.

[11] Uhlig H. H., Revie R. W. (1985): Corrosion and Corrosion Control, J. Wiley & Sons., New York, pp. 278.

[12] G 46–94 (1997): *Standard Guide for Examination and Evaluation of Pitting Corrosion*, 1997 Annual Book of ASTM Standards, ASTM, Easton, pp. 169.

[13] Grant A., Henon B. K., Mansfeld F. (1997): Pharm. Engineering. Vol. 1, pp. 46.

[14] Grant A., Henon B. K., Mansfeld F. (1997): Pharm. Engineering. Vol. 2, pp. 94.

Processing of PK 324 Duplex Stainless Steel: Influence of aging temperature and cooling rates on precipitation - preliminary results

Preoblikovanje dupleksnega nerjavnega jekla PK 324: Vpliv temperature staranja in ohlajevalnih hitrosti na izločanje – preliminarni rezultati

Matevž Fazarinc[1], Tatjana Večko Pirtovšek[1], David Bombač[1], Goran Kugler[1], Milan Terčelj[1]

[1]University of Ljubljana, Faculty of Natural Sciences and Engineering, Department of Material Science and Metallurgy, Aškerčeva cesta 12, SI-1000 Ljubljana, Slovenia;
E-mail: matevz.fazarinc@ntf.uni-lj.si, tpirtovšek@metal.com, david.bombac@ntf.uni-lj.si, goran.kugler@ntf.uni-lj.si, milan.tercelj@ntf.uni-lj.si

Received: October 6, 2008 **Accepted:** December 8, 2008

Abstract: Knowledge on precipitation phenomena in the PK 324 duplex stainless steel (DSS) is an important step in improving its final microstructure in the production process. Due to increased content of Cr, Ni and C the DSS exhibits complex microstructure, consisting of ferrite, austenite, intermetallic phases (sigma) and carbides. Several tests were applied in order to obtain necessary knowledge for improving the processing of the DSS. Aging-treatment tests revealed that sigma phase precipitated in the range between 680 °C and 900 ºC. Additionally, the influence of cooling rates on the precipitation and transformation behaviour of samples, previously aged in the range between 950 °C and 1300 ºC, has been studied. With sufficiently high cooling rates the precipitation of sigma phase could be reduced to negligible values.

Izvleček: Razumevanje izločanja v dupleksnih nerjavnih jeklih PK 324 je pomemben korak k izboljšavi končne mikrostrukture v procesu izdelave. Zaradi povišane koncentracije Cr, Ni in C tvori ta vrsta jekel kompleksno mikrostrukturo, ki je sestavljena iz ferita, avstenita, intermetalnih spojin (σ-faza) in karbidov. Izvedenih je bilo več različnih preizkusov, ki so služili za nabiranje potrebnega znanja za izboljšanje procesov izdelovanja teh jekel. S staranjem je bilo ugotovljeno, da se σ-faza izloča v temperaturnem intervalu med 680 °C in 900 °C. Dodatno je bila narejena še analiza vpliva ohlajevalnih hitrosti na vzorce, ki so bili predhodno starani v temperaturnem intervalu med 950 °C in 1300 °C. Pokazalo se je, da se je mogoče izogniti izločanju σ-faze z zadostno visoko ohlajevalno hitrostjo.

Original scientific paper

Key words: PK 324 duplex stainless steel, aging treatment, cooling rates, precipitation
Ključne besede: dupleksno nerjavno jeklo PK 324, staranje, ohlajevalne hitrosti, precipitacija

Introduction

Duplex stainless steels, composed manly of austenite and ferrite grains, posses excellent corrosion resistance as well as mechanical properties, i.e. good ductility and strength, where austenite contributes to the ductility while ferrite, which is harder, improves the strength and the welding characteristics. In the temperature range between 500 °C and 1100 ºC the precipitation of secondary phases such as sigma phase (σ) - $(FeNi)_x(CrMo)_y$ intermetallic compound, chromium nitride (Cr_2N), secondary austenite (γ_2) and Chi phases (χ) takes place in this type of stainless steels. When the composition is changed in the nominal concentration region the range of precipitation usually changes. Larger content of the ferrite-stabilizing elements, such as Mo and Si promote the σ-phase precipitation during the cooling process, while on the other hand the austenite-stabilizing elements, such as Ni, Mn, C and N reduce the σ-phase precipitation. Type M_7C_3 and $M_{23}C_6$ carbides usually commence to precipitate at temperatures bellow 1100 ºC or 950 ºC, respectively. The precipitation takes place on grain boundaries between the ferrite and austenite grains as well as on other incoherent boundaries (non-metallic inclusions). The σ-phase is one of the most influential phases according to the Fe-Cr binary system. It usually precipitates in the temperature range between 600 °C and 1000 ºC, is very brittle and consequently increases the hardness of stainless steel but decreases ductility, toughness, corrosion resistance and consequently cold and hot deformability. Cooling rate influences the amount of precipitated carbides as well as the amount of sigma and other phases and consequently the obtained mechanical properties. Thus an appropriate processing parameters should be chosen in order to obtain the desired properties of the stainless steel in question that are needed in further processing steps for its quality production. After hot forming, cold forming is usually applied during the manufacturing of items whit fine dimensions (8 mm wire). The cold formability of stainless steel is highly influenced by present sigma phase as well

Table 1. Chemical compositions of various batches, used in our experiments
Tabela 1. Kemična sestava različnih šarž, uporabljenih pri preizkusih

BatchNo.		*w*(C)/%	*w*(Si)/%	*w*(Cr)/%	*w*(Mn)/%	*w*(Ni)/%	*w*(Mo)/%	*w*(S)/%	*w*(P)/%	*w*(Al)/%	*w*(Cu)/%
1	Φ 13	0.12	0.39	29.66	1.87	10.00	0.17	0.003	0.028	0.024	0.15
2	⌀ 90	0.10	0.22	30.1	1.96	9.66	0.32	0.02	0.032	0.006	0.19
3	cast	0.10	0.26	30.1	1.91	9.5	0.04	0.004	0.020	0.007	0.06

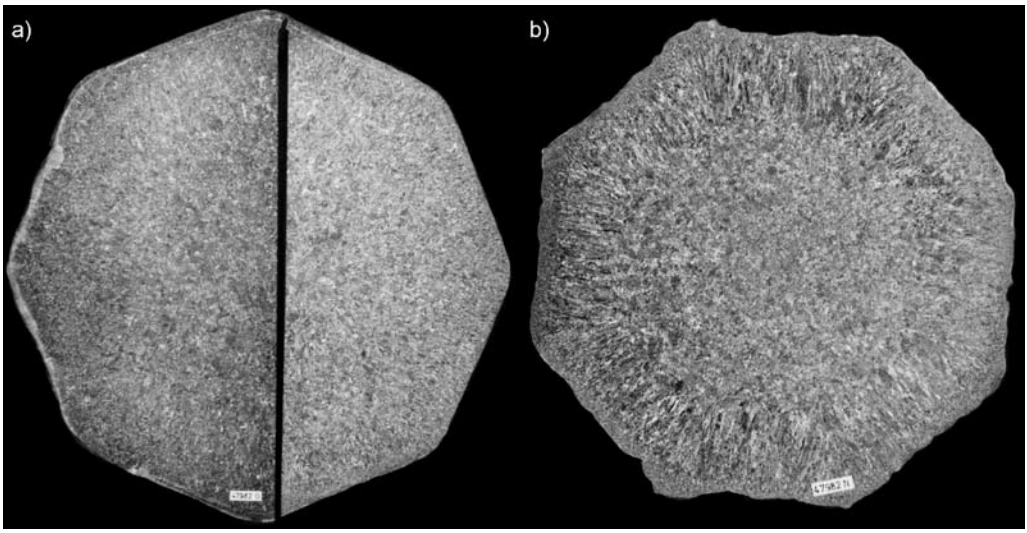

Figure 1. Observed macrostructures on the cross sections of the PK 324 DSS ingot; a) in the ingot head (G), and b) in the ingot foot (N)
Slika 1. Optična makrostruktura prečnega prereza ingota jekla PK 324; a) glava ingota (G) in b) noga ingota (N)

as by present carbides [1-14].

PK 324 is a ferrous alloy, usually used as welding material, grouped among super duplex stainless steel (DSS). Its production is still characterised by appearance of cracks as a consequence of precipitation processes. Thus this paper presents the results of influence of aging temperatures and cooling rates on the transformation and precipitation processes.

EXPERIMENTAL PROCEDURE

Applied materials, methods of characterization and analyses

The specimens made of PK 324 DSS and applied in testing were cut from a rolled wire with diameter Φ = 13 mm (Batch no. 1), from a square rod (90 mm x 90 mm, Batch no. 2) and from 380 kg ingots prepared in a vacuum electric furnace (Batch no. 3). Chemical compositions of the applied batches of the PK 324 DSS are given in Table 1. They differed from the standard DSS since they contained higher mass fraction of C (over 0.1 %), Cr (about 30 %), and Ni (about 10 %). An isopleths cross section of the Fe-Cr-Ni ternary diagram at 8 % Ni is given in [3].

(OM) ZEISS JENA VERT apparatus was applied for the light microscopy. Murakami's etchant (KLEMM [15]) was used to tint σ phase grey, α phase brown, carbides red, green and blue, while γ phase remained uncoloured. Further, XRD was used to verify the percentage of phases in the microstructure. Chemical compositions of the γ, α, σ phases and of carbides were determined with the EDS. Microanalyses were performed using the Leitz - AMR 1600 T scanning electron microscope and using the PGT IV EDX system.

Figure 1a and b present the macrostruc-

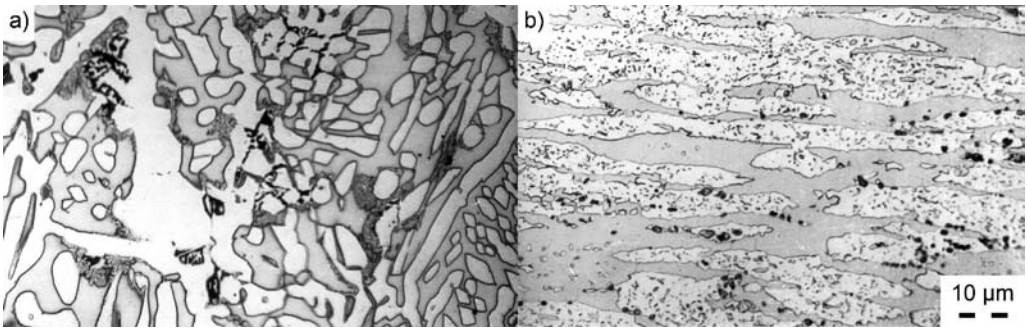

Figure 2. LM micrograph of PK 324 DSS; a) initial as-cast ingot; b) as-wrought, after 30 minutes of solution annealing at 1050 °C and subsequent water quenching
Slika 2. Posnetek mikrostrukture jekla PK 324; a) ulit ingot; b) predelan, po 30 min žarjenja na 1050 °C in po gašenju v vodi

tures in the cross-sections in the ingot's head (in the text marked with G) and in the ingot's foot (in the text marked with N), respectively. Figure 1a made evident that an area 5 mm below the surface of the ingot consists of globular grains. Towards the ingot centre, a 10 mm wide area consisting of dendritic grains can be observed while the areas further towards the centre contain equiaxial grains that gradually change into globular grains in the centre of ingot's head. The macrostructure of the cross section of ingot foot is presented in Figure 1b. The 5 mm wide area of globular grains in the outer part of ingot was clearly visible. Towards the ingot centre this area is followed by a 30 mm wide area of dendritic grains that gradually change into equiaxial grains and finally globular grains are found in the centre of ingot's foot.

The calculated value for Cr_{ekv}/Ni_{ekv} ratio according to the equation given in [2] is 2.3, pointing to the presence of both phases at room temperature.

During the solidification process ferrite dendrites form first. After the solidification is complete the alloy consisted only of ferrite grains. Further cooling causes the $\alpha \rightarrow \gamma$ transformation and afterwards, due to the decreased solubility of C in austenite, precipitation of carbides takes place. With further cooling the decomposition of ferrite according to the $\alpha \rightarrow \sigma + \gamma$ eutectoid reaction takes place. During the cooling process the precipitation of carbides and of σ phase also takes place. Final microstructure consists of γ-phase in the interdendritic spaces, phases α and γ inside the dendrite grains, intermetallic phases (phases σ and χ) and eutectic carbides. Figure 2a shows the final as-cast microstructure of the batch no. 3 taken from the ingot centre. Type M_7C_3 and $M_{23}C_6$ carbides predominately precipitate on the α/γ boundaries in the interdendritic spaces (due to the segregation of C during the solidification process) and in a smaller extent also inside the grains close to the α/γ boundaries while σ-phase precipitates in the ferrite area. Measured volume fraction of ferrite in the ingot centre was about 48 %, austenite about 52 % and below 1 % of sigma phase and carbides at room temperature. In the samples that were taken from the ingot surface the volume fraction of ferrite was 45.2 %, of austenite about 54.8 % and below 1 % of

sigma phase and carbides.

In order to equalize fractions of ferrite and austenite in the initial microstructure, all the heat treated specimens were solution annealed in an electric furnace at 1050 °C for 30 min and quenched in water. According to the phase diagram given in reference [3] for this temperature approximately equal parts of α and γ were obtained. The obtained microstructure after aging heat treatment of the as-wrought material is presented in Figure 2b. The microstructure consists of approximately equal parts of ferrite and austenite and carbides (M_7C_3 and $M_{23}C_6$) which precipitated in austenite and on the α/γ interfaces. In austenite small islets of ferrite were found as a mixture of Widmannstätten microstructure and small islets of austenite.

High temperature aging treatments and cooling

After initial solution annealing the specimens underwent various aging treatments in the temperature range between 620 °C and 1050 °C in 20 °C increments. The temperature was kept constant for 30 min. All the samples were quenched after the annealing process. Samples from batch no. 1 were applied for these tests. Based on these aging tests the temperature range of precipitation of sigma phase was determined. Detailed data of all the test conditions, characterizations, etc. that were performed in the research are given in Table 2.

To analyze the influence of cooling rates on the precipitation processes, the as-wrought (batch no. 2) and as-cast (batch no. 3) samples were quenched in water (with the cooling rate of approximately 200 °C/s) and cooled in air (with the cooling rate of approximately 4 °C/s), respectively, after they were aged for two hours in the temperature range between 1000 °C and 1300 °C. This served as a basis for characterisation of the influence of cooling rates (quenching in water, and cooling on air) on the achieved microstructure. Longer aging time (120 min) in the temperature range between 900 °C and 1250 °C (1300 °C) was chosen instead of shorter aging time (30 min) in the temperature range

Table 2. Applied aging conditions and applied tests
Tabela 2. Uporabljeni pogoji staranja in uporabljeni preizkusi

	Temp. range 620–1050 °C	Temp. range 900–1250 (1300) °C	
Batch No.	1	2	3
Initial state	wrought, wire Φ 13 mm	wrought, ▯ 90 mm	as-cast
Aging time (min)	30	120	120
Cooling	water	water, air	water, air
Microhardness: measured	Yes	No	No
OM, XRD, EDS	Yes	Yes	Yes

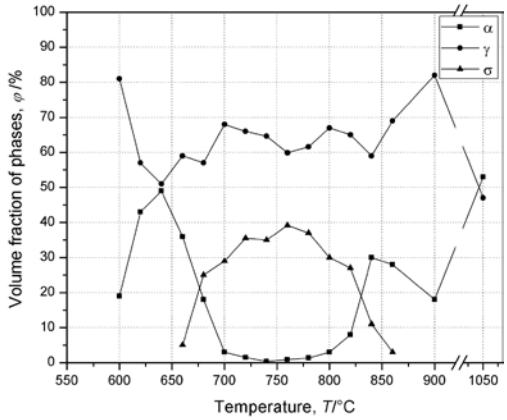

Figure 3. a) Volume concentrations of phases vs. aging temperature in the temperature range between 620 °C and 1050 °C, aging time of the as-wrought specimen (Φ = 13 mm) was 30 min and b) the obtained LM microstructure of the as-wrought sample aged at 800°C for 30 min, (3 % α, 30 % σ, 67 % γ)

Slika 3. a) Prostorninska koncentracija faz v odvisnosti od temperature staranja v območju med 620 °C in 1050 °C pri času staranja predelanega jekla (Φ = 13 mm) 30 min; b) mikrostruktura, posneta z optičnim mikroskopom (3 % α, 30 % σ, 67 % γ)

between 620 °C and 1050 °C, since the hot forming process usually takes place in that temperature range. This meant also longer holding times of workpiece at higher temperatures. Consequently the influence of cooling rate in the predetermined temperature range on the precipitation process was more relevant.

Results

Stable microstructure, characterized by α/γ ratio, was obtained at 1050 °C and has become thermodynamically metastable at lower temperatures. This consequently results in the decomposition of ferrite phase into austenite and sigma phase (α → γ + σ). Figure 3a presents volumetric concentrations of phases vs. aging temperatures for aging time of 30 min in the temperature range between 620 °C and 1050°C. The samples were taken from batch no. 1. The sigma phase precipitated in the temperature interval between 660 °C and 860 °C, reaching maximum volume fraction of 39.5 % at approximately 760 °C. Figure 3a makes evident that with the decomposition of α phase the amount of σ and γ phases increase. At the aging temperature of 1050 °C the obtained α/γ phase ratio was approximately 1 and indicates that it remained the same as after initial solution heat treatment. In Figure 3b the microstructure of the sample that was aged for 30 min at 800 °C is presented. The areas with (α → γ + σ) eutectoid are clearly visible; the sigma phase commenced to precipitate at the triple points as well as on the grain boundaries (α/α and α/γ) and it grew into the interior of ferrite grains.

The authenticity of the mentioned phases was also proved by micro-hardness measurements. The micro-hardness values $HV_{0.1}$ for ferrite (α) were in the range of 433–525, 230–309 for austenite (γ), austenite (γ) plus sigma phase (σ) in the range of 630–661 and of austenite (γ) plus carbide (K) in the range of 322–405. These values were in agreement with the obtained results by Martins et all [1, 4, 5].

As presented in Table 2, similar aging tests

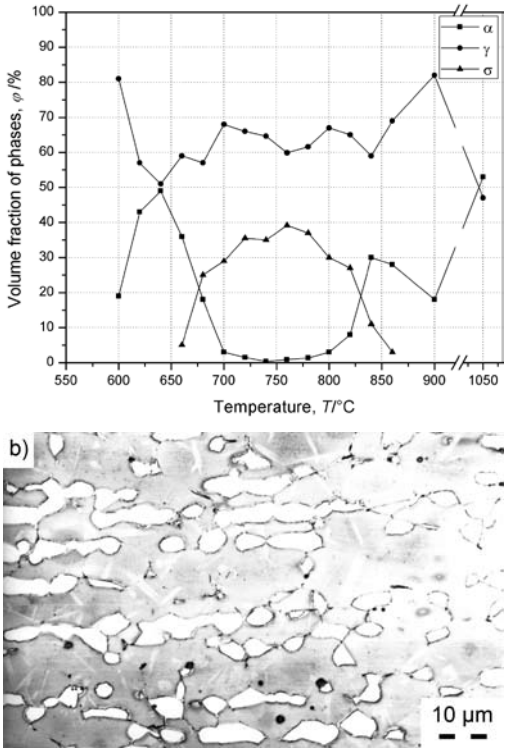

Figure 4. a) Volume concentration of phases after the two-hour aging vs. the aging temperature (900–1250 °C); b) microstructure of the specimen, aged at 1250 °C. As-wrought (⌀ 90 mm), quenched in water, Batch no. 2.

Slika 4. a) Volumenska koncentracija faz po dveurnem staranju v odvisnosti od temperature staranja (900–1250 °C); b) mikrostruktura vzorca, staranega pri 1250 °C. Predelano jeklo (⌀ 90 mm), gašeno v vodi, skupina 2.

for 120 min were carried out with specimens from the batches no. 2 and 3 in the temperature interval 900 °C and 1250 °C, being subsequently quenched in water and cooled in air in order to analyze the influence of cooling rates on the precipitation process. The volumetric concentration of phases, depending on the aging temperature, is presented in Figure 4a. It was evident that volume fraction about 3.5 % of σ-phase appeared after 2 h aging at 900 °C. This could be ascribed to the increased content of Mo in the batch no. 2 (w(Mo) = 0.32 %) compared to batch no.1 (w(Mo) = 0.17 %). In general, the content of ferrite phase increased with the increasing temperature. Intensive $\gamma \rightarrow \alpha$ phase transformation commenced at the temperature around 1150 °C where at the temperature of 1250 °C the volume fraction of ferrite amounted to about 82 % but carbides were predominately dissolved (Figure 4b). On the other hand, the amount of ferrite in general decreased at temperatures below 1050 °C (down to 900 °C).

After all the specimens were aged for 2 h at selected temperatures in the range between 950 °C and 1300 °C they were cooled with two different cooling rates. They were quenched in water and cooled in air. The obtained microstructures of the as-cast and the as-wrought specimens are presented in Figures 5 and 6, respectively.

During the cooling of the as-cast specimens from the aging temperatures of 1300 °C and 1250 °C in water, the austenite and carbides precipitated predominately in ferrite and on the α/α grain boundaries (Figure 5a). At the lower cooling rate (i.e. in air) carbides precipitated predominately on the α/γ grain boundaries and to smaller extent in the ferrite phase (Figure 5b). Precipitated austenite had Widmannstätten morphology. The amount of precipitated carbides increased with decreasing the annealing temperature. The precipitation of carbides and austenite took place predominately on the α/γ phase grain boundaries (Figure 5c–d) and only a small difference was observed in the obtained microstructures of specimens that were quenched in water and cooled on air.

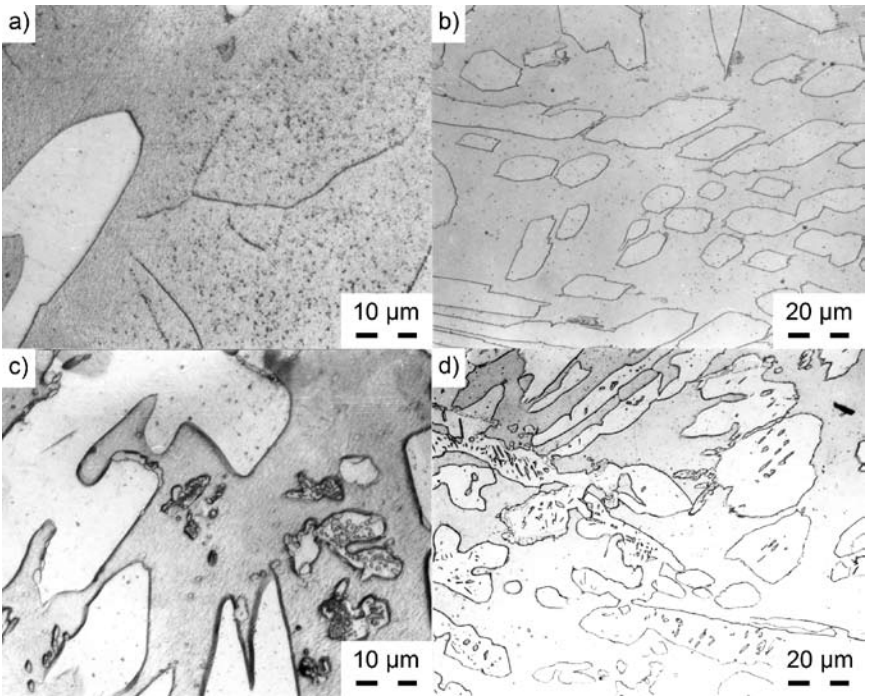

Figure 5. Obtained microstructures of the as-cast specimens of the batch no. 3 that were aged for 2 h at 1250 °C and consequently quenched in water (a) and air cooled (b); aging at 1050 °C, quenched in water (c), and air cooled (d), LM
Slika 5. Mikrostruktura, dobljena z optičnim mikroskopom vzorcev litega stanja, skupina 3, starana 2 h pri temperaturi 1250 °C in gašena v vodi (a) ter ohlajana na zraku (b); staranje pri temperaturi 1050 °C gašena v vodi (c) in ohlajana na zraku (d)

Similar results were obtained for the as-wrought specimens, where the only difference was that carbides precipitated during the quenching in water from the annealing temperature of 1300 °C and 1250 °C to smaller extent in the ferrite phase and to greater extent on the α/γ grain boundaries (Figures 6a-b, compared to Figures 5a-b). The annealing temperature and the cooling rate influenced the morphology of the precipitated carbides in the as-cast as well as in the as-wrought specimens. At higher annealing temperature the morphology of precipitated carbides was lamellar but with decrease of annealing temperature the mentioned morphology slightly changed from lamellar to spherical. This change occurred in the as-wrought specimens that were quenched in water from the temperature range between 1150 °C and 1100 °C (Figure 6d) while in the specimens that were cooled in air this phenomenon occurred already at approximately 1175 °C (Figure 6c).

With the decrease of aging temperature (1050 °C) the amount of precipitated carbides increased. They predominately precipitated on the α/γ grain boundaries and their form varied from stick-shaped to spherical. The morphology of precipitates did not change only with the aging

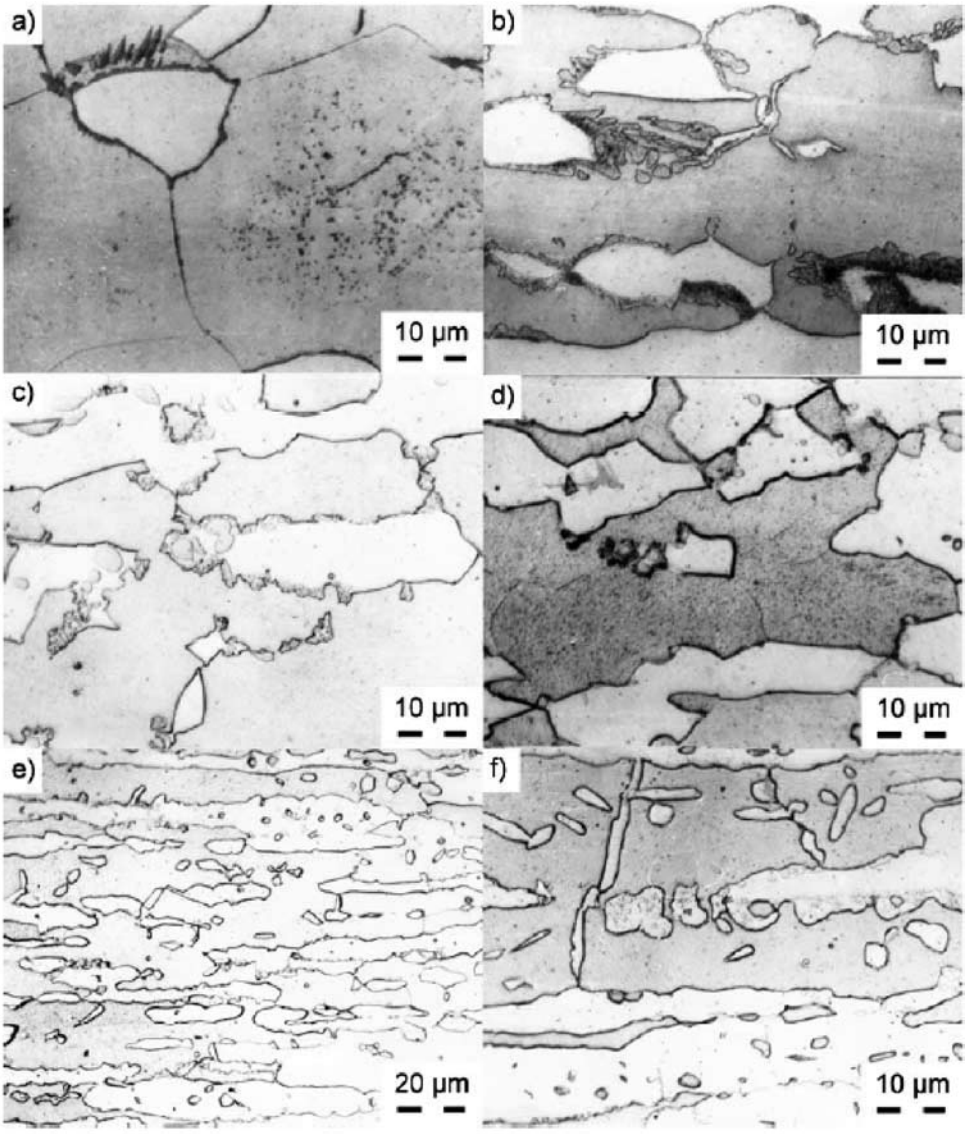

Figure 6. Obtained microstructures of the as-wrought specimens from the batch no. 2 being aged for 2 h in the temperature range of 1300–1000 °C, and subsequently quenched in water or cooled in air; aging at 1250 °C, water quenching (a), aging at 1250 °C, air cooling (b), aging at 1175 °C, air cooling (c), aging at 1150 ºC, water quenching (d), aging at 1050°C, water quenching (e) and air cooling (f), LM

Slika 6. Mikrostruktura, dobljena z optičnim mikroskopom predelanega jekla, skupina 2, po dvournem staranju pri temperaturi 1250 °C, gašena v vodi (a) ter ohlajana na zraku (b); staranje pri temperaturi 1050 °C, gašena v vodi (c) in ohlajan na zraku (d); staranje pri 1050 °C in ohlajana v vodi (e) ter na zraku (f)

temperature but also with the cooling rate (Figures 6e–f).

Examination with the EDS revealed that $M_{23}C_6$-type carbides precipitated on the α/γ grain boundaries.

Table 3. Chemical composition (*w*/%) of phases, and the (*I*α/γ) distribution coefficient of elements in the sample aged for 30 min at 1050 °C, batch no. 1

Tabela 3. Kemična sestava (*w*/%) faz in razdelitveni koeficient (*I*α/γ) faz v vzorcih, staranih 30 min pri temperaturi 1050 °C, skupina 1.

w/%	α	γ	Carbides	*I*α/γ
Cr	33.76	25.75	68.12	1.32
Mn	1.98	2.31	1.57	0. 86
Fe	55.78	58.71	20.17	0.95
Co	0.35	0.45	0.11	0.78
Ni	7.07	12.68	2.69	0.56
Mo	0.22	0.13	0.61	1.69

The amounts of α and γ-phases depend on the annealing temperature where as the cooling rate showed a negligible influence.

Chemical analyses of austenite, ferrite and carbides (M_7C_3) in the specimen that was aged for 30 min at 1050 °C were performed using the EDS microanalyzer. They are presented in Table 3 together with the (Iα/γ) distribution coefficient. The highest difference of chemical elements content between ferrite and austenite was found for Mo and Ni, followed by Cr, Co, Mn and Fe. Transformation of ferrite into austenite took place only by diffusion of Cr and Mo to certain regions (carbides) thus enriching them and leading to the formation of sigma phase. The regions that were enriched with the mentioned elements due to segregation were favourable for commencement of the α → γ transformation [6]. The carbides (M_7C_3) were mainly composed of Cr and Fe (see Table 3). The presence of M_7C_3 carbides was discovered on the base of transforming the chemical composition of carbides from mass fractions into molar fractions, taking in account that molar fraction of carbon, N_C, was obtained by subtracting the sum of molar fractions of the other alloying elements that were composing carbides from the value 1. The calculated ratio between the sum of molar fractions of chromium and iron (x(Cr) + x(Fe)) and the x(C) was approximately 7 : 3 that indicated the presence of M_7C_3-type carbides.

Conclusions

Precipitation behaviour in the PK 324 ferrous alloy at various testing conditions was examined. Two aging treatment tests were applied; shorter aging time (30 min) in lower temperature range (620–900 °C (1050 °C)), and longer aging time (120 min) in higher temperature range (900–1300 °C). The aged specimens in the higher temperature range were cooled with two cooling rates; i.e. quenched in water and cooled in air. The following conclusions, useful for increasing the final quality of PK 324 ferrous alloy, can be stated:

- As-cast microstructure consisted of austenite, ferrite, sigma phase and M_7C_3 and $M_{23}C_6$ carbides. The carbides were mainly composed of Cr and Fe.
- The sigma phase nucleated on ferrite-austenite interfaces and grew into ferrite grains.
- The sigma phase precipitated in the temperature range of 660–860 °C, having peak value of the maximal amount of 39.5 % at about 750 °C and it was then completely dissolved at about 900 °C. The upper temperature limit of the σ phase precipitation is depended on the chemical

composition. The final hot forming steps should be performed above 900 °C.
- The concentration of sigma phase could be minimized if the cooling rate in the range of its precipitation was high enough. This would improve the cold deformability as well as the final microstructure.
- The 2 h aging process at about 1250 °C, gave the content of ferrite above 80 %; at around 1100 °C this content was reduced below 60 %, at around 1000 ºC the content was already below 50 %, and at around 900 °C the content of ferrite was even lower than 40 %.

Povzetek

Raziskana je bila precipitacija v dupleksnem jeklu PK 324 pri različnih pogojih preizkušanja. Uporabljena sta bila dva poteka preizkušanja: kratki preizkus staranja (30 min) pri nižjih temperaturah (620–900 °C (1050 °C)) ter daljši preizkusi staranja (120 min) pri višjih temperaturah (900–1300 °C). Preizkušanci so bili ohlajani na sobno temperaturo z dvema različnima hitrostma ohlajanja; gašeni so bili v vodi, drugi pa so bili ohlajani na zraku.

Pri tem so bile dobljene naslednje ugotovitve:
- Lita struktura je vsebovala avstenit, ferit, fazo sigma ter karbida M_7C_3 in $M_{23}C_6$. Karbida sta v večji meri vsebovala Cr in Fe.
- Faza sigma je nukleirala na fazni meji avstenit/ferit in je rastla v notranjost feritnih zrn.
- Faza sigma se je izločala v temperaturnem območju med 660 °C ter 860 °C, vrh (φ = 39.5 %) pa je dosegla pri 750 °C. Popolnoma je bila raztopljena pri 900 °C. Ta temperatura je odvisna od kemijske sestave in kaže na to, da bi se morali zadnji vtiki med kovanjem izvesti nad 900 °C.
- Koncentracijo izločene faze sigma bi bilo mogoče zmanjšati s pospešenim ohlajanjem skozi področje njenega izločanja. S tem bi se izboljšala preoblikovalnost v hladnem ter končna mikrostruktura izdelka.
- Dveurni proces staranja pri 1250 °C je pokazal, da je v mikrostrukturi prostorninski delež ferita večji od 80 %. Pri 1100 °C je bilo ferita le še 60 %, pri 1000 °C 50 % ter pri 900 °C manj kot 40 %.

References

[1] Martins, M. & Rodrigues Nogueira Forti, L. (2008): Effect of aging on impact properties of ASTM A890 Grade 1C super duplex stainless steel. *Materials Characterization*; 59/2, pp.162–166.

[2] The group of authors, (1977): *A guide to the Solidification of Steels*. Jernkontoret, Box 1721 87 Stockholm, Sweden, pp. 5–111.

[3] Hayes, F. H., Herherington, M. G., Longbottom, R. D. (1990): Thermodynamics of duplex stainless steels. *Materials Science and Engineering*, Vol. 6, pp. 263–272.

[4] Martins, M. & Casteletti, L. C. (2005): Heat treatment temperature influence on ASTM A890 GR 6A super duplex stainless steel microstructure. *Materials Characterization*, 55/3, pp. 225–233.

[5] Martins, M., Mazzer Rossitti, S., Ritoni, M. & Carlos Casteletti,

L. (2007): Effect of stress relief at 350 °C and 550 °C on the impact properties of duplex stainless steels. *Materials Characterization*, 58/10, pp. 909–916.

[6] Flasche, L. H. (1983): Weldability of Ferralium alloy 225, in R. A. Lula: Duplex Stainless Steel, Conference Proceedings. *American Society of Metals*, Ohio, pp. 553–571.

[7] Chi-Shang Huang & Chia-Chang Shih, (2005): Effects of nitrogen and high temperature aging on σ phase precipitation of duplex stainless steel. *Materials Science and Engineering*, 402/(1–2), pp. 66–75.

[8] Cabrera, J. M., Mateo, A., Llanes, L., Prado, J. M. & Anglada, M. (2003): Hot deformation of duplex stainless steels. *Journal of Materials Processing Technology*, 143-144, pp. 321–325.

[9] Josefsson, B., Nilsson, J. O., Wilson, A. (1991): Phase transformation in duplex steels and relation between continous cooling and isothermal heat treatment, in Duplex stainless steels '91, 28-30, ed.: Charles, J. & Bernhardsson, S., Beaune Bourgogne, France.

[10] Chen, T. H. & Yang, J. R. (2001): Effects of solution treatment and continuous cooling on σ-phase precipitation in a 2205 duplex stainless steel. *Materials Science and Engineering A*, 311/(1-2), pp. 28–41.

[11] Chen, T. H., Weng, K. L. & Yang, J. R. (2002): The effect of high-temperature exposure on the microstructural stability and toughness property in a 2205 duplex stainless steel, *Materials Science and Engineering* A, Vol. 338, No. 1–2, pp. 259–270.

[12] Pohl, M., Storz, O. & Glogowski, T. (2007): Effect of intermetallic precipitations on the properties of duplex stainless steel. *Materials Characterization*, 58/1, pp. 65–71.

[13] Sieurin, H. & Sandström, R. (2007): Sigma phase precipitation in duplex stainless steel 2205. *Materials Science and Engineering* A, 444/(1–2), pp. 271–276.

[14] Rieck, W., Pohl, M., Padihla, A. F. (1998): Recrystallization-Transformation Combined Reactions during Annealing of a Cold Rolled-Austenitic Duplex Stainless Steel. *ISIJ International*, 38/6, pp. 567–571.

[15] Klemm, B. (1962): Handbuch der metallographischen Ätzverfahren. *Deutscher Verlag für Grundstoffindustrie*, Leipzig.

The possibility of using soil instead of rock samples for a petrological interpretation

Možnost uporabe tal namesto kamnin za petrološko interpretacijo

Nina Zupančič[1], Maja Plaskan[1]

[1]University of Ljubljana, Faculty of Natural Sciences and Engineering, Department of Geology, Aškerčeva cesta 12, SI-1000 Ljubljana, Slovenija; E-mail: nina.zupancic@ntf.uni-lj.si

Received: September 22, 2008 **Accepted:** December 01, 2008

Abstract: In the area of the Pohorje Mts. (NE Slovenia, Eastern Alps) igneous complex we tried to test whether the sampling of soil instead of fresh rock yields adequate results for a petrological interpretation. In 22 locations granodiorite, dacite, gabbro and lamprophyre with corresponding soil were sampled. Whole rock and trace element analysis was performed using ICP – MS and – ES. A statistical t-test showed that the major element content as well as Ba, Nb, Rb, and Sr are generally significantly different in both media. On the petrological diagrams based on these elements soil and rock samples from the same location plot in different fields. In the case of major elements the use of soil samples instead of rock is not advisable. However for diagrams constructed with immobile elements – such as diagrams for tectonic setting and REE patterns – a soil sample might possibly be used quite safely in place of fresh rock.

Izvleček: Na področju pohorskega magmatskega masiva (SV Slovenija, Vzhodne Alpe) smo skušali preveriti, ali vzorčenje tal na mestu vzorcev kamnin daje enakovredne rezultate za petrološko interpretacijo. Na 22 lokacijah smo vzorčili granodiorit, dacit, gabbro in lamprofir ter tla nastala na teh kamninah. Vsebnost glavnih in slednih prvin smo določili z ICP – MS in – ES. Statistični t-test je pokazal, da se vzorci značilno razlikujejo po vsebnosti glavnih prvin ter Ba, Nb, Rb in Sr. Na petroloških diagramih, ki so zasnovani na teh prvinah, se vzorci kamnin in tal uvrščajo na različna področja. Uporaba vzorcev tal v diagramih, ki vključujejo glavne prvine, zato ni primerna. V diagramih, zasnovanih z nemobilnimi prvinami – kot na primer diagrami tektonskega okolja ter vzorci REE – pa lahko vzorci tal dokaj dobro nadomestijo vzorce kamnin.

Key words: geochemistry, weathering, petrological diagrams, soil, granodiorite, Eastern Alps

Ključne besede: geokemija, preperevanje, petrološki diagrami, tla, granodiorit, Vzhodne Alpe

Original scientific paper

Introduction

The Pohorje Mts. (NE Slovenia, Europe) consist of prevailing granodiorite pluton with a small satellite gabbro body, a minor dacite stock and several lamprophyre veins. In previous years studies on these igneous rocks have been performed to establish their origin and genesis (Zupančič, 1997a, b). During field work it has become obvious that in a temperate climate at altitudes of below 2000 m fresh rock samples are quite difficult to obtain due to the rapid weathering and formation of soil. Silicate rocks are often covered by deep soil and vegetation. Sampling is limited to outcrops which are not uniformly distributed. That is why the reliability of petrological and statistical studies may often be in question.

In this study we tried to test weather it is possible to use soil samples instead of fresh rock and still obtain authentic data for a petrological interpretation. The applicability of the different classification and discrimination diagrams constructed with data from the soil samples is discussed.

Materials and methods

Five kilogram samples of different igneous rocks and the corresponding two kilograms of soil (the upper 20 cm) were collected. Altogether, there were 22 sampling localities distributed throughout the massive in accordance with the volume of different rock types. Both media were collected as close as possible to ensure that the soil was truly a weathering product of the treated rock. In randomly chosen locations replicate samples were obtained to control the sampling quality. To control the quality of analytics some duplications were added. The chemical composition of three gabbro and two corresponding soils, three lamprophyres and their soils, five dacites with appropriate soils and 16 granodiorites with 19 soils were analyzed at the ACME Laboratories in Vancouver, Canada. For an analysis of major elements a 2 g sample was digested in 5 % HNO_3 after a $LiBO_2$ fusion. The contents were determined by inductively coupled plasma – emission spectroscopy (ICP – ES). For the trace elements analysis, a 0.5 g sample was leached with 3 mL of an $HCl – HNO_3 – H_2O$ (2 : 2 : 2) mixture at 95 °C for one hour, then diluted to 10 mL and analyzed using an inductively coupled plasma – mass spectroscopy (ICP – MS). According to the added replicates and AGV-1 and RGM-1 standards the analytical error is below 10 % for the elements used in the proceeding study (SiO_2, TiO_2, Al_2O_3, Fe_2O_3, FeO, MnO, CaO, Na_2O, K_2O, P_2O_5, MnO, LOI, Ba, Nb, Rb, Sc, Sr, Th, V, Zr, Y and REE). For REE chondrite the normalization values suggested by Nakamura (1977) were used.

Results and discussion

Generally in more basic rock types (gabbro and lamprophyre) the mean values (Table 1) of the majority of analyzed elements are higher in soils than in rock, while the opposite is true for more acid rocks (granodiorite and dacite). The situation is reverse concerning data scattering i.e. standard deviations (Table 2). These are higher in soils formed on acid rock types and lower in soils weathered from basic rocks. But it should be noted that for both basic rock types the number of observations is ex-

Table 1. Mean values of major (%) and trace (μg/g) values in rock and soil samples from Pohorje Mts. Number of observations: gabbro soil = 2, rock = 3, dacite soil = 5, rock = 5, lamprophyre soil = 3, rock = 3, granodiorite soil = 19, rock = 16.
Tabela 1. Srednje vrednosti glavnih (%) in slednih (μg/g) prvin v pohorskih vzorcih kamnin in tal. Število opazovanj: gabbro (tla) = 2, kamnina = 3, dacit (tla) = 5, kamnina = 5, lamprofir (tla) = 3, kamnina = 3, granodiorit (tla) = 19, kamnina = 16.

	Gabbbro soil	Gabbro rock	Dacite soil	Dacite rock	Lamprophyre soil	Lamprophyre rock	Granodiorite soil	Granodiorite rock
SiO_2	57.95	54.57	54.31	67.99	52.93	56.82	58.53	68.59
TiO_2	0.61	0.41	0.45	0.34	0.97	0.85	0.44	0.30
Al_2O_3	11.50	8.01	13.61	15.58	16.91	16.99	13.89	15.97
Fe_2O_3	2.55	2.75	1.79	1.67	4.04	2.63	1.70	1.29
FeO	2.08	2.24	1.46	1.44	3.30	3.42	1.33	1.41
MnO	0.11	0.15	0.06	0.06	0.14	0.11	0.04	0.07
MgO	6.49	12.27	0.66	1.03	2.62	4.74	0.64	0.96
CaO	6.51	14.01	1.79	3.10	1.80	6.04	1.91	3.23
Na_2O	2.22	2.20	2.42	3.93	1.14	3.74	2.51	4.01
K_2O	1.27	0.19	2.17	3.02	2.27	1.94	2.10	2.84
P_2O_5	0.21	0.13	0.14	0.16	0.16	0.29	0.12	0.13
LOI	8.42	3.04	21.06	1.53	13.99	2.41	16.73	1.04
Ba	907.5	81.66	780.80	1124.60	611.66	1197.66	994.84	1246.81
Nb	9.25	11.56	14.16	2.80	14.83	6.93	13.38	7.66
Rb	37.40	9.90	82.10	110.00	120.56	62.85	73.57	103.67
Sc	39.50	69.33	4.60	5.28	16.66	20.33	4.36	4.31
Sr	440.45	417.33	326.92	509.60	206.96	822.80	426.79	666.84
Th	12.20	9.56	13.34	13.20	15.76	11.16	15.80	16.28
V	141.50	143.33	40.40	36.40	138.00	106.33	41.15	32.31
Zr	89.65	64.36	156.64	164.60	181.83	150.30	162.53	156.52
Y	16.50	16.43	13.46	15.80	28.00	19.53	14.04	16.07
La	34.75	25.13	34.98	33.40	46.43	41.40	40.71	37.06
Ce	66.75	46.96	69.36	67.92	97.86	84.83	75.88	70.57
Pr	7.14	5.28	6.33	6.10	10.34	8.29	7.45	6.68
Nd	26.15	19.70	21.72	21.42	38.06	21.70	25.42	23.33
Sm	5.25	4.30	3.58	3.72	7.63	5.50	4.16	3.98
Eu	1.23	1.07	0.79	0.99	1.59	1.51	0.87	1.04
Gd	4.05	3.73	2.62	3.24	6.36	4.70	2.96	3.22
Tb	0.53	0.49	0.38	0.42	0.88	0.59	0.41	0.43
Dy	3.09	2.93	2.36	2.28	5.36	3.47	2.45	2.54
Ho	0.58	0.55	0.46	0.41	1.02	0.63	0.46	0.46
Er	1.74	1.67	1.44	1.12	3.05	1.75	1.46	1.37
Tm	0.23	0.23	0.21	0.18	0.38	0.23	0.20	0.20
Yb	1.52	1.53	1.49	1.12	2.82	1.64	1.48	1.39
Lu	0.24	0.24	0.24	0.33	0.42	0.41	0.24	0.29

Table 2. Standard deviations of major (%) and trace (μg/g) values in rock and soil samples from Pohorje Mts. Number of observations is the same as in Table 1.
Tabela 2. Standardni odkloni glavnih (%) in slednih (μg/g) prvin v pohorskih vzorcih kamnin in tal. Število opazovanj je enako kot v tabeli 1.

	Gabbbro soil	Gabbro rock	Dacite soil	Dacite rock	Lamprophyre soil	Lamprophyre rock	Granodiorite soil	Granodiorite rock
SiO_2	0.452	0.618	5.064	2.828	0.856	0.631	3.727	1.632
TiO_2	0.021	0.015	0.071	0.068	0.070	0.201	0.186	0.076
Al_2O_3	0.063	0.170	1.427	0.549	0.258	0.639	1.607	0.469
Fe_2O_3	0.007	0.015	0.313	0.723	0.297	0.573	0.916	0.559
FeO	0.007	0.011	0.254	0.296	0.245	0.646	0.540	0.311
MnO	0.000	0.000	0.048	0.021	0.020	0.010	0.034	0.017
MgO	0.014	0.125	0.271	0.237	0.157	0.421	0.545	0.245
CaO	0.035	0.820	1.102	0.681	0.086	0.260	0.402	0.648
Na_2O	0.042	0.057	0.295	0.235	0.257	0.226	0.544	0.208
K_2O	0.021	0.141	0.273	0.253	0.100	0.302	0.275	0.570
P_2O_5	0.106	0.010	0.087	0.040	0.030	0.041	0.040	0.037
LOI	0.282	0.001	5.968	1.350	0.669	0.200	4.861	0.371
Ba	0.707	22.030	78.017	101.455	137.128	138.896	165.891	510.820
Nb	0.494	0.472	1.789	0.836	0.378	7.695	2.269	5.769
Rb	0.141	0.435	12.399	14.142	9.176	4.030	14.201	24.739
Sc	0.707	2.081	1.516	1.517	1.527	2.300	3.531	1.339
Sr	5.727	16.510	41.609	46.516	25.364	109.393	105.749	138.180
Th	1.555	3.629	1.289	2.387	1.501	2.020	3.975	3.469
V	4.949	1.527	13.630	11.653	19.000	60.467	33.258	10.150
Zr	1.060	3.957	11.866	36.390	19.062	21.035	23.852	28.336
Y	1.131	0.650	3.870	1.643	3.593	1.858	4.713	4.845
La	7.283	4.880	6.460	7.893	5.750	8.190	10.431	9.294
Ce	12.515	6.815	5.073	11.646	12.444	4.916	18.904	14.415
Pr	1.195	0.528	1.140	0.913	1.401	1.118	2.120	1.611
Nd	4.596	0.818	4.470	2.751	4.735	16.674	7.696	5.266
Sm	0.212	0.360	0.858	0.593	1.457	0.700	1.554	0.878
Eu	0.091	0.017	0.224	0.120	0.183	0.026	0.314	0.169
Gd	0.254	0.393	0.788	0.427	1.000	0.300	1.153	0.696
Tb	0.028	0.025	0.115	0.044	0.117	0.085	0.177	0.108
Dy	0.325	0.201	0.558	0.238	0.729	0.654	0.909	0.748
Ho	0.042	0.043	0.127	0.040	0.134	0.136	0.181	0.147
Er	0.091	0.142	0.351	0.130	0.376	0.444	0.491	0.484
Tm	0.028	0.015	0.047	0.044	0.064	0.063	0.066	0.065
Yb	0.084	0.051	0.297	0.178	0.215	0.338	0.400	0.425
Lu	0.007	0.037	0.019	0.232	0.043	0.253	0.047	0.123

Table 3. t-values of comparison of soil and rock samples from Pohorje Mts. Number of observations is the same as in Table 1. * - value is statistically significant at 95 % probability level.
Tabela 3. t-vrednosti primerjave pohorskih vzorcev kamnin in tal. Število opazovanj je enako kot v tabeli 1. * - vrednost je statistično značilna na 95 % stopnji verjetnosti.

	Gabbro	Dacite	Lamprophyre	Granodiorite
SiO_2	6.50*	–5.27*	–6.32*	–9.99*
TiO_2	12.63*	2.61*	0.94	2.76*
Al_2O_3	26.49*	–2.86*	–0.18	–4.98*
Fe_2O_3	–16.55*	0.35	3.79*	1.55
FeO	–17.23*	0.12	–0.30	–0.48
MnO		0.08	2.75	–3.52*
MgO	–61.69*	–2.33*	–8.17*	–2.15*
CaO	–12.25*	–2.26	–26.74*	–7.35*
Na_2O	0.34	–8.96*	–13.13*	–10.35*
K_2O	10.19*	–5.10*	1.79	–4.98*
P_2O_5	1.50	–0.51	–4.47*	–1.23
LOI	36.20*	7.13*	28.71*	12.85*
Ba	50.28*	–6.00*	–5.20*	–2.03
Nb	–5.28*	12.85*	1.77	3.98*
Rb	82.50*	–2.61*	8.05*	–4.50*
Sc	–18.69*	–0.70	–2.29	0.059
Sr	1.82	–6.54*	–9.49*	–5.81*
Th	0.93	0.11	3.16*	–0.37
V	–0.64	0.49	0.86	1.02
Zr	8.42*	–0.46	1.92	0.68
Y	0.08	–1.24	3.62*	–1.25
La	1.81	0.34	0.87	1.08
Ce	2.37	0.25	1.68	0.92
Pr	2.51	0.35	1.98	1.19
Nd	2.58	0.12	1.63	0.91
Sm	3.26*	–0.29	2.28	0.41
Eu	3.29*	–1.73	0.74	–1.97
Gd	0.98	–1.53	2.75	–0.78
Tb	1.53	–0.68	3.44*	–0.26
Dy	0.67	0.30	3.33*	–0.28
Ho	0.76	0.83	3.52*	0.11
Er	0.61	1.90	3.85*	0.51
Tm	–0.35	1.16	2.81*	–0.20
Yb	–0.22	2.42*	5.09*	0.67
Lu	0.05	–0.82	0.04	–1.76

tremely low so the data are not very trustworthy, and the results rather on the level of indications.

The statistical significance of the differences has been checked by the t-test (Table 3). Mainly the differences are statistically significant for all major elements except for Fe, Mn and P, and for the most part for Ba, Nb, Rb and Sr. REE seem to be unaffected by weathering except for HREE in the case of lamprophyre (where the observation number is low and so the conclusion is not so indicative). Between the soil and rock in all four rock types the largest differences are observed for the loss of ignition (LOI). This is normal, since weathering includes hydratation. What was less expected was the statistically significant change in SiO_2, MgO and Rb in all four rock types. These observations are well expressed on the standard petrological plots.

Diagrams using major elements

In igneous petrology major elements are used for different types of rock classification. In recent times (Wilson, 1989) a TAS (total alkalis/silica) diagram (Cox et al., 1979) has also been used for plutonic rocks. It is obvious in Figure 1 that the rock samples plot in the appropriate fields – granodiorite and dacite in the field of granite and granodiorite, gabbro in the area between gabbro and diorite and lamprophyre in the field of diorite. Yet the soil samples show quite a different classification. The majority of samples indicate a far more basic character with less silica and alkalis i.e. they all plot in the fields of diorite, the fields between diorite and gabbro and some soils from dacites and granodiorite even in the field of gabbro.

According to the silica saturation index (Thornton & Tuttle, 1960), all rock samples are described as silica oversaturated, which is supported by free quartz observed in hand specimen and under the microscope. On the contrary, soils from granodiorites and dacites seemed to be predominantly silica saturated or even under saturated, which is not in accordance with the true situation in the igneous body.

Saturation with aluminia is expressed with the A/CNK ($Al_2O_3/(CaO+Na_2O+K_2O)$) and A/NK (Al_2O_3/Na_2O+K_2O)) index (Shand, 1947). In the diagram (Figure 2) granodiorites and dacites are in the field of peraluminous rocks, close or even partly in the field of metaluminous rocks. Gabbro and lamprophyre of a more pronounced mantle source are, as expected, in the metaluminous field. Again, the soil samples behave differently. They showed a much more pronounced peraluminous character. Only soil derived from gabbro is metaluminous. The same diagram enables a distinction between I- and S-type granites as proposed by Chapell & White (1974). In this case, the allocation of soil samples far from their rock counterparts is crucial. Instead of the I-type, the soils are prevailingly classified as the S-type, with the exception of soil from gabbro and one soil sample from dacite.

The interpretation of trends and magma evolution is performed with the use of Harker diagrams (Rollinson, 1993). In those diagrams the major and trace elements are plotted versus SiO_2. Figure 3 indicates that normally there is much more data scatter when using soil samples in place of fresh rock samples. The low silica content in the soil samples in comparison to adequate rock samples is one of the main characteristics.

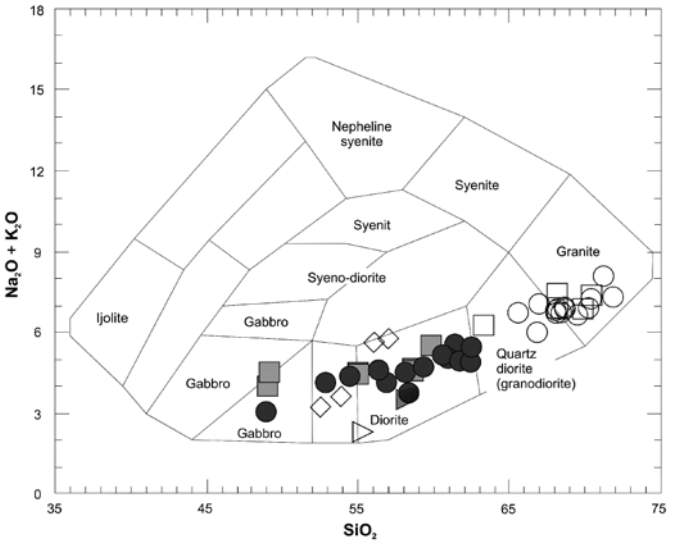

Figure 1. TAS classification of rock (empty symbols) and soil samples (full symbols) from the Pohorje Mts. ■ - gabbro, ▶ - dacite, ◆ - lamprophyre, ● - granodiorite.
Slika 1. TAS-klasifikacija vzorcev kamnin (prazni znaki) in tal (polni znaki) s Pohorja. ■ - gabbro, ▶ - dacit, ◆ - lamprofir, ● - granodiorit.

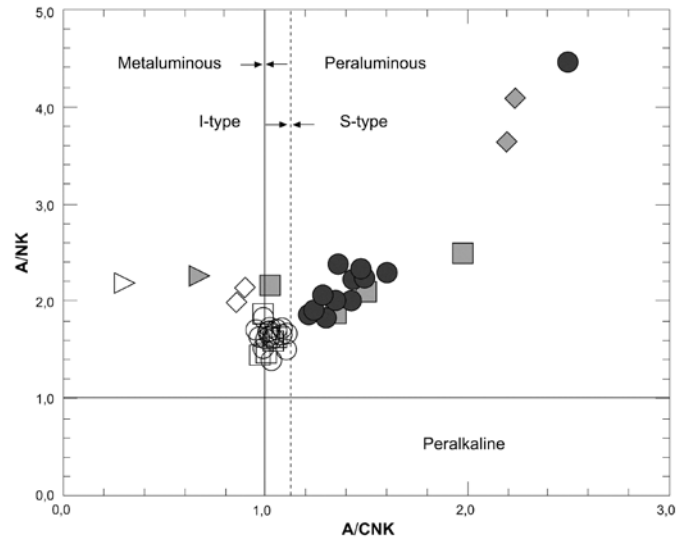

Figure 2. Aluminia saturation index and the I- and S-type division of Pohorje rock (empty symbols) and soil samples (full symbols). Legend: see Figure 1.
Slika 2. Indeks nasičenja z glinico ter razdelitev pohorskih kamnin (prazni znaki) in tal (polni znaki) v I- in S-tip. Legenda: glej sliko 1.

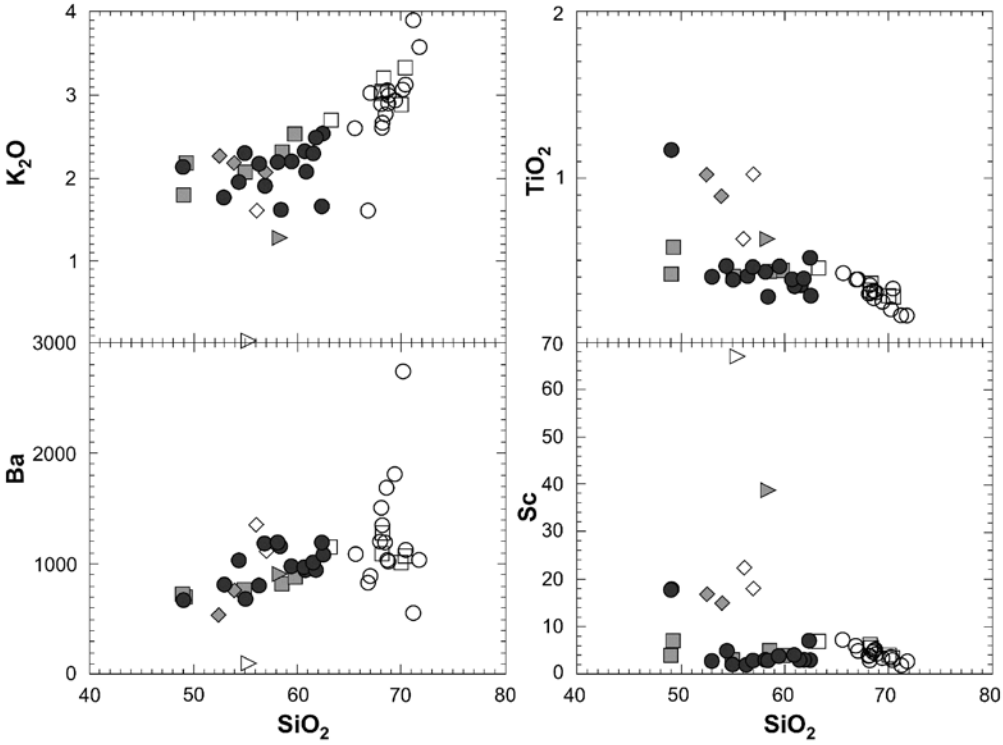

Figure 3. Harker diagrams of Pohorje rock (empty symbols) and soil samples (full symbols). Major elements in *w*(%), trace in *w*(μg/g). Legend: see Figure 1.
Slika 3. Harkerjevi diagrami vzorcev kamnin (prazni znaki) in tal (polni znaki) s Pohorja. Glavne prvine so izražene z *w*(%), sledne pa z *w*(μg/g). Legenda: glej sliko 1.

In some instances (i.e. TiO_2 in Figure 3) we can still trace the same trend as if using rocks, but in others (i.e. K_2O in Figure 3) this information is completely missing. In the soil samples with some trace elements (i.e. Ba in Figure 3) we even observed trends not shown by the rock samples. The petrogenetic interpretation of such a trend is, of course, misleading.

Trace elements

Although the statistical t-test indicates that the Ba, Rb and Sr content in soils does not reflect the amount of the mentioned elements in the rock, Figure 4 makes it obvious that in the ternary diagram of El Bouseily & El Sokkary (1975) all the samples fall within the same area.

Pearce et al. (1984) started with use of geochemical parameters to distinguish between the different tectonic settings of basalts and granites. One of the conditions for constructing such diagrams was that the elements involved should not be subject to mobilization during weathering or other alteration processes. The appropriate selection of elements in tectonic setting diagram proposed by Pearce et al. (1984) is

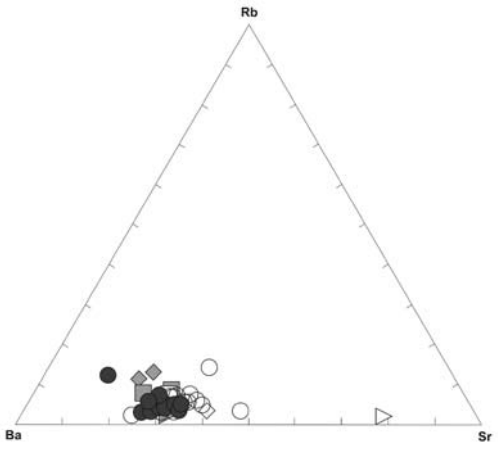

Figure 4. Ternary diagram Rb-Ba-Sr of Pohorje rock (empty symbols) and soil samples (full symbols). Legend: see Figure 1.
Slika 4. Trikotni diagram Rb-Ba-Sr pohorskih kamnin (prazni znaki) in tal (polni znaki). Legenda: glej sliko 1.

clearly demonstrated in the Figure 5 where the soil and rock samples overlap in the field of volcanic arc granites.

REE patterns

REE show various degrees of mobility during weathering or metamorphic alteration (HUMPHRIES, 1984; PRICE et al., 1991). They could be even mobilized inside the soil profile (NESBITT, 1979; SHARMA & RAJAMANI, 2000; PANAHI et al., 2000; AUBERT et al., 2001). HREE are reported to be more mobile than LREE (NESBITT, 1979; BRAUN et al., 1998; MINAŘIK, 1998; AUBERT et al. 2001,). Figure 6 indicates that during weathering and soil formation the REE patterns of each rock type preserved their form as well as their REE content, which is consistent with the work of certain authors (SHARMA & RAJAMANI, 2000; MUCHANGOS, 2006). There are some isolated

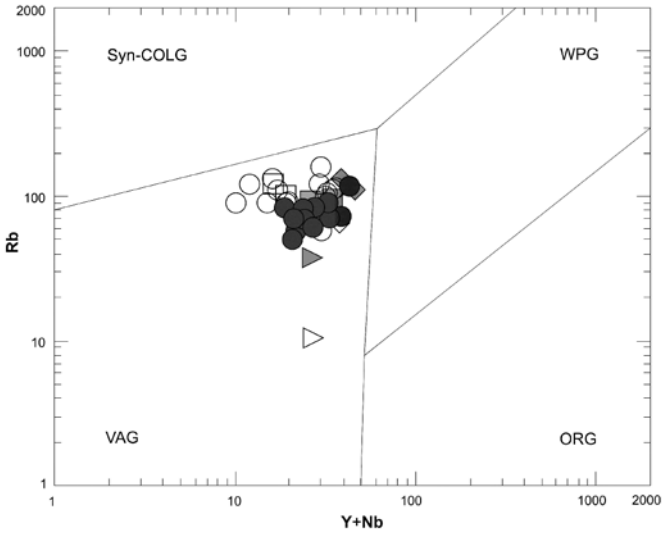

Figure 5. Tectonic setting diagram of Pohorje rock (empty symbols) and soil samples (full symbols). Values in *w*(µg/g). Legend: see Figure 1.
Slika 5. Diagram tektonskega okolja Sr pohorskih kamnin (prazni znaki) in tal (polni znaki). Vrednosti so izražene z *w*(µg/g). Legenda: glej sliko 1.

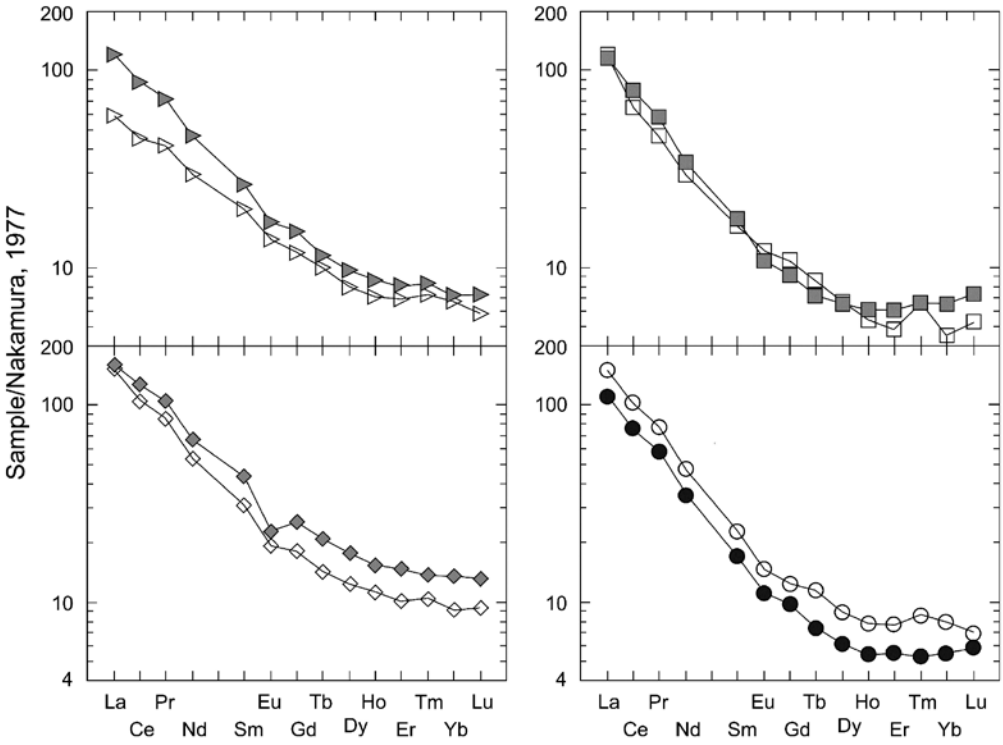

Figure 6. REE patterns of selected Pohorje rock (empty symbols) and soil samples (full symbols). Legend: see Figure 1.
Slika 6. Vzorec REE izbranih pohorskih kamnin (prazni znaki) in tal (polni znaki). Legenda: glej sliko 1.

cases with a deviation from the original rock pattern. In particular, there was one lamprophyre sample with a pronounced negative Eu anomaly and a higher HREE fractionation, which caused significant differences in the t-test results (Table 3). In spite of low number of samples for significant results, generally with some precaution the REE data from the soil samples can be used in the same manner as rock samples.

Conclusions

During weathering and soil formation major and some trace element (Ba, Nb, Rb and Sr) content becomes more or less changed. In basic rock types (gabbro and lamprophyre) we noticed their increase, while in more acid rocks (granodiorite and dacite) we observed their decrease. Only Fe, Mn, and P seemed to be an exception.

Consequently it appears inappropriate to use soil samples instead of fresh rocks for the majority of petrological classifications – i.e. TAS diagram, silica and aluminia saturation indexes, and the division between I- and S-type granites. The use of Harker diagrams based on soil samples is also highly unreliable.

More promising appears to be the application of soil samples in the construction of

variation diagrams with less mobile elements. Diagrams such as Ba-Rb-Sr, or Rb/(Y+Nb) for the tectonic setting and REE patterns do not show discrepancies between the soil and rock samples.

POVZETEK

Zaradi preperevanja in nastajanja tal se bolj ali manj spremeni vsebnost glavnih in nekaterih slednih prvin (Ba, Nb, Rb in Sr). V bazičnih kamninah (gabbro, lamprofir) je njihova količina narasla, v bolj kislih (granodiorit in dacit) pa padla. Izjeme so le Fe, Mn in P.

Zato je uporaba vzorcev tal namesto svežih kamnin za večino petroloških klasfikacij (TAS–diagram, indeks nasičenja s kremenico in glinico, ločevanje I- in S-tipa granitov) neustrezna. Tudi uporaba Harkerjevih diagramov je pri talnih vzorcih skrajno nezanesljiva.

Bolj ustrezna je videti uporaba talnih vzorcev v primeru variacijskih diagramov, ki temeljijo na manj mobilnih prvinah. Diagrami, kot so Ba-Rb-Sr ali Rb/(Y+Nb), za tektonska okolja ter vzorci REE ne kažejo razlik med kamninskimi in talnimi vzorci.

REFERENCES

AUBERT D., STILLE P. & PROBST A. (2001): REE fractionation during granite weathering and removal by waters and suspended loads: Sr and Nd isotopic evidence, *Geochimica et Cosmochimica Acta* 65, 3, 387–406.

BRAUN J. J., VIERS J., DUPRE B., POLVE M., NDAM J. & MULLER J. P. (1998): Solid/liquid REE fractionation in the lateritic system of Goyoum, East Cameroon - the implication for the present dynamics of the soil covers of the humid tropical regions. *Geochimica et Cosmochimica Acta* 62, 2, 273–299.

CHAPELL B. W. & WHITE A. J. R. (1974): Two contrasting granite types. *Pacific Geology* 8, 173–174.

COX K. G., BELL J. D. & PANKHURST R. J. (1979): The interpretation of igneous rocks. *George, Allen and Unwin*, London.

EL BOUSEILY A. M. & EL SOKKARY A. A. (1975): The relation between Rb, Ba and Sr in granite rocks. *Chemical Geology* 16, 207–219.

HUMPHRIES S. E. (1984): The mobility of REE in the crust. In: Henderson, P. (ed.), Rare earth element geochemistry. *Elsevier*. Amsterdam.

MINAŘIK L., ŽIGOVA A., BENDL. J., SKŘIVAN P. & ŠTASTNY M. (1998): The behaviour of rare-earth elements and Y during the rock weathering and soil formation in the Ricany massif, Central Bohemia. *Science of the Total Environment* 215, 1–2, 101–110.

MUICHANGOS A. C. (2006): The mobility of rear-earth and other elements in the process of alteration of rhyolitic rocks to bentonite (Lebomo Volcanic Mountainous Chain, Mozambique). *Journal of Geochemical Exploration* 88, 300–303.

NAKAMURA N. (1974): Determination of REE, Ba, Fe, Mg, Na and K in carbonaceous and ordinary chondrites. *Geochimica et Cosmochimica Acta* 38, 757–775.

Nesbitt H. W. (1979): Mobility and fractionation of REE during weathering of a granodiorite. *Nature* 279, 206–210.

Panahi A., Young G. M. & Rainbird R. H. (2000): Behavior of major and trace elements (including REE) during Paleoproterozoic pedogenesis and diagenetic alteration of an Achaean granite near Ville Marie, Quebec, Canada, *Geochimica et Cosmochimica Acta* 64, 13, 2199–2220.

Pearce J. A., Harris N. B. W. & Tindlle A. G. (1984): Trace element discrimination diagrams for the tectonic interpretation of granitic rocks. *Journal of Petrology* 25, 956–983.

Price R. C., Gray C. M, Wilson R. E., Frey F. A. & Taylor S. R. (1991): The effects of weathering on rare earth elements, Y and Ba abundances in Tertiary basalts from southeastern Australia. *Chemical Geology* 93, 3/4, 245–265.

Rollinson H. (1993): Using geochemical data: Evaluation, presentation, interpretation. *Longman Scientific and Technical*, Essex.

Shand S. J. (1947): Eruptive rocks. Their genesis, composition, classification, and their relation to ore deposits. J. *Wiley & Sons*.

Sharma A. & Rajamani V. (2001): Weathering of gneissic rocks in the upper reaches of Cauvery river, south India: implications to neotectonics of the region. *Chemical Geology* 166, 3–4, 203–223.

Thornton C. P. & Tuttle O. F. (1960): Chemistry of igneous rocks I: Differentiation index. *American Journal of Science* 258, 664–684.

Wilson M. (1989): Igneous petrogenesis. *Unwin Hyman*, London.

Zupančič N. (1994a): Petrographical characteristics and classification of Pohorje igneous rocks. *Rudarsko-metalurški zbornik* 41, 1/2, 101–112. (in Slovene)

Zupančič N. (1994b): Geochemical characteristics and genesis of Pohorje igneous rocks. *Rudarsko- metalurški zbornik* 41, 1/2,113–128. (in Slovene)

Determination of heavy metals in paddy soils (Kočani Field, Macedonia) by a sequential extraction procedure

Določitev težkih kovin v tleh riževih polj (Kočansko polje, Makedonija) z uporabo postopka zaporednega izluževanja

Nastja Rogan[1], Tadej Dolenec[1], Todor Serafimovski[2], Goran Tasev[2], Matej Dolenec[1]

[1]University of Ljubljana, Faculty of Natural Sciences and Engineering, Department of Geology, Aškerčeva 12, SI-1000 Ljubljana, Slovenia;
E-mail: nastja.rogan@guest.arnes.si, tadej.dolenec@ntf.uni-lj.si
[2]Faculty of Mining and Geology, Goce Delčev 89, 2000 Stip, Macedonia;
E-mail: todor.serafimovski@ugd.edu.mk, goranktasev@yahoo.com

Received: October 20, 2008 **Accepted:** December 8, 2008

Abstract: In this study we examine the distribution of heavy metals (As, Cd, Cu, Pb and Zn) in paddy soil samples from Kočani Field (Macedonia) by ICP-EAS and sequential extraction procedure. Very high concentrations of As (42 mg/kg), Cd (5.6 mg/kg), Cu (99 mg/kg), Pb (892 mg/kg) and Zn (1134 mg/kg) were found in the paddy soil sample from location VII-2 in the western part of Kočani Field, close to the Zletovska River, which drains the untreated effluents of the Pb-Zn mine in Zletovo and is used for the irrigation of the Kočani paddy fields. The mobility potential of heavy metals in the investigated paddy soil samples increases from As–Pb–Zn–Cu–Cd. We concluded that the paddy soil sample from location VII-2 had highly elevated heavy metal concentrations and revealed that the extraction characteristics of heavy metals represents a serious environmental potential risk for the surrounding ecosystems.

Izvleček: V študiji smo raziskovali razporeditev težkih kovin **(**As, Cd, Cu, Pb in Zn) v vzorcih tal riževih polj (Kočansko polje, Makedonija) z uporabo ICP-EAS in postopka zaporednega izluževanja. V vzorcu iz lokacije VII-2, ki se nahaja blizu reke Zletovske v zahodnem delu Kočanskega polja, smo našli zelo visoke koncentracije As (42 mg/kg), Cd (5,6 mg/kg), Cu (99 mg/kg), Pb (892 mg/kg) in Zn (1134 mg/kg). Visoke koncentracije težkih kovin so bile v vzorcu VII-2 zato, ker reka Zletovska odvaja neprečiščene odplake in odpadke z območja rudnika Pb-Zn Zletovo, kmetje pa jo uporabljajo za namakanje okoliščnih riževih polj. V raziskovanih vzorcih narašča potencial mobilnosti v naslednjem zaporedju: As–Pb–Zn–Cu–Cd. Na podlagi zelo visokih koncentracij in izluževalnih lastnosti težkih kovin, prisotnih v vzorcu VII-2, smo ugotovili, da pomeni območje okoli imenovanega vzorca resno ekološko grožnjo bližnjim ekosistemom.

Original scientific paper

Key words: heavy metal contamination, paddy soil, sequential extraction procedure, Kočani Field, Macedonia
Ključne besede: težke kovine, tla, postopek zaporednega izluževanja, Kočansko polje, Makedonija

Introduction

Environmental pollution by heavy metals from base-metal mining operations and from abandoned mines can become a very important source of contamination of soils and poses a long-term risk to ecosystem health (Adriano, 1986). Elevated concentrations of heavy metals can be found in and around abandoned and active mines due to the discharge and dispersion of the untreated mines waste materials into nearby agricultural soils, food crops, riverine water and stream sediments (Jung, 2001; Korre et al., 2002; Lee et al., 2001; Liu et al., 2005; Lu & Zhang, 2005; Simmons et al., 2005).

The chemical behaviour of heavy metals in soils is controlled by a number of processes, including metal cation release from contamination source materials (e.g., fertilizer, sludge, amelter dust, slag), cation exchange and specific adsorption onto the surfaces of minerals and soil organic matter, and precipitation of secondary minerals (Manceau et al., 2000; McBride et al., 1997; McBride, 1999; Morin et al., 1999). Only soluble, exchangeable and chelated metal species in the soils are the labile fractions available for plants (Kabata-Pendias, 1993). For this reason, the measurements of the total amount of heavy metals in soils should be complemented with the measurements of the available fraction. A method widely used to assess the lability of heavy metals in soils and to provide detailed information on the heavy metal binding forms is the leaching of soils by means of chemical extractants. During recent decades, several leaching/extraction tests have been developed and modified for these purposes in the fields of geochemistry, marine chemistry and agricultural sciences (Tack & Verloo, 1995). Among the various sequential procedures presented, the most widely applied is that proposed by Tessier et al. (1979).

Studies about heavy metal concentrations in soil derived from the past and present mining activities in Macedonia are very rare (Dolenec et al., 2007). Consequently, very little is known about the distribution and concentrations of heavy metals in the soil from different parts of Macedonia, which could be affected due to historical and/or recent base-metal mining. Such an example is Kočani Field in eastern Macedonia, where the base-metal mining history of the region is very long and paddy rice (Oryza sativa L.) is one of the main agricultural products of the region. Previous investigations have shown that the riverine water from the Zletovska River and the Bregalnica River, used for the irrigation of the Kočani paddy fields, was contaminated with heavy metals as the result of acid mine water and the untreated effluents from the ore-processing facilities from the Zletovo-Kratovo and Sasa-Toranica ore district (Serafimovski et al., 2005). Therefore, it is very likely that the paddy soil in this area displays raised levels of heavy metals.

In this context, the present paper comprises the following:

(a) the determination of the total heavy metal concentrations in paddy soil samples from sampling points in Kočani Field;
(b) an application of the sequential extraction method (leaching procedure) for the definition of available fractions in soil samples from the Kočani Field;
(c) the estimation of the heavy metal distribution and mobility characteristics in the investigated soil samples and
(d) environmental risk assessment.

MATERIALS AND METHODS

Study area

Kočani Field, well known for its paddy fields and thermal waters, is located in the eastern part of Macedonia, about 115 km from the capital city, Skopje. With an average length of 35 km and width of 5 km, it is situated in the valley of the Bregalnica River between the Osogovo Mountains in the north and the Plačkovica Mountains in the south (Figure 1). The paddy soil of Kočani Field was estimated to originate from the composite material of the sediment derived from igneous, metamorphic and sedimentary rocks transported by the Bregalnica River and its tributaries and deposited in the Kočani depression (DOLENEC et al., 2007).

The broader region has a long history of mining dating to the pre-Middle Ages, with the most recent phase of mining starting after the Second World War. The mining activities, the abandoned old mine sites and bare tailings, the large amounts of untreated waste material as well as the effluents from the Pb-Zn Zletovo and Sasa mines induced the expansion of heavy metal loads across the entire region. The acid mine waters and the untreated effluents from the ore-processing facilities and the tailings were discharged into the Zletovska and Bregalnica Rivers, which were used for the irrigation of paddy fields and therefore represented a further pollution source that could seriously affect the soil as well as the food and feed crops of Kočani Field.

Soil sampling and analysis

The sampling of the soil was carried out in autumn 2005 in order to investigate the distribution and concentrations of the potentially toxic heavy metals, including As, Cd, Cu, Pb and Zn, related to the base-metal mining activities of the region. The soil was sampled from 5 locations across the Kočani paddy fields. The sampling locations of the study area are shown in Figure 2. Near-surface soils were collected, because it is not possible to distinguish the A, B and C horizons in the agricultural soil. Each soil sample was made up of a composite of 5 sub-samples taken from within a 1 m × 1 m square. After air-drying at 25 °C for a week, the soil samples were disaggregated, sieved to 2 mm and then ground in a mechanical agate grinder to a fine powder (< 63 μm) for subsequent geochemical analysis.

All the paddy soil samples were analysed for their As, Cd, Cu, Pb and Zn concentrations in a certified commercial Canadian laboratory (Acme Analytical Laboratories, Ltd.) after extraction for 1 h with 2-2-2-HCl-HNO_3-H_2O at 95 °C by inductively coupled plasma mass spectrometry (ICP-MS). The accuracy and precision of the soil analyses were assessed by using international reference material such as CCRMR SO-1 (soil) and USGS G-1 (granite). The analytical precision and the

Figure 1. Map of the study area, Kočani Field
Slika 1. Geografska karta Kočanskega polja

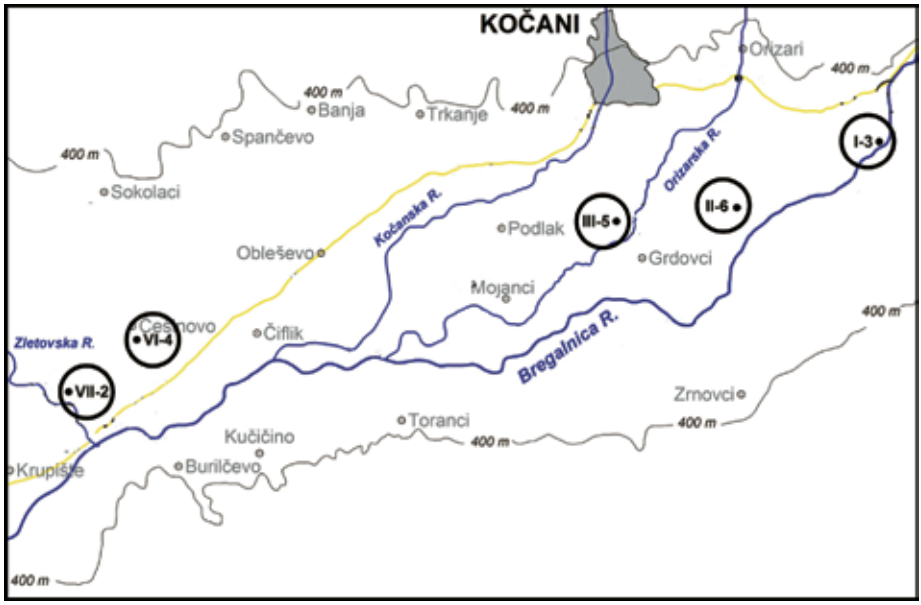

Figure 2. Sampling locations map of the study area
Slika 2. Geografski položaj vzorčnih točk

accuracy were better than ± 5 % for the analysed elements.

Sequential extraction procedure

Selected soil samples were also analysed for the chemical partitioning of As, Cd, Cu, Pb and Zn using a sequential chemical extraction method (LI et al., 1995; TESSIER et al., 1979). The soil samples weighing 1 g were placed in screw-top test tubes. To the sample was added 10 mL of leaching solution, the caps were screwed on and the tubes were subjected to the appropriate extraction procedure depending on the stage of the leach. For sequential leaching, the sample was leached, centrifuged, decanted, washed and then the residue was leached again, in a process of 5 steps from the weakest to the strongest solution. The sequential extraction procedure of heavy metals is precisely described in Table 1.

After sequential extraction, the sample solutions were analysed by a Perkin Elan 6000 ICP-MS for the determination of 60 or more elements. QA/QC protocol incorporated a sample duplicate to monitor the analytical precision, a reagent blanks measured background and an aliquot of an in-house reference material to monitor accuracy.

RESULTS AND DISCUSSION

Heavy metal concentration

The total concentrations of heavy metals (As, Cd, Cu, Pb and Zn) in the paddy soil samples from Kočani Field together with the assumed permissible level of heavy metals adopted by the National Environmental Protection Agency of Slovenia (Uradni list RS 1996) and the maximum allowable concentrations (MAC) of trace elements in agricultural soil proposed by the German Federal Ministry of Environment (1992) as well as the critical soil total heavy metal concentration ranges given by KABATA-PENDIAS & PENDIAS (1984) are presented in Table 2. The critical total soil heavy metal concentration is defined as the range of values above which toxicity is considered to be possible.

The data clearly show that the paddy soil samples from locations I-3, II-6, III-5 and VI-4 contain slightly increased heavy metal concentrations but the paddy soil sample from section VII-2 in the vicinity of the Zletovska River is highly impacted with As, Cd, Cu, Pb and Zn. The concentration values in paddy soil sample VII-2 strongly exceeded the limit emission values reported by KABATA-PENDIAS AND PENDIAS (1984) and the national environmental protection agencies of Slovenia and Germany (Table 2).

Arsenic (As)

An elevated concentration of As (42.0 mg/kg) was detected in the paddy soil sample from section VII-2, which significantly exceeded the limit value of 20 mg/kg reported by the Environmental Protection Agency of Slovenia (Table 2).

Cadmium (Cd)

An increased Cd concentration (5.6 mg/kg) was determined in the paddy soil sample from location VII-2. The limit emission value for Cu concentrations in soils reported by the environmental protection agencies of Slovenia is 1 mg/kg and of Germany is 1.5 mg/kg (Table 2).

Copper (Cu)

A high concentration of Cu (99 mg/kg) found in the paddy soil sample from sam-

Table 1. Sequential extraction of heavy metals
Tabela 1. Postopek zaporednega izluževanja težkih kovin

Step	Fraction	Chemical reagents
1	water soluble	distilled water
2	exchangeable and carbonate bound	1 M ammonium acetate
3	organic (oxidizable)	0.1 M sodium pyrophosphate
4	reducible	cold 0.1 M hydroxylamine hydrochloride
5	reducible plus residual	hot 0.25 M hydroxylamine hydrochloride

Table 2. Total elemental concentrations in the paddy soil samples of Kočani Field: **1**) critical soil total concentration ranges given by Kabata-Pendias & Pendias (1984); **2**) limits for elemental concentrations in soil (Environmental Protection Agency of Slovenia (Uradni list RS 1996); **3**) maximum allowable concentrations (MAC) of trace elements in agricultural soils proposed by the German Federal Ministry of the Environment (1992)
Tabela 2. Celotne koncentracije elementov v vzorcih tal riževih polj: **1**) kritične koncentracije težkih kovin v tleh, Kabata-Pendias & Pendias (1984); **2**) mejne vrednosti težkih kovin v tleh (Agencija za okolje in prostor, Slovenija (Uradni list RS 1996)); **3**) maksimalne dovoljene vrednosti slednih elementov v agrikulturnih tleh (Nemško zvezno ministrstvo za okolje, 1992)

Concentration	c(As)/(mg/kg)	c(Cd)/(mg/kg)	c(Cu)/(mg/kg)	c(Pb)/(mg/kg)	c(Zn)/(mg/kg)
Location					
I-3	18.7	0.5	40	81	162
II-6	11.8	0.3	26	32	100
III-5	8.3	0.2	33	24	102
VI-4	9.9	0.3	29	41	105
VII-2	42.0	5.6	99	892	1134
1	-	3-8	60–125	100–400	70–400
2	20	1	60	85	200
3	-	1.5	60	100	200

pling site VII-2 exceeded the limit emission value of 60 mg/kg, suggested by the environmental protection agencies of Slovenia and Germany (Table 2).

Lead (Pb)

The highest Pb concentration (892 mg/kg) was noticed in the paddy soil sample from section VII-2 and it is above the limits provided by the environmental protection agencies of Slovenia and Germany (85 mg/kg and 100 mg/kg) and the limit values by Kabata-Pendias & Pendias (1984), (100–400 mg/kg) (Table 2).

Zinc (Zn)

A very elevated concentration of Zn (1134 mg/kg) highly exceeding all the limit values (200 mg/kg and 70–400 mg/kg, Table 2) was found in the paddy soil sample from section VII-2.

All the studied heavy metals are important ore-forming elements and are paragenetically related to the Pb-Zn polymetalic mineralization of the Zletovo-Kratovo ore district (Zletovo mine) predominately drained by the Zletovska River (Dolenec et al., 2007). However, in the case of the paddy

soil sample from sampling location VII-2 in the vicinity of the Zletovska River and Zletovo mine, it is clear that the continued mining activities producing enormous untreated mining wastes from Zletovo mine are the main source of As, Cd, Cu, Pb and Zn contamination.

Sequential extraction (heavy metal binding forms)

The highly stable forms contained in the residual are unlikely to be released under weathering conditions. On the other hand, soluble, exchangeable and chelated fractions are quite labile and hence more accessible to plants and the food chain (KABATA-PENDIAS, 1993). In the applied sequential extraction procedure, the labile/residual fractions considered were: water soluble (1), exchangeable and bound to carbonates fraction (2), bound to organic matter – oxidizable fraction (3), bound to amorphous Mn hydroxide – reducible fraction (4) and bound to amorphous Fe hydroxide and crystalline Mn hydroxide – reducible and residual fraction (5).

The water soluble fraction includes highly mobile and hence potentially available metal species. The exchangeable fraction contains weakly bound (electrostatically) heavy metal species, that can be released by ion-exchange with cations such as Ca^{2+}, Mg^{2+} or NH_4^+. Metals in the exchangeable fraction are also very available for plant uptake and therefore the most labile. The oxidizable fraction releases under oxidizing conditions metals linked to organic matter within the soil matrix into solution. The reducible fraction provides unstable metal forms connected with amorphous Mn hydroxides, which are easily discharged and approachable by the surrounding biota under reducing conditions. In the reducible plus residual fraction, the metals are bound to amorphous Fe hydroxides (reducible part) and under reducing conditions they are expected to be released into nature. The residual includes naturally occurring crystalline Mn hydroxide minerals, which may hold heavy metals within their cristalline matrix. Thus, heavy metals are not likely to be discharged under normal environmental conditions (DEAN, 2007; FILGUEIRAS et al., 2002; FUENTES et al., 2004; KAZI et al., 2002). Figure 3 displays the results of the sequential extraction procedure (heavy metal binding forms).

Arsenic (As)

A significant fraction of As in the paddy soil samples from all five sampling locations was present in the reducible plus residual fraction (5) and the oxidizable fraction (3) (Figure 3A). The highest proportion of As in the reducible plus residual fraction was found in the paddy soil sample from location VII-2 (64 %) and the highest part of As in the oxidizable fraction was extracted from the paddy soil sample from sampling site III-5 (42.45 %).

Cadmium (Cd)

Figure 3B shows that Cd from all the paddy soil samples was strongly associated with the exchangeable phase (2), closely followed by the reduction phase (4). The highest share of Cd in the exchangeable phase was detected in paddy soil samples from sites I-3 (49.21 %) and VI-4 (47 %). The dominant part of Cd in the reduction phase was found in the paddy soil sample from section III-5 (68 %).

Copper (Cu)

Cu in all the paddy soil samples (Figure 3C) was almost entirely connected with

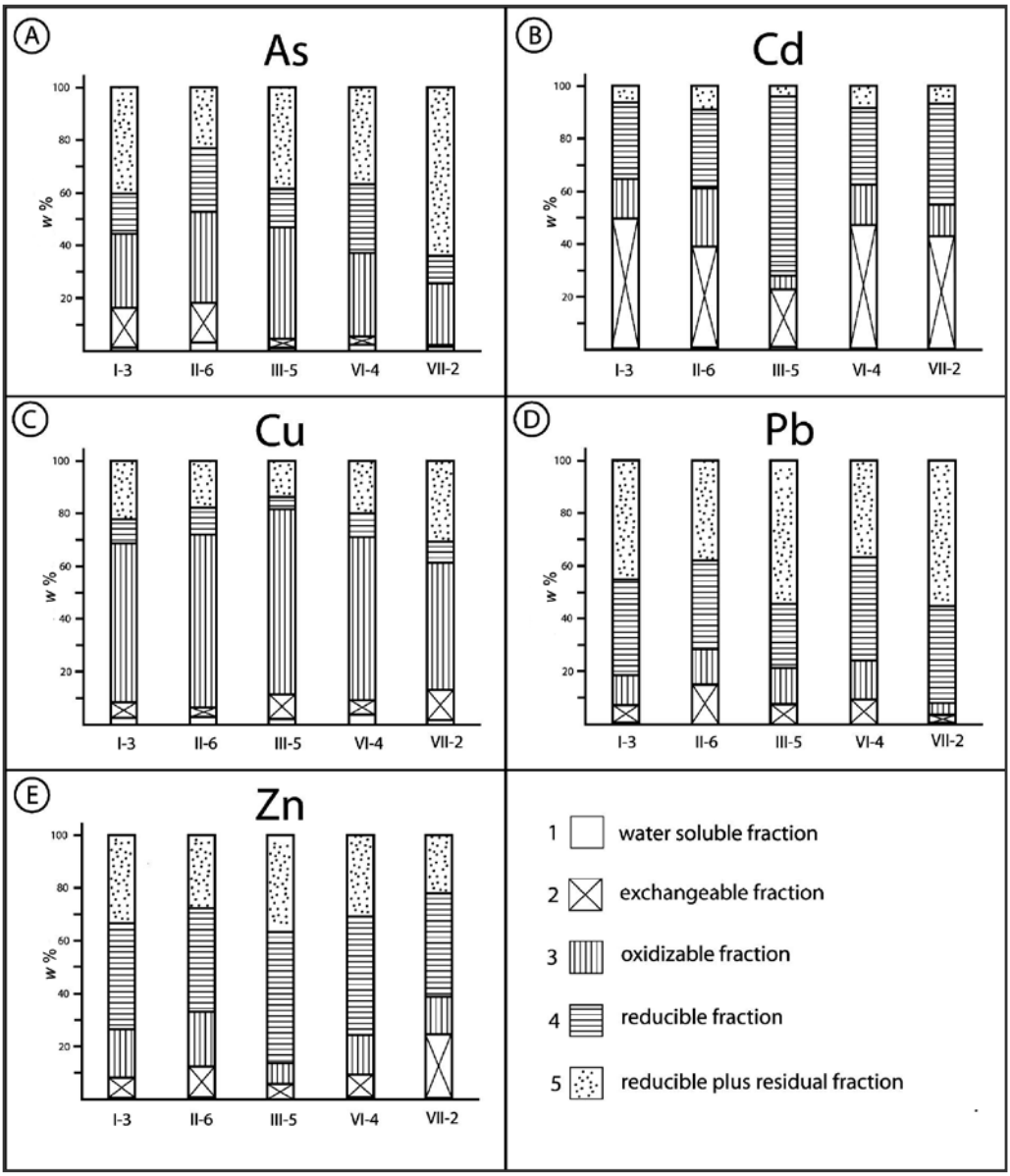

Figure 3. Heavy metal binding forms in paddy soil samples from different locations

Slika 3. Vezava težkih kovin v vzorcih tal riževih polj iz izbranih lokacij

the oxidizable fraction (3). The highest part of Cu in the oxidizable fraction was extracted from the soil sample from section III-5 (70 %).

Lead (Pb)

In the paddy soil samples, a large part of Pb (Figure 3D) was bound to the reducible plus residual fraction (5) and the second most important fraction was the reducible phase (4). The highest amount of Pb in the reducible plus residual fraction was in the paddy soil sample from sampling site III-5 (54.46 %) and the highest share of Pb in the reducible phase was found in the paddy soil sample from section VI-4 (38.96 %).

Zinc (Zn)

The chemical partitioning of the Zn (Figure 3E) in the investigated paddy soil samples displayed that Zn was mainly associated with the reducible fraction (4) and weakly with the reducible plus residual fraction (5). The highest amount of Zn in phases (4) and (5) was determined in the soil sample from location III-5 (49.19 % and 36.9 %).

The most exchangeable, highly mobile and readily available element to biota in the surrounding ecosystems in all the paddy soil samples is Cd, closely followed by Pb and Zn, mainly bound to amorphous Fe and Mn hydroxides in the reducible fraction. Pb and Zn are thus under reduction conditions thermodynamically very unstable and available to plants. Cu is dominantly linked to organic matter and under oxidizing conditions is potentially released into the environment. As is also weakly bound to organic matter. However, in larger proportions, As is connected to amorphous Fe hydroxides, which are to some extent leachable and thus potentially bioavailable and furthermore to potentially the least harmful, non-mobile residual fraction (crystalline Mn hydroxides). Consequently, the mobility characteristics and potential of heavy metals in the investigated paddy soil samples increases from As–Pb–Zn–Cu–Cd.

In general, a high proportion of heavy metals in the non-residual fractions of all the paddy soil samples may suggest a greater contribution of anthropogenic metals. From the environmental and utilization point of view, it is notable that the paddy soil sample from location VII-2 near the Zletovska River and Zletovo mine, which had highly elevated heavy metal concentrations exceeding the limits proposed by the environmental agencies and KABATA-PENDIAS & PENDIAS, (1984) and introduced heavy metal mobility characteristics, represents a serious potential risk for the surrounding ecosystems.

To assess the possible health risk, more detailed studies on heavy metal contamination in agricultural soils, irrigation and drinking water, rice and other edible crops as well as a dietary study of the local population are needed.

CONCLUSIONS

The present study examined the distribution of heavy metals (As, Cd, Cu, Pb and Zn) in paddy soil samples from Kočani Field, Macedonia. The heavy metal concentrations were determined by ICP-EAS analysis and heavy metal binding was defined with the sequential extraction procedure.

The results showed that the paddy soil sample (section VII-2) from the western

part of Kočani Field in the vicinity of the Zletovska River exhibited very elevated concentrations of As, Cd, Cu, Pb and Zn, which significantly exceed the limits proposed by the Slovenian and German environmental agencies and critical soil total concentration ranges given by Kabata-Pendias & Pendias (1984). The elevated concentrations of As, Cd, Cu, Pb and Zn in paddy soil sample VII-2 undoubtedly indicate heavy metal contamination related to mining activities and acid mine drainage impacted on the riverine water, which is used by local farmers for irrigation purposes.

The most exchangeable, labile and available element for plant uptake and furthermore for the possible contamination of the surrounding ecosystem in all the paddy soil samples is Cd, closely followed by Pb and Zn. Elements Pb and Zn are mainly linked to amorphous Mn hydroxides and amorphous Fe hydroxides in the reducible fraction and thus under reduction conditions are very unstable and mobile. Cu is dominantly bound to organic matter and consequently released under oxidizing conditions into the environment. As is also weakly bound to organic matter. However, in larger proportions, As is connected to amorphous Fe hydroxides, which are usually released from the soil and more crystalline Mn hydroxides, which are not expected to escape under normal environmental conditions. The mobility potential of heavy metals in the investigated paddy soil samples increases from As–Pb–Zn–Cu–Cd.

It was found out that the paddy soil sample from location VII-2, with highly elevated heavy metal concentrations and the revealed mobility characteristics of heavy metals As, Cd, Cu, Pb and Zn, represents a serious environmental potential risk for the surrounding ecosystems.

To assess the possible health risk, more detailed studies on heavy metal contamination in the surrounding ecosystems as well as a dietary study of the local population are needed.

Povzetek

Izkoriščanje nahajališč kovinskih mineralnih surovin in predelava rude sta pomemben vir onesnaženja okolja s težkimi kovinami. Rudarjenje, drobljenje in mletje rude skupaj z odlagališči jalovine in odpadkov predelave je očiten vir onesnaženja. Povišane vsebnosti težkih kovin, ki izhajajo iz rudnikov kovin, so zabeležene na območju rudnikov in v njihovi širši okolici, v okolnih tleh, pridelkih, rečnih in podzemnih vodah ter rečnih sedimentih, kamor migrirajo zaradi dispergiranja in odlaganja rudniškega odpadnega materiala. Posledica tega onesnaženja so velike površine onesnažene pridelovalne površine. Posebno pozornost smo namenili predvsem koncentraciji težkih kovin v pridelovalnih tleh, saj preko užitnih rastlin in prehrambene verige lahko vstopajo v živalski in človeški organizem.

V študiji smo raziskovali razporeditev težkih kovin (As, Cd, Cu, Pb in Zn) v vzorcih tal riževih polj (Kočansko polje, Makedonija) z uporabo ICP-EAS in postopka zaporednega izluževanja. V vzorcu iz lokacije VII-2, ki se nahaja blizu reke Zletovske v zahodnem delu Kočanskega polja, smo našli zelo visoke koncentracije As (42 mg/kg), Cd (5,6 mg/kg), Cu (99 mg/kg), Pb (892 mg/kg) in Zn (1134 mg/kg).

Visoke koncentracije težkih kovin so bile v vzorcu VII-2 zato, ker reka Zletovska odvaja neprečiščene odplake in odpadke z območja rudnika Pb-Zn Zletovo, kmetje pa jo uporabljajo za namakanje okolišnih riževih polj. V raziskovanih vzorcih narašča potencial mobilnosti v naslednjem zaporedju: As–Pb–Zn–Cu–Cd. Na podlagi zelo visokih koncentracij in izluževalnih lastnosti težkih kovin, prisotnih v vzorcu VII-2, smo ugotovili, da pomeni območje okoli imenovanega vzorca resno ekološko grožnjo bližnjim ekosistemom.

References

Adriano, D. C. (1986): Trace Elements in the Terrestrial Environment. New York, *Springer-Verlag*.

Dean, J. R. (2007): Bioavailability, Bioaccessibility and Mobility of Environmental Contaminants. *John Wiley and Sons Ltd*, England, 292 p, pp. 92–106.

Dolenec, T., Serafimovski, T., Tasev, G., Dobnikar, M., Dolenec, M. & Rogan, N. (2007): Major and trace elements in paddy soil contaminated by Pb–Zn mining: a case study of Kočani Field, Macedonia. *Environmental Geochemistry and Health*; 29, pp. 21–32.

Filgueiras, A. V., Lavilla, I., Bendicho, C. (2002): Chemical sequential extraction for metal partitioning in environmental solid samples. *J. Environ. Monit*; 4, pp. 823–857.

Fuentes, A., Lorens, M., Saez, J., Soler, M., Ortuno, J., Meseguer, V. (2004): Simple and sequential extraction of heavy metals from different sewage sludges. *Chemosphere*; 54, pp. 1039–1047.

Jung, M. C. (2001): Heavy metal contamination of soils and waters in and around the Imcheon Au-Ag mine, Korea. *Applied Geochemistry*; 16, pp. 1369–1375.

Kabata-Pendias, A. (1993): Behaviour properties of trave metals in soils. *Applied Geochemistry*; 2, pp. 3–9.

Kabata Pendias, A. & Pendias H. (1984): Trace elements in Soils and Plants. *CRC Press*; Boca Raton, FL.

Kazi, T., Jamali, G., Kazi, G., Arain, M., Afridi, H., Siddiqui, A. (2002): Evaluating the mobility of toxic metals in untreated industrial wastewater sludge using a BCR sequential procedure and a leaching test. *Anal. Bioanal. Chem.*; 374, pp. 255–261.

Korre, A., Durucan, S. & Koutroumani, A. (2002): Quantitative-spatial assessment of the risks associated with high Pb loads in soils around Lavrio, Greece. *Applied Geochemistry*; 17, pp. 1029–1045.

Lee, C. G., Chon, H. T. & Jung, M. C. (2001): Heavy metal contamination in the vicinity of the Daduk Au-Ag-Pb-Zn mine in Korea. *Applied Geochemistry*; 16, pp. 1377–1386.

Li, X. D., Coles, B. J., Ramsey, M. H., Thornton, I. (1995): Sequential extraction of soils for multielement analysis by ICP-AES. *Chemical Geology*; 124, pp. 109–123.

Liu, H., Probst, A. & Liao, B. (2005): Metal

contamination of soils and crops affected by the Chenzhou lead/ zinc mine spill (Hunan, China). *Science of the Total Environment*; 339, pp. 153–166.

Lu, X. & Zhang, X. (2005): Environmental geochemistry study of arsenic in Western Hunan mining area, P.R. China. *Environmental Geochemistry and Health*; 27, pp. 313–320.

Manceau, A., Lanson, B., Schlegel, M. L., Harge, J. C., Musso, M., Eybert-Berard, L., Hazemann, J. L., Chateigner, D. & Lamble, G.M. (2000): Quantitative Zn speciation in smelter-contamintaed soils by EXAFS spectroscopy. *Am. J. Sci*; 300, pp. 289–343.

McBride, M. B. (1999): Chemisorption and precipitation reactions. p. B265-B302. *In* M.E. Sumner (ed.) *Handbook of soil science*; CRC Press, Boca Raton, FL.

McBride, M. B., Sauve, S. & Hendershot, W. (1997): Solubility control of Cu, Zn, Cd and Pb in contaminated soils. *Eur. J. Soil Sci*.; 48, pp. 337–346.

Morin, G., Ostergren, J. D., Juillot, F., Ildefonse, P., Calas G., & Brown, Jr. G. E. (1999): XAFS determination of the chemical form of lead in smelter-contaminated soils and mine tailings: Importance of adsorption processes. *Am. Mineral*;. 84, pp.420–434.

Serafimovski, T. & Aleksandrov, M. (Eds.) (1995): Lead and zinc deposits and occurences in the Republic of Macedonia. *Special edition of RGF*, No. 4, 387 pgs., with extended summary in English, Stip.

Simmons, R. W., Pongsakul, P., Saiyasitpanich, D. & Klinphoklap, S. (2005): Elevated Levels of Cadmium and Zinc in Paddy Soils and Elevated Levels of Cadmium in Rice Grain Downstream of a Zinc Mineralized Area in Thailand: Implications for Public Health. *Environmental Geochemistry and Health*, 27, pp. 501–511.

Tack, F. M. G & Verloo, M. G. (1995): Int. J. Environ. *Anal. Chem*., pp. 59–225.

Tessier, A., Campbell P. G. C. & Bisson, M. (1979): Sequential extraction procedure for the spetiation of particulate trace metals. *Analytical Chemistry*, 51, pp. 844–851.

Applicability of User Defined Functions in Mine Surveying

Aleksandar Ganić[1], Dragan Đorđević[1], Branko Leković[1]

[1]University of Belgrade, Faculty of Mining and Geology, Djušina 7, 11000 Belgrade, Serbia;
E-mail: aganic@rgf.bg.ac.yu, dragand@rgf.bg.ac.yu, blekovic@rgf.bg.ac.yu

Received: November 7, 2008 **Accepted:** December 8, 2008

Abstract: MS Excel is one of the most popular programs for tabular calculations. As such, it is widely applicable in mine surveying. This work shows the possibilities for creation and usage of the User Defined Functions (UDF), which can replace classic forms, but also the possibility to transfer, by using of those functions, data from Excel into the AutoCAD.

Key words: Mine Surveying, MS Excel, Visual Basic for Applications (VBA), User Defined Function (UDF)

Introduction

As we know, Excel is a program, which is a part of Microsoft Office package. It is one of the most applied programs and one of the most popular programs for tabular calculations. However, apart from processing numerical data, Excel is also very useful for the creation of charts, organization of table lists, automation of complex tasks, as well as for the data import from other programs (Walkenbach, 2003). This all is responsible that Excel is widely applied in mining surveys, both scientific and engineer discipline, which is, apart from performance of appropriate surveys, based also on the large number of calculations of various complexity.

Excel and calculations in mining surveys

Mine surveying are a specific segment of mining science and technique. If we would like to define them in simple terms, then this is a discipline by which necessary surveys, calculations and display of recorded mine areas and facilities on digital plans or in the form of digital terrain model are to be performed. In view of the large number of calculations of various size and complexity, the application of Excel in this stage of mining and surveying works is very significant.

During the earlier period of computation technique (logarithmic tables and pocket calculators), necessary calculations were, for the reason of uniformity, easy reference and reduction of computation errors, performed on appropriate printed patterns – forms. Those forms are being in use today, as well, however, on a much lesser scale.

Excel has got a large number of already made functions, which are divided into nine categories (database functions, date and time functions, financial functions, information functions, logical functions, lookup and reference functions, math and

Original scientific paper

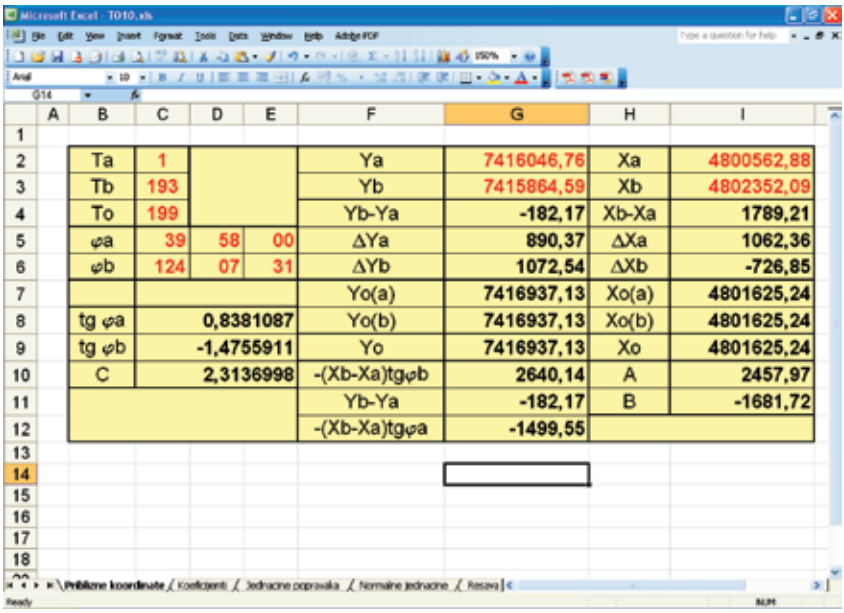

Ta	1			Ya	7416046,76	Xa	4800562,88
Tb	193			Yb	7415864,59	Xb	4802352,09
To	199			Yb-Ya	-182,17	Xb-Xa	1789,21
φa	39	58	00	ΔYa	890,37	ΔXa	1062,36
φb	124	07	31	ΔYb	1072,54	ΔXb	-726,85
				Yo(a)	7416937,13	Xo(a)	4801625,24
tg φa	0,8381087			Yo(b)	7416937,13	Xo(b)	4801625,24
tg φb	-1,4755911			Yo	7416937,13	Xo	4801625,24
C	2,3136998			-(Xb-Xa)tgφb	2640,14	A	2457,97
				Yb-Ya	-182,17	B	-1681,72
				-(Xb-Xa)tgφa	-1499,55		

Figure 1. First page of trigonometry form number 10, made in Excel

trig functions, statistical functions, text functions), which enable wide application of this program for various fields.

Thanks to these functions, above all regarding the categories math and trig functions and statistical functions, practically all calculations to be performed within mine surveying, regardless of their complexity, can be performed in Excel. If we add wide possibilities in organizing and formatting of worksheets, it is no problem, at all, to organize worksheets as existing forms. In this way, visual identity of forms is maintained both while working as while printing.

Figure 1 shows how the first page of the form number 10 looks like in Excel, which is used to calculate temporary coordinates of unknown trigonometric points by using the method of forward cut through (Mijatović, 2006).

Basic element of each worksheet is the cell. There are 16777216 cells on one worksheet, which are distributed in 65536 rows and 256 columns (Excel 2007 has 1048576 rows marked with numbers, i.e. the number of rows and columns is limited by the memory of the computer and by the available system resources). This is so big space, that all existing forms can be put on one worksheet and yet to have large part of the cells free. However, a worksheet formatted in such a way would be inefficient and not economical (imagine scrolling or jumping on a worksheet such like that while searching the appropriate form).

This can be resolved by adding and formatting new worksheets within one worksheet, or by formatting new worksheets. Figure 1 shows several of totally seven worksheets, that are used to perform the complete alignment of coordinates of one trigonometric point, as well as the assessment of accuracy of the survey results and coordinates of the unknown point, on the model of the form number 10.

By acknowledging the standpoint of single individuals, according to which they do not want to waste their time in order to search for the appropriate worksheet, but also by taking into account the fact that the largest number of cells is actually occupied by provisional results, which had their significance only while calculation "by hand", brings us to the other application concept of Excel at calculations in the field of mining surveys.

User Defined Functions (UDF) for the solution of classic formulas

The other concept for the solution of the problem is based on the application of macro language called Visual Basic for Applications (VBA). The VBA macro (procedure) may be either subprogram (Sub) or a function. The Result of the VBA function is a single result, and execution of those functions is made from other VBA procedures or in the manner, which is also used by the other existing functions within the Excel itself. To put it briefly, we are going to create our own User Defined Functions within the VBA (VULIĆ, BRECELJ, 2007) and (VULIĆ, DURGUTOVIĆ, 2007), which are to be used as any other existing function.

In this way, the number of the cells used is significantly being reduced, since we need only the cells with input and output data (without hiding the columns and rows where provisional calculations are made). Also, the output data, just like the input data, may be situated anywhere on the worksheet in any cell.

VBA functions, which are newly created, are stored in files with the extension *xla*. Those files are the so called Microsoft Excel VBA Add-In files, to which modules, functions or other tools are to be added, and which are created by users.

The download of those files into Excel may be performed in two ways:

- open the new, empty worksheet, select with *Save As* from the menu *File*, choose option *Microsoft Office Excel Add-In (*.xla)* and set the desired name and location;
- if the desired *xla* file already exists somewhere in the computer, the download is to be performed from the menu *Tools→ Add-Ins*.

After file download, function writing or correction of the functions already existing is to be performed in VBA editor, which is accessible from the menu *Tools→Macro→Visual Basic Editor* or by pressing key buttons *ALT-F11* (Figure 2).

The possibility of solution of particular formulas within the mining surveys will be, for the purpose of comparison, shown on the example of calculation of temporary coordinated of a trigonometric point by using the method of forward cutting. Function *TO10nap* has the following shape:

```
Function TO10nap(ya As Double, xa As Double, yb As Double, xb As Double, fiast As Integer, fiamn As Integer, fiase As Double, fibst As Integer, fibmn As Integer, fibse As Double) As Variant
        Dim fiadec As Double, fiarad As Double, fibdec As Double, fibrad As Double
        Dim a As Double, b As Double, c As Double
        Dim yoa As Double, yob As Double, yo As Double
        Dim xoa As Double, xob As Double, xo As Double
        Dim toOut(1) As Double
        Dim ro As Double
        ro = 57.29577951
```

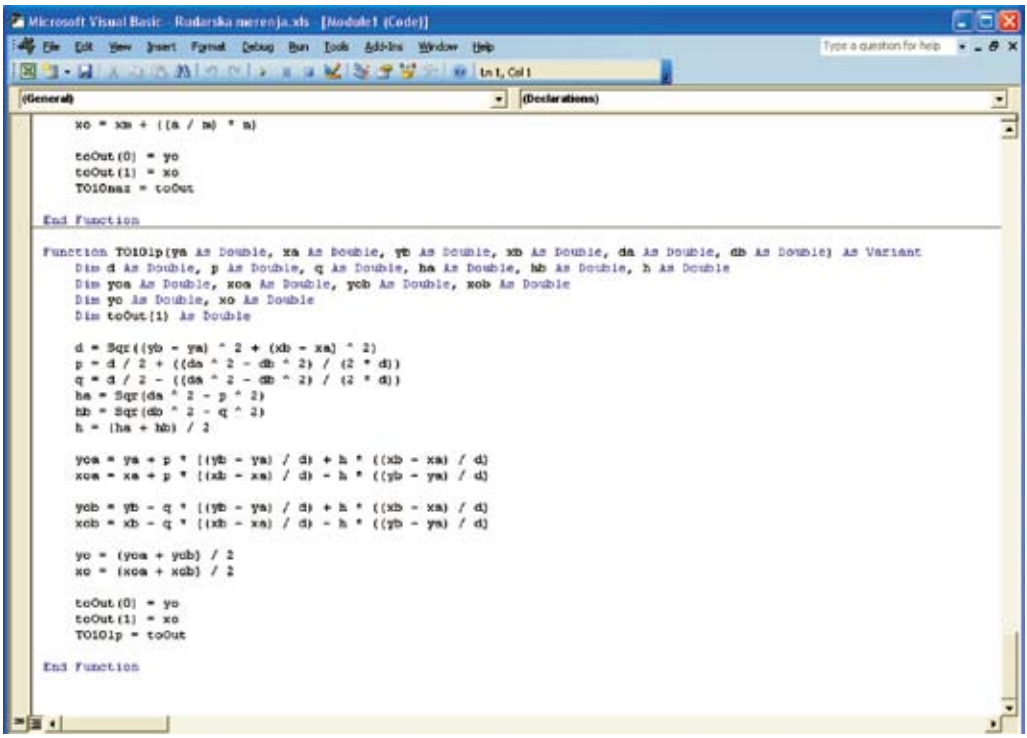

Figure 2. Preview of VBA Editor with the function TO10lp for calculation of temporary coordinates by using the method of arch cross section

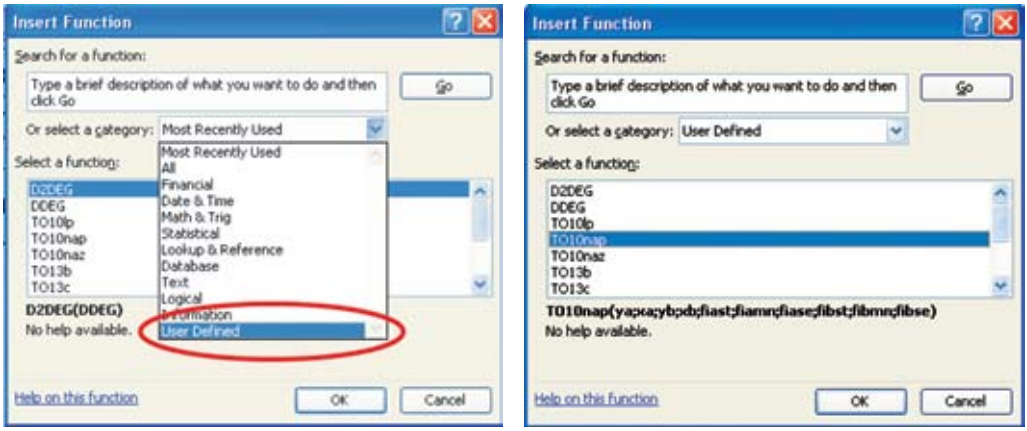

Figure 3. Download of the TO10nap function

```
        fiadec = fiast + fiamn / 60 + fiase / 3600
        fiarad = fiadec / ro
        fibdec = fibst + fibmn / 60 + fibse / 3600
        fibrad = fibdec / ro
        a = (yb - ya) - (xb - xa) * Tan(fibrad)
        b = (yb - ya) - (xb - xa) * Tan(fiarad)
        c = Tan(fiarad) - Tan(fibrad)
        yoa = ya + (a / c) * Tan(fiarad)
        yob = yb + (b / c) * Tan(fibrad)
        yo = (yoa + yob) / 2
        xoa = xa + a / c
        xob = xb + b / c
        xo = (xoa + xob) / 2
        toOut(0) = yo
        toOut(1) = xo
        TO10nap = toOut
End Function
```

The function *TO10nap* is to be requested in the same way as any other already existing Excel function. By clicking on the icon for *Insert function*, which is on the Toolbar, a window for the selection of a category, where the function can be found (newly formed category *User Defined*) appears. After this, in the next window, the selection of the function from the selected category (figure 3) is made.

Subsequently, in the next window (figure 4), the arguments of the function, i.e. worksheet cells, where those arguments are located, are entered. In this case, the coordinates y and x of the given points A and B, as well as oriented directions of given points in relation to the unknown are entered. Since the degrees, minutes and seconds of oriented directions are located within the separate cells, it is necessary, while entering arguments of this function, to locate ten cells, in which said input data are located, which is also shown by the afore mentioned procedure of this function.

As the result of those activities, the coordinates of the unknown trigonometric point (figure 5) will be obtained within previously marked cells for which we want the printout.

As partially shown by the figure 3, the procedures for calculation of temporary coordinates of trigonometric points by using the method of backward cutting *TO10naz* and by using arch cross cutting *TO10lp* (figure 2) are also written within those UDFs. Furthermore, functions for calculation of both grid bearings of sides *TO8ni* and horizontal lengths between side *TO8ni* defining points are also written. Functions, which are used to solve triangles by using sine or tangent theorem, are also made (*TO13b, TO13c, TO13gama, TO14a, TO14beta, TO14gama*). Those functions are used to calculate separate elements of triangles, and there is no connection between them in terms of obligation to maintain some order of calculation or obligation to calculate all elements. Due to the size of this function, they are not shown during work.

Data transfer from Excel into AutoCAD

As already said at the beginning, one of the main tasks of mining surveys is also to display the space or the facility recorded in form of digital cards and plans or in form of a digital terrain model. AutoCAD is a standard for the development of digital plans as well as other technical drawings, so that, in terms of mine surveyings, the idea of connecting Excel and AutoCAD

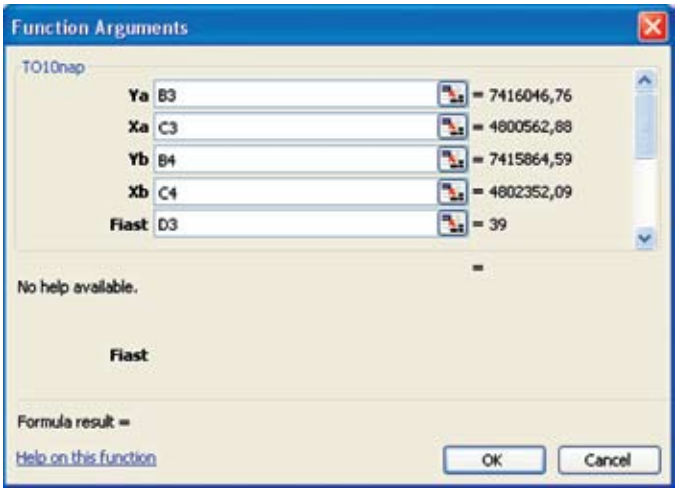

Figure 4. A part of entry of the arguments of the function TO10nap

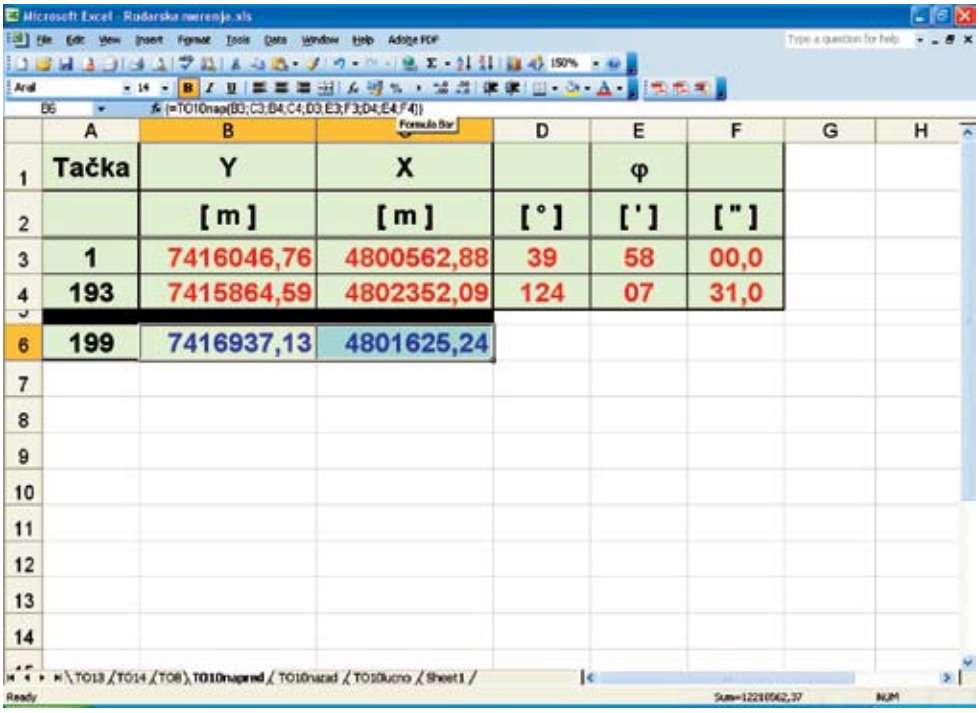

Figure 5. Preview of a worksheet, in which the function TO10nap was used

is very interesting. Our desire was to use large calculation potentials of Excel, i.e. to export those calculated data into AutoCAD.

A program called XLPoint Plus, which is intended for the plotting of large number of points by using AutoCAD and 3D model generation by using of coordinates of points in Excel can be found on the Internet. Since this program is not free to download, UDFs were written, which, by complying with the syntax of AutoCAD, group the corresponding data from cells and practically write down the AutoCAD commands in Excel (points with UDF *pointW*, lines with *lineW*, ellipses with *ellipseW*, etc) (http://www.geo.ntf.uni-lj.si/mvulic/udf/vule4acad.xla).

Subsequently, the corresponding cells – commands are copied (*Ctrl+C*), AutoCAD is being opened and, within the command line, copied commands (*Ctrl+V*) are being transferred. At the same time, copied points, lines, circles, ellipses, etc are being plotted in AutoCAD.

CONCLUSIONS

MS Excel, a program for tabular calculation, has a very significant place within mine surveying today. It is able to perform not only some auxiliary calculations, but also the complete solutions for corresponding problems, as well as complex equalizations based on matrix calculus. All of this opens the possibility for Excel to be alternative in situations where there is no corresponding application software available.

The objective of this paperwork was to show that the User Defined Functions may also be used for more complex calculations, i.e. that the use of one or several functions created in this way can replace the entire classic calculation formula. Of course, this requires that the user has a certain elementary foreknowledge in the field of programming.

Due to its size, some functions are completely shown, and some of them are only mentioned, namely those who are able to show all benefits of the UDF in the best way possible. In other words, functions replacing those so called “trigonometric formulas”, which are most frequently used in mining surveys, are shown and thus is the autonomy, simple application, but also the ability and reliability of functions created in this way is demonstrated.

This is just one of the methods to solve problems related to calculations in mine surveying. Each user shall for him/her, depending on his/her expertise, ability and the desire, define how to solve a particular problem.

At the same time, it is necessary to emphasize again, a very simple method, by which calculated values can be moved into AutoCAD and to show calculations, but also measurements, in 2D or 3D.

References

Mijatović, R. (2006): *Uglovno-dužinsko izravnanje koordinata trigonometrijske tačke primjenom softvera za tabelarno računanje.* Diplomski rad, Univerzitet u Beogradu – Rudarsko-geološki fakultet, Beograd, p. 66.

Vulić, M., Brecelj, U. (2007): Distance reduction with the use of UDF and Mathematica. *RMZ –Materials and Geoenvironment, Ljubljana*; Vol. 54, No. 2, pp. 265–286.

Vulić, M., Durgutović, A. (2007): "UDF" for volume calculation with use of "NTF" method. *RMZ –Materials and Geoenvironment, Ljubljana*; Vol. 54, No. 3, pp. 412–425.

Walkenbach, J. (2003): Microsoft Office Excel 2003 Bible. *Wiley Publishing Inc*., 897 p., Indianapolis. http://www.geo.ntf.uni-lj.si/mvulic/udf/vule4acad.xla

Analysis of seismic events at the Velenje Coal mine

Analize seizmičnih dogodkov v območju Premogovnika Velenje

Milan Medved[1], Evgen Dervarič[2], Goran Vižintin[2], Jakob Likar[2], Janez Mayer[1]

[1]Premogovnik Velenje, d. d., Partizanska 78, 3320 Velenje; Slovenia;
E-mail: milan.medved@rlv.si, janez.mayer@rlv.si
[2]University of Ljubljana, Faculty of Natural Sciences and Engineering,
Aškerčeva 12, SI-1000 Ljubljana, Slovenia; E-mail: evgen.dervaric@ntf.uni-lj.si,
goran.vizintin@guest.arnes.si, jakob.likar@ntf.uni-lj.si

Received: November 10, 2008 **Accepted:** December 8, 2008

Abstract: Complaints due to ground shaking and tremors were regularly addressed to the management of the Velenje Coal Mine. The micro-seismic monitoring system was set up on the surface in the nearby urban areas and also directly in the vicinity of mining activities. Results of these measurements were carefully analysed and openly presented to the public together with various safe vibration limit standards (national standards). The system for automatic publishing of measurements immediately after the event recorded was also set up. This resulted in a drastic reduction of complaints. Routine micro-seismic monitoring became part of the regular monitoring of mining activities as some patterns of seismic response to mass mining were revealed.

Izvleček: Na Premogovnik Velenje so se redno naslavljale pritožbe zaradi povečanega tresenja tal. Postavljen je bil mikroseizmični sistem za spremljanje tresljajev na površini, v bližnjih naseljih, pa tudi na odkopih. Rezultati meritev so bili detajlno analizirani in predstavljeni zainteresirani javnosti skupaj z raznimi standardi in predpisi za varno tresenje tal, ki veljajo v posameznih državah. Taki predpisi in standardi v slovenski regulativi ne obstajajo. Poleg tega je bil postavljen tudi sistem za avtomatsko zapisovanje podatkov o tresenju tal in objavljanje teh na spletnih straneh. Navedeno je imelo za posledico drastično zmanjšanje števila pritožb. Rutinske mikroseizmične nadzorne meritve tresenja tal so tako postale del obratovalnega nadzora, saj so se pokazala določena pravila pri seizmičnem odzivu okolne hribine na rudarska dela.

Key words: rockbursts, seismicity, coal mine, longwall mining, caving, Velenje, Slovenia, public response
Ključne besede: stebrni udar, seizmičnost, premogovnik, širokočelno odkopavanje, rušenje krovnine, odziv javnosti

Original scientific paper

Introduction

The Velenje coal basin has very thick layer of lignite. Modern mining technology on big excavation plates assures viability of operation despite low combustion value. The main consumer is the nearby thermo power plant.

Mine tremors and even rockbursts follow the excavation, although the geological formation is soft. Seismic monitoring systems on the surface and in the mine gave us invaluable insight into the processes that took place at the excavation.

Geology of coal deposit

The lignite seam at the Velenje Coal Mine extends under almost the entire Šaleška Valley, its deposit being 8.3 km long and 2.5 km wide.

The thickness of the coal ranges from 20 m to 160 m. The nearest coal is 60 m under the surface, in the seam, which is 10 m to 35 m thick. The greatest amount of the coal can be found at the depth of 290 m where the thickest seam has been confirmed. The coal layer is 100 m thick at the depth of 400 m. The north area of the coal seam inclines at the angle of 10° to 15°, and gradually becomes thinner in the depth from 100 m to 300 m, where in the south area it ends up abruptly at the depth of 150 m under the surface. The quality of the coal decreases from the hanging wall to the footwall of the seam. The lower calorific value for the coal seam still being exploited is down to 7.5 MJ/kg. The longitudinal section of the coal seam is shown in Figure 1.

River and lake alluvia consisting of sand and clay, whose thickness totals 460 m at the most, represent the hanging wall of the seam. Immediately above the coal seam

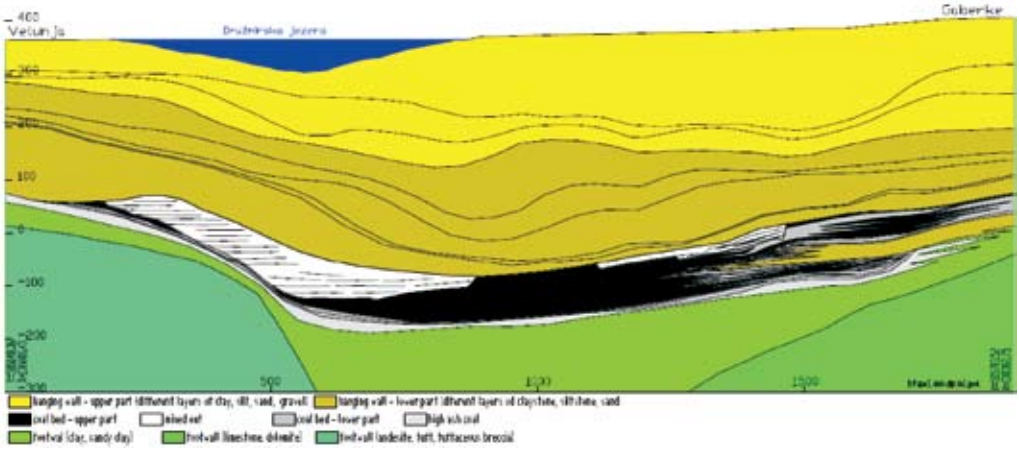

Figure 1. Longitudinal section of the coal seam (geomechanical interpretation)
Slika 1. Vzdolžni prerez skozi sloj premoga (geomehanski profil)

Table 1. Geomechanical properties of different layers
Tabela 1. Geomehanske lastnosti različnih slojev

	Density (kN/m^3)	Moisture content (%)	Uniaxial compressive strength (MPa)	Tensile strength (MPa)	Young modulus (MPa)	Poisson modulus (/)	Cohesion (MPa)	Friction angle (°)
Hanging wall – upper part	20.9	24.4	0.85	0.08	140	0.35	0.4	15
Hanging wall – lower part	19.2	32.6	2.5	0.23	430	0.2	0.7	17
Coal bed upper part	12.6	39	8.4	0.92	480	0.25	0.7	30
Coal bed – lower part	13.6	35	5.4	0.59	480	0.3	0.7	30
High ash coal	17.7	25.6	1.6	0.17	375	0.35	-	-
Footwall	23.6	10	4.9	0.44	2917	0.3	1.4	21.6

there are clay layers ranging from a few hundred meters to minimum of six meters. They prevent water inflow into haulages.
The footwall of the seam consists of clay and marl lying on triassic limestone and dolomites. In a hydrological sense, the depression is extremely water bearing, especially in the Pliocene area.
The coal seam, in whose hanging wall and footwall most roadways can be found, is tectonically not much cracked, and the fractures caused by sinking of the seam are mostly of local character.
The whole formation is soft with low values of geomechanical properties. Brittle failure of coal can be expected based on experiences with laboratory compressive strength tests. Geomechanical properties are collected[11] in Table 1.

MINING METHOD

The mining method used in Velenje Coal Mine is known as Velenje Mining Method and is unique in world mining technology. The basic principle of work on the faces was based on winning the lower and the upper excavation part of the face at the floor level height of 10–15 m.
The cracking of roof influences considerably further mining. The first floor level advances only with the lower excavation part, and crushes the hanging wall and the coal to the extent that efficient excavation from the upper area is made possible with the following floor level.
With the Velenje mining method the length of longwalls amounts from 80 m to 210 m and the length of panels varies from 600

m to 800 m. Maximum face inclination in the direction of advancing totals 15° and 7° inclined along the face.

Technological coal mining procedure is divided into:

- winning the lower excavation section of the coalface and
- winning the upper excavation section of the coalface.

The double-drum shearer excavates the coal in the lower section of the longwall face.

The coal in the upper section of the face is excavated by winning the coal through the gate in the shield, or over the canopy of the shield of the section.

Working cycle is completed when all the coal from the upper excavation part is extracted. The coal from the upper excavation part is mined systematically after a certain number of cuttings in the lower part. The number of cuttings in the cycle depends on:

- working height,
- coal face length,
- slope and inclination of the face,
- number of sectors in the upper excavation section along the face and
- degree of coal crushing in the upper excavation section of the coalface.

The sequence of working phases is changed with regard to what was stated above. They can also be carried out simultaneously, in case of favorable conditions.

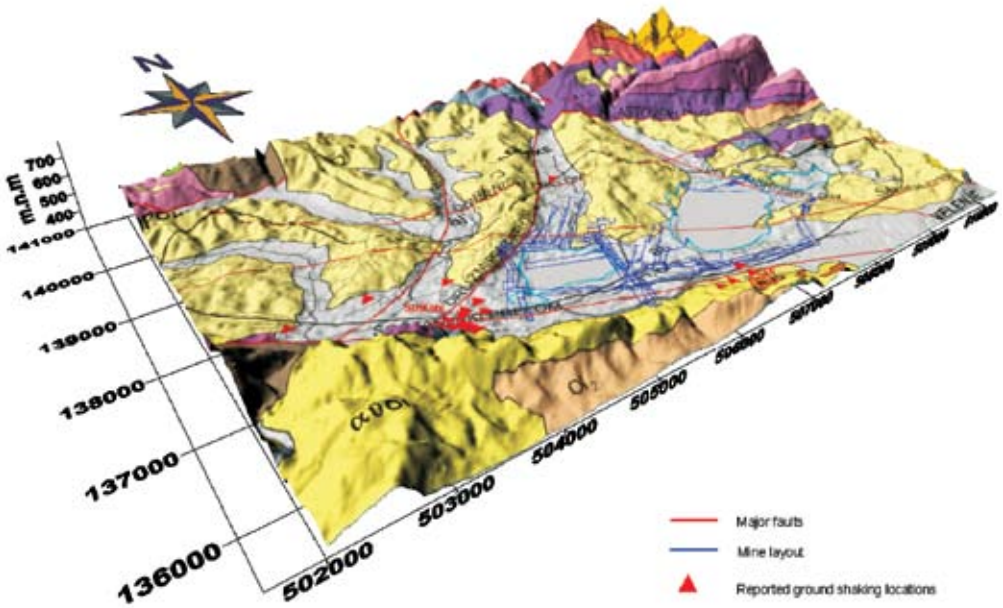

Figure 2. Reported locations of seismic events
Slika 2. Prijavljene lokacije tresenja tal

TREMORS AND MINING

Tremors regulary accompany longwall mining. They are felt by local inhabitants of the nearby town of Šoštanj and village Pesje which is only few hundred meters away measured in horizontal distance from longwall faces (Figure 2). Most of the tremors that were felt by local inhabitants were not observed in the mine and also did not cause any damage to the mine infrastructure. But the local community has organized and started strong media campaign against the mine authorities, which was from time to time very disagreeable. Regularly new minor superficial cracks were reported to the mine and damage compensation was claimed. After careful examination of reported damages it was found out that cracks were not to ascribe to tremors and were rather ascribed to other causes like uneven settlements of foundation, changes in humidity and constructional reasons.

It was very difficult to explain to local inhabitants that these cracks were not caused by mining. The approach to the problem was very systematical. First we started to collect public response on a toll free phone line, where every caller was asked to report the location of event felt and the description of event. Then all locations were summarized and plotted on a map with relation to the mine layout. In the centre of the areas with greater density of complaints – in area of Šoštanj and Pesje - ground vibration monitors were installed. The system is trigger based. The trigger is set to 0.1mm/s which is about 5 times less than the human sensitivity to ground vibrations. This means that we make sure that we do not miss an event which can be felt by local inhabitants.

RESULTS OF MICRO SEISMIC MONITORING

The results of measurements soon revealed that at most seismic active days three to five seismic events were recorded with maximum peak particle velocities from 2–3 mm/s at frequencies of 7–10 Hz. Typically recorded values were from 0.7 mm/s to 1.1 mm/s at same frequencies. So most of the tremors were weak which could not cause any damage to the buildings.

When the results were presented to the public, lot of skepticism and disbelief among local inhabitants was present. Up to date measurements were collected for period of more than one year and sent to independent and internationally acknowledged blasting techniques and vibration expert. In his "Experts opinion" it was officially confirmed, that damage due to vibration in terms of a reduction in utility values is unlikely to have occurred. The vibrations at recorded levels were not able to damage buildings in a causal manner according to standard DIN 4150[2]. However already existing damages could change. If damages are found, it is to be assumed that other causes are responsible for this damage.

We openly presented the conclusions from "Experts opinion" and analyzed measurements to the public. In the meantime we also set up a system for automatic measurements and publishing of results on company's web pages – which was the most convincing proof that we are ready to assist local inhabitants with information. In the first months we received lots of calls immediately after the tremor from people asking where the results of measurements could be seen. So instead of complaint calls we are now receiving calls from people who

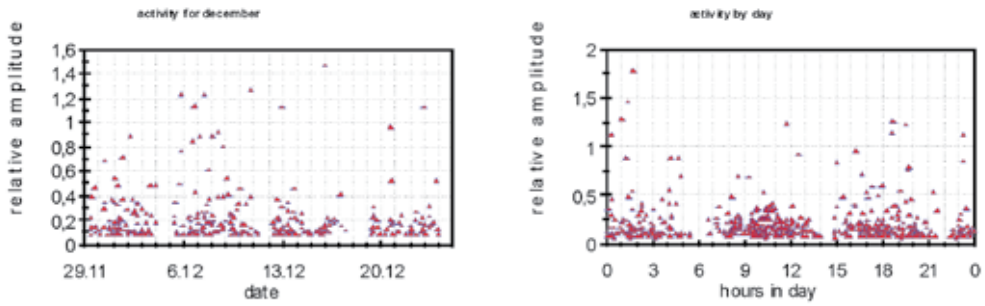

Figure 3. Activity for December 2004 (a) and its display by hours in day (b)
Slika 3. Aktivnost decembra 2004 (a) in prikaz po urah (b)

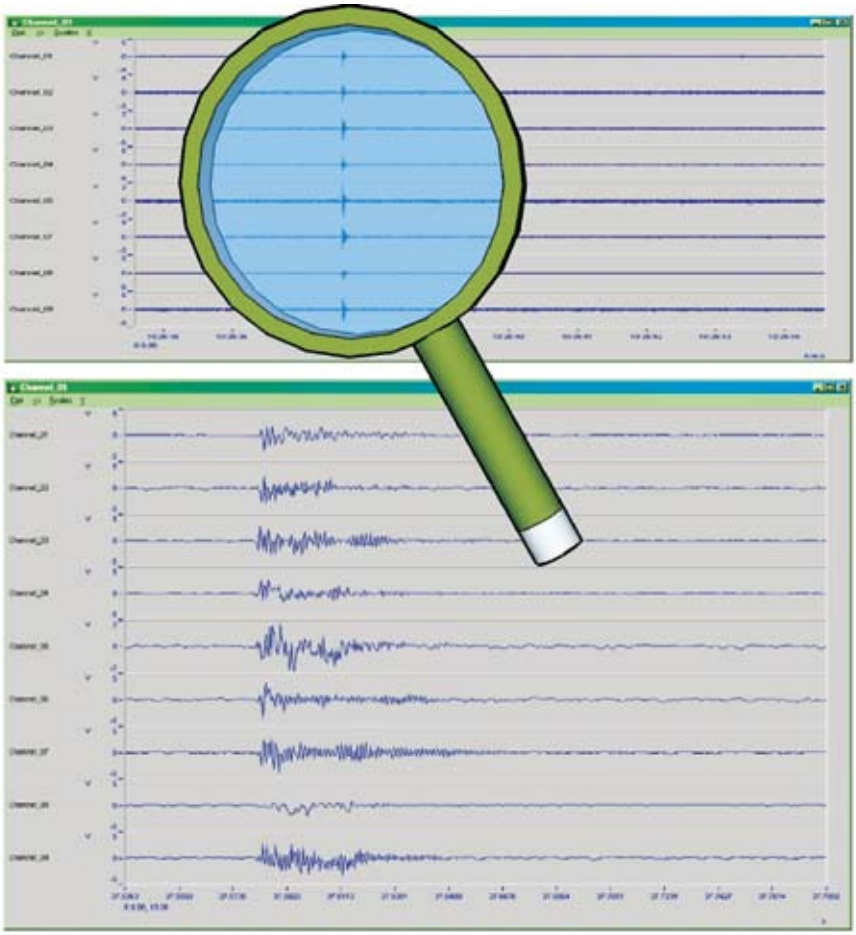

Figure 4. An example of the accelerogram recorded by the in-mine system. Time is in seconds, amplitude in Volts.
Slika 4. Akcelerogram, zapisan z jamskim mikroseizmičnim sistemom. Čas je v sekundah in amplituda v voltih.

are interested in things like "What are safe vibration limits", "What are mm/s", "What other can cause cracks in my house". To answer these and other questions we have supplemented web pages with answers to these frequently asked questions. These measures resulted in a drastic reduction of complaints.

CHARACTERISATION OF EVENTS

Seismic monitoring system on the surface and in the mine gave us invaluable insight into the processes that took place.

Figure 3 displays seismic activity for December 2004 by days and by hour in day. Stronger events occur in the beginning of week and are connected with the cracking of the console in the hanging wall that is built for the weekend. With the constant and not too fast progress of longwall the level of activity decreases and the number of events increases. The accumulated energy is released in smaller amounts[1]. We can see the decrease of activity in the time of shifts in Figure 3b (6, 14 and 22 o'clock). Relative amplitude shown on figure 3 was used to calculate energy of seismic events by considering distance and depth difference from seismic event to seismic station.

Caving is the most critical process at coal extraction. There have been studies of the caving processes associated with the longwall mining, for example HATHERLY et al[3]. Accurate location of the mine tremors is possible only with the use of in-mine seismic system. We have deployed also a mine wide seismic system consisting of accelerometers and signal transmission to the surface[10]. An example of accelerogram is displayed in Figure 4.

Values are measured in Volts and a factor of sensitivity $1/G = 9.684$ m/(V s^2) should be used to convert values to ground vibration accelerations. The locations of events are usually above the level of excavation[10]. The process of caving is taking place in that area. High stresses fracture the coal. The process can be improved by destress blasting or preconditioning (TOPER et al [4]).

ANALYSIS OF FOCAL MECHANISM

Even if the shaking tremors were now better described, some uncertainty still remains. Especially the question, if all big events are originated because of mine works, or their natural origin still remains unsolved. For these purposes the analysis was widened and also the national seismological station was used for analyzing the tremors (Figure 5). The question has its reasons in facts that some stronger tremors were also registered on the Slovenian seismological stations and some were not. Another reason was that only for the national seismological stations sensors orientations data are provided well enough for the first motion analysis. Because of these reasons, the selection of events registered on mine and Slovenian seismological observations network was needed. In fact there were just few events which we were able to prove that their origin was in the area of mining works. For better understanding of governing mechanism we decided for an analysis of a fault plane solution. A fault plane solution (or focal-mechanism solution) is a method to identify the type of an earthquake (COX[8], 1986). The fault plane solution is constructed from the detected signals of different stations and

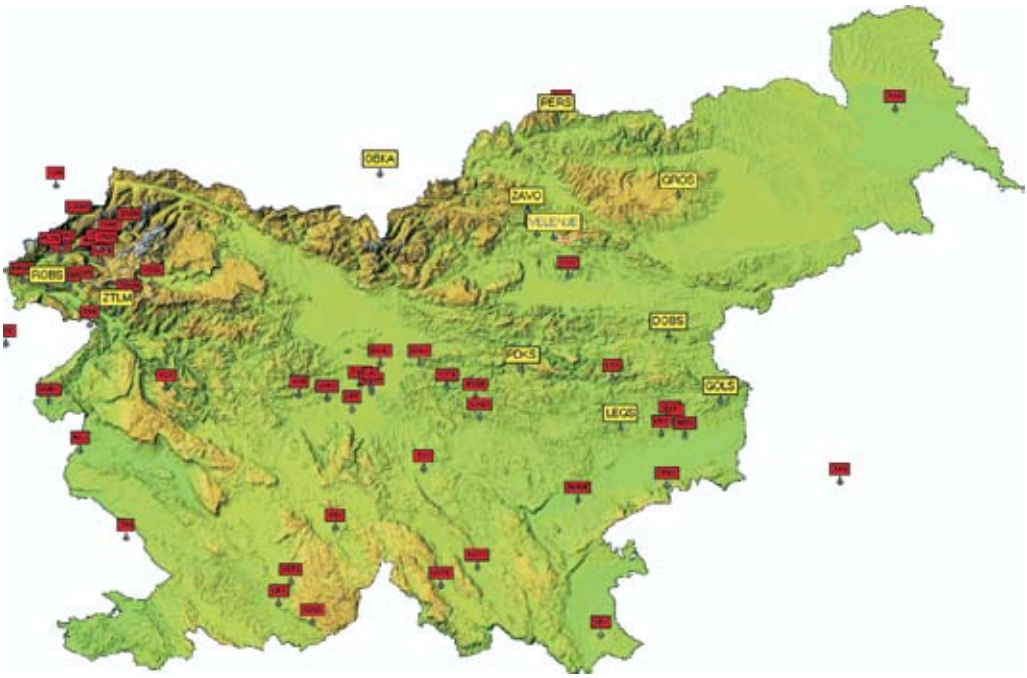

Figure 5. Seismological stations used for the analysis of focal mechanisms. Yellow stations had enough good signals for making the analysis.
Slika 5. Seizmološke opazovalnice, uporabljene za analizo žariščnega mehanizma. Rumeno označene opazovalnice so dale dovolj dober signal za analizo.

gives insight into the type or the source of the earthquake (normal fault, thrust fault or strike slip). To accomplish a fault plane solution, the azimuth as well as the angle of incidence and the type of the first wave (compression or dilatation), which reaches the detecting station, is necessary. The lower hemisphere projection of data is used in the way that the azimuth is taken as an angle and the angle of incidence is taken as the length of a line. At the end of the line a mark is placed depending on the type of the wave.

Our aim was to identify, if the events observed on the mine and national observations nets have manly their origin in normal fault movements or there are also components of thrust fault movements. If they would have their origin in thrust fault movements their origin would be unlikely due to the mining works. The events were first compared on the basis of their frequency and calculated seismic moments. Seismic moment is a quantity used to measure the size of an earthquake (Aki[9], 1966). The seismic moment of an earthquake is typically estimated using whatever information is available to constrain its factors. For earthquakes, moment is usually estimated from ground motion recordings of earthquakes (Westway[5], 1992). In 1970 Brune[6] set up this relation of dislocation along the fault:

$$u = (\sigma / G)\beta \cdot t'' \qquad (1)$$

Where
σ - effective stress (difference in effective stress on a fault before and after dislocation)
G - shear modulus
β - velocity of shear waves
R - distance between the hypocenter and seismological station
r - fault plane distance
t'' - t-R/β
$f = (S/0.8)^{1/2}$ where S is a conversion factor of shear waves in compression waves

Using a Fourier transformation on the equation (1) a equation (2) can be found (STANKOVIĆ[7], 1988):

$$u(\omega) = R_{\Theta\phi} f (r/R)(\sigma\beta/G)(\omega^2 + \alpha^2)^{-1/2} \quad (2)$$

The equation (2) is describing amplitude spectra of dislocation on the free distance from the fault plane. In the equation (2) a factor ($R_{\Theta,\varphi}$) is defining a seismic waves we are observing. The α and f are very well known factors, usually $f = 1$ when $S = 0.8$ and $\alpha = 2.21\ \beta/r$. If we are calculating the specter of dislocation movement along fault using the equation (2) and putting the calculated values on abscise composed of log(ω) and ordinate of log(u (ω)) we are getting the diagram presented on the figure 6.

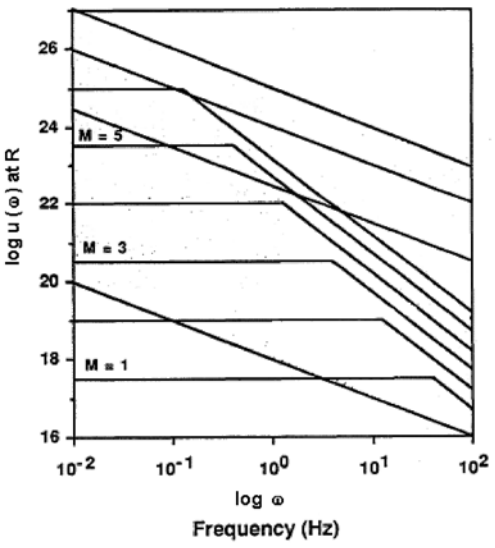

Figure 6. Displacement spectra (BRUNE[6] 1970)
Slika 6. Spekter po Bruneju

Looking at the equation (2) and taking in consideration well known expressions for seismic moment $M_o = (18/7)\sigma r^3$ and $\sigma^2 = (14\pi/9)\ (\beta/r)^2$ (BRUNE[6], 1970) and sending ω to 0 we can get the following equation:

$$u(\omega) = R_{\Theta\phi} M_o \eta (4\pi\rho\beta^3)^{-1} \quad (3)$$

From the equation (3) we can see that the seismic moment is depending on the spectrum of dislocation at low frequencies. This implicit that the using the low spectrum frequencies we are able to compare the events registered on the mining seismological nets with those on the Slovenian seismological net.

On the basis of theory shown before, only few events could be identified on both observation networks. The uncertainty was even greater if we looked at the first arrivals on the seismological stations. So at the end only four events had data good enough (ŽIVEC[12], 2005) for first motions analysis (Figure 7).

It seems that in the four analyzed events the normal movements are present in the governing mechanisms of the tremors. This can be associated with the dilatations occurring due to the excavations of coal seam. Because of data uncertainty we can not for sure associate all big events with the mining works but on the basis of first analysis as some indications are strong

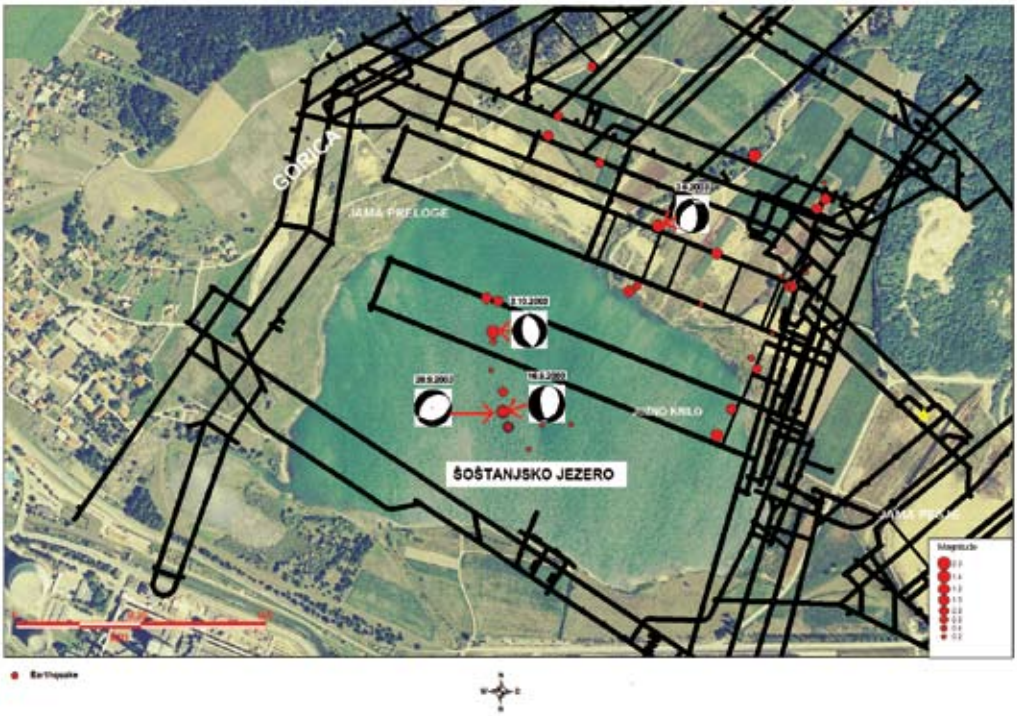

Figure 7. Focal mechanisms of four events which were good enough for the first motion analysis
Slika 7. Žariščni mehanizem štirih dogodkov, katerih signal je bil dovolj dober za analizo prvih premikov

enough that further work in this direction will be done.

Conclusions

Mine wide seismic monitoring system became essential part of mining surveillance monitoring systems especially for mines operating near urban areas. It serves with data about time and intensity of recorded seismic events at the locations where most of complaints are coming from.

The surface station in the nearest village Pesje and town of Šoštanj convinced us that the mine tremors don't cause damage to the buildings, as they are much smaller then allowed values according to the DIN 4150 standard. Independent experts opinion confirmed that statement on the basis of measurements for a period of more than one year. A first motions analysis was also made with the aim of better knowing of tremors governing mechanism. It seems that some big events had also the origin in the mining works rather than in the natural geological events.

We openly presented the conclusions and made the results of on-line measurements available to the public. So instead of complaining calls we are now receiving calls from people who are interested in things like "What are safe vibration limits", "What are mm/s", "What other can cause cracks

in my house". These measures resulted in a drastic reduction of complaints.
Seismic monitoring helped us to gain back information about the processes in the mine and to get response of the coal formation to the mass mining. The response is immediate and therefore it is controllable. It was also found out, that some parts of the longwall face responded to mining with lower intensity of seismic events than other. This phenomena is especially noticeable at the start of the longwall excavation.
With time the database of measurements is increasing and also the knowledge base in that area, so it is very important to keep uninterrupted seismic monitoring of mining operations also in the future.

POVZETEK

Na Premogovnik Velenje so se v preteklosti redno naslavljale pritožbe zaradi povečanega tresenja tal. Način reševanja problematike je bil večplasten in sistematičen. Postavljena je bila merilna oprema za spremljanje dogodkov na površini, v bližnjih naseljih, pa tudi na odkopih. Rezultati meritev so pokazali, da se dogodki dogajajo v materialu, ki ima v geomehanskem smislu precej šibke karakteristike in ga je težko vzročno povezati z nastajanjem dogodkov. V premogu, ki je najtrši, nastane le manjši del seizmičnih dogodkov. Meritve so obsegale tudi spremljavo intenzitete vibracij tal na površini, ne glede na to, od kod prihajajo. Za vse dogodke brez izjeme je bilo ugotovljeno, da s svojo intenziteto ne morejo povzročiti škode na gradbenih objektih, saj so prešibki in so v okviru najstrožjih tujih standardov. Domačih standardov, ki bi na nivoju današnjega stanja tehnike obravnavali problematiko vpliva vibracij tal na površinske objekte, nimamo, zato smo uporabili nemški standard DIN 4150, ki je najstrožji. Rezultate meritev v daljšem obdobju je ovrednotil tudi ekspert s področja vibracij tal, ki je potrdil pravilnost postopkov in rezultatov. Rezultati meritev so vedno na vpogled okoliški javnosti, ki jih ti dogodki motijo, skupaj z razlago, ki pojasnjuje postopke in rezultate meritev na za javnost sprejemljivem nivoju. Pojasnjena je bila tudi osnovna dilema, ki povzroča skrb zaradi tresenja tal, namreč da je človeška občutljivost za vibracije več desekrat nižja od tiste, ki v najneugodnejših razmerah lahko povzroči majhne razpoke na objektih.
Navedeno je imelo za posledico drastično zmanjšanje števila pritožb glede tresenja tal, saj je vsak dogodek izmerjen in tudi zapisan. Ni se še namreč zgodilo, da bi se kdo pritožil zaradi tresenja tal, ki ne bi bilo tudi izmerjeno.
Nekateri od teh dogodkov so zapisani tudi na več postajah državne mreže potresnih opazovalnic, kar je omogočilo tudi bolj poglobljeno analizo mehanizma izvora dogodka. Ugotovljen je bil dilatacijski mehanizem nastanka seizmičnih dogodkov. Seizmičnost je spremljana tudi z jamskim sistemom. Primerjava podatkov s površine in tistih iz jame je pokazala le delno skladanje dogodkov, kajti veliko več dogodkov se zgodi na površini, v jami pa sploh niso ugotovljeni oziroma so pod pragom zaznavanja inštrumentov. Po drugi strani pa lahko z jamskim sistemom ugotovimo direkten odziv na pridobivalna dela, kar nam daje možnost spremljanja odziva hribine na rudarska dela. To je sedaj postalo pomemben del obratovalnega nadzora, saj nam meritve dajejo vpogled v intenzivnost odziva hribine in na dogajanje na površini.

References

[1] Brown, E. T. (1984): Rockbursts. Prediction and Control, *Tunnels and Tunneling*, pp. 17–19.

[2] DIN 4150 Teil 1 bis Teil 3-Erschutterungen im Bauwesen, DIN Deutsches Institut fur Normung, Berlin (Germany), 1993.

[3] Hatherly, P., Luo, X., Dixon, R. & McKavanagh, B. (1997): Seismic monitoring of ground caving processes associated with longwall mining of coal. *Rockbursts and seismicity in mines*, Rotterdam, pp. 121–124.

[4] Toper, A. Z., Grodner, M., Stewart, R., D. & Lightfoot, N. (1997): Preconditioning a rockburst control technique. *Rockbursts and seismicity in mines*, pp. 267–272.

[5] Westway, R. (1992): Seismic Moment Summation for historical Earthquakes in Italy. Tectonic implications, J. Geophys. Res. 97, Washington, pp. 15437–15464.

[6] Brune, J. (1970): Tectonic stress and the Spectra of Seismic Shear Waves from Earthquakes. J. Geophys. Res. 75, Washington, pp. 4997–5009.

[7] Stanković, R. S., Stojić, M. R., Bogdanović, S. M. (1988): Fourier transformations of seismic signals. *Naučna knjiga Beograd*, 142 p.

[8] Cox, A. & Hart, R. (1986): *Plate Tectonics – How it works?* Blackwell, Oxford, 392 pp.

[9] Aki, K. (1966): Generation and propagation of G waves from the Niigata earthquake of June 16, 1964, Part 2 Estimation of earthquake moment, released energy, and stress-strain drop from the G wave spectrum. Bull. Earthq. Res. Inst. 44, pp. 73–88.

[10] Mayer, J. et al. (2002): Spremljanje rudarsko induciranih seizmičnih pojavov v Premogovniku Velenje. *RMZ* 49/1, pp. 51–60.

[11] Žorž, Z. et al., (1984) : Geomehanski model intaktne premoške kadunje Rudnika lignita Velenje, *GZL*, Ljubljana pp. 15–18.

[12] Živec, T. (2005): Analiza potresne dejavnosti na območju premogovnika Velenje, diplomsko delo, Ljubljana, 69 p.

Determination of the adhesive fracture energy G_C of structural adhesives using DCB and Peel tests

Določitev raztržne žilavosti strukturnih adhezivov G_C z uporabo DCB in odluščnih preizkusov

Martin Lamut[1], Rado Turk[2], Matjaž Torkar[1]

[1]Institute of Metals and Technology, Lepi pot 11, SI-1000 Ljubljana, Slovenia;
E-mail: martin.lamut@imt.si, matjaz.torkar@imt.si
[2] University of Ljubljana, Faculty of Natural Sciences and Engineering, Aškerčeva cesta 12, SI-1000 Ljubljana, Slovenia; E-mail: rado.turk@uni-ntf.si

Received: October 13, 2008 **Accepted:** November 24, 2008

Abstract: Due to the increasing use of adhesively bonded load bearing joints in demanding Engineering applications, the failure properties of adhesives need to be known.The fracture testing of adhesive joints has been developed to yield engineering data used for comparative analysis between adhesives and also the different substrates used. A large number of different tests have been developed to measure the adhesive fracture toughness, G_C, of adhesive joints. In this work two different types of test are presented, an elastic plastic peel test and a double cantilever beam test, based on linear elastic fracture mechanics (LEFM). Ideally, adhesive fracture toughness should be a geometry independent value, a characteristic adhesive property.

Izvleček: Zaradi vse večje uporabe adhezivnih spojev v avtomobilski in letalski industriji je poznavanje mehanskih lastnosti adhezivov izrednega pomena. Preizkušanje zlepljenih spojev z uporabo strukturnih adhezivov je bilo v prvi vrsti razvito za pridobitev primerjalnih podatkov različnih adhezivov in podlag, uporabljenih pri spojih. Obstaja veliko različnih geometrijskih oblik preizkusov za določitev energije raztržne žilavosti strukturnih adhezivov. V tem delu sta predstavljena dva osnovna tipa geometrije, in sicer: elastoplastični odluščni preizkus in preizkus z uporabo dvojnega konzolnega nosilca (DCB), ki je osnovan na linearni mehaniki loma. Idealno je energija raztržne žilavosti adhezivov neodvisna karakteristična veličina adheziva.

Key words: fracture tests, adhesives, Peel tests, DCB test
Ključne besede: lomni preizkusi, adhezivi, odluščni preizkusi, DCB-preizkusi

Review paper

Introduction

Adhesive joints are an effective way of connecting structural components such as metals and polymers. Comparing to the traditional joining techniques riveting and welding adhesively bonded structures experience many advantages. The most important in aerospace and automotive industry are weight savings and good dynamic fatigue properties [1]. The effective bonding of sheet materials also makes it very appealing for the packing industry.

There have been a large number of different tests developed to obtain the fracture resistance of structural adhesive joints [1], among them are two of particular interest for this work: the double cantilever beam bending test (DCB), which is based on a linear-elastic fracture mechanics (LEFM), and the elastic-plastic T-peel test, both tests yield the adhesive fracture toughness G_C.

Guidance on conducting fracture tests is described in various standards, e.g. for a DCB test geometry there is a British standard BS 7991 [2], the existing ISO standards: ISO 8510-1 1990 [3] and ISO 8510-2 1990 [4] "Peel test for a flexible bonded to rigid specimen assembly, Part 1 90° peel and Part 2 180°", ISO 11339 1993 "180 peel test for flexible to flexible bonded assemblies" (T-peel test), indicate how to measure peel strength, force per unit width for peeling. To determine the adhesive fracture toughness from the measured peel strength described in the ISO standards, a special protocol was developed at the Imperial College, called ICPeel [5].

DCB test principles

Introduction

One of the most frequently used test geometries for generating Mode I adhesive fracture energy, G_{IC}, is the double cantilever beam specimen. In this test the substrates, usually made from metal, are bonded together with the adhesive and the crack is propagated along the adhesive layer in opening mode by pin loading at the beam-ends. The method used to determine the fractural resistance is based on linear elastic fracture mechanics (LEFM). From this test, both the resistance to crack initiation and propagation can be determined and the resistance curve (plot of G_{IC} vs. crack length) can be produced [2].

DCB specimen geometry

Generally a DCB test specimen is suited for testing joints, where relatively thin sheets of fibre composite materials are adhesively bonded, but may also be used for metallic substrates. A typical specimen used for metallic substrates is shown in Figure 1.

Test procedure

Test is preformed under normal conditions (23 °C ± 2 °C, 50 % ± 5 % r. h.) on a tensile testing machine, capable of producing a constant cross-head displacement rate between 0.1 mm/min and 5 mm/min in displacement control. A special fixture is used to introduce the load to the pins inserted into substrate beams.

The tensile testing machine compliance must be taken into account. If the machine compliance is not known, it should be determined using the calibrated specimens [2].

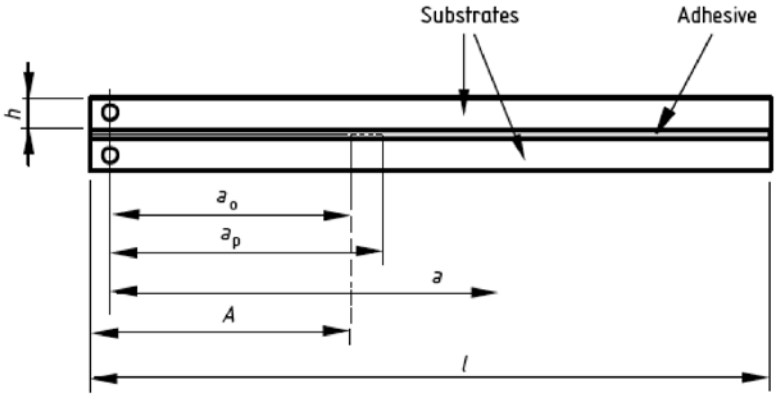

Figure 1: DCB test specimen geometry [2]. Where: *A* - insert film length, distance between the end of the specimen and the tip of the insert film, *a* - crack length, distance between the load line and the tip of the crack, a_0 - initial crack length, a_p - precrack length, distance from the load line to the tip of the precrack, *B* - specimen width, *h* - arm thickness, h_a - adhesive layer thickness, *l* - specimen length.
Slika 1: Geometrija DCB-preizkušanca. Oznake: *A* - dolžina vstavljenega traku, razdalja med koncem preizkušanca in začetkom razpoke, *a* - dolžina razpoke, razdalja med linijo obremenitve in vrhom razpoke, a_0 - začetna dolžina razpoke, a_p - dolžina predrazpoke, *B* - širina preizkušanca, *h* - širina konzolnega nosilca, h_a - debelina adheziva, *l* - dolžina preizkušanca.

During the test progress, recording of the complete load versus displacement curves are taken. At the same time the crack is measured using a travelling microscope or a video camera.

Analysis methods or determining the values G_{IC}

There are three analyses methods that may be used to calculate G_{IC} from the DCB test data, where $_I$ denotes Mode I loading condition.
(1) simple beam theory (SBT),
(2) corrected beam theory (CBT), and
(3) experimental compliance method (ECM).
All of them are essentially derived from Equation (2.1), and all require the monitoring of load, crack opening displacement, and crack growth to determine variation of compliance with crack growth. A brief outline of every analysis method is discussed at this point.

Simple beam theory.

The value of adhesive fracture energy G_{IC} may be deduced from:

$$G_C = \frac{1}{2B} P^2 \frac{dC}{da} \tag{2.1}$$

where *C* is the compliance and is given by load-line *displacement(δ)/load(P)*. The compliance change with crack length was derived by MOSTOVOY at al. [6] where bending and shear deflection contribute to the specimen compliance. The specimen was treated as a pair of cantilever beams with length *a,* representing the crack length, measured from the point of loading. The

dC/da may be written as

$$\frac{dC}{da} = \frac{8}{E_S B}\left(\frac{3a^2}{h^3} + \frac{1}{h}\right) \quad (2.2)$$

where E_S is the flexural or tensile modulus of the substrate. This value is quoted for the standard grade materials, otherwise should be measured from an independent modulus test.

Inserting expression for dC/da into equation (2.1) gives G_{IC}

$$G_{IC} = \frac{12P^2a^2}{E_S B^2 h^3}\left(1 + \frac{1}{3}\frac{h^2}{a^2}\right) \quad (2.3)$$

This value can be further simplified if the condition $a^2 >> h^2$ is met, it means that the crack length is much larger than the beam arm thickness and deflection due to shear stress can be neglected

$$G_{IC} = \frac{12P^2a^2}{E_S B^2 h^3} \quad (2.4)$$

where h, B, and E_S are the height, width and Young's modulus of the substrate, respectively.

Corrected beam theory

The simple beam theory does not account for the important effect of beam root rotation, which affects compliance and G_{IC}. It has been shown that this effect can be modelled by adding a length, Δ, to the measured crack length [8]. Adhesive fracture energy may be calculated using the following equation

$$G_{IC} = \frac{3P^2\delta}{2B(a+\Delta)}\frac{F}{N} \quad (2.5)$$

where δ is the measured load-line displacement, F is a correction factor which accounts for the reduction in bending moment caused by large displacements and N is the load block correction. When piano hinges are drilled directly through the substrate, as is the case for metal substrates, N = 1. Further information can be found [8, 2, 9], where detailed explanations and derivation of the variables are provided.

Experimental compliance method

In order to estimate the change of compliance in relation to crack growth, compliance is plotted against crack length and then curve fitted using the Berrys method [9], which employs a power-law compliance calibration

$$C = ka^n \quad (2.6)$$

where k and n are regression coefficients determined from experiments. Differentiating this equation with respect to crack length, a, and combining the differential with Equation (2.1) leads to

$$G_{IC} = \frac{nP\delta}{2Ba}\frac{F}{N} \quad (2.7)$$

Elasto-plastic peel tests

Introduction

Peel test is a widely used method for measuring the peeling energy between flexible joints [1]. The level of the bond strength is a critical issue since laminates act as engineering structures, therefore it is very important to be able to control adhesive fracture toughness. Ideally, adhesive fracture toughness should be a characteristic adhe-

sive property, independent of test geometry such as the thickness of the peel arm or peel angle [1]. Due to the fact of wide application of peel tests, several test geometries have been used. Two particular forms used in this work are the fixed arm peel test and T-peel test (Figures 3, 4). Since the T peel test may be seen as a two fixed arm tests combined, the fixed arm peel test is analysed firstly and then extended to T-peel test.

Peel specimen geometry

There are two basic types of test geometry, a fixed arm peel test, and a T-peel test. The specimen for the peel test should be of a rectangular shape, where the two parts of the joint have already been adhered but where there is a region of unadhered material (of nominal length 30 mm) [5]. The peel arms should be thick enough to withstand the expected tensile force, their dimensions are carefully measured and assembled with great caution. The overall dimensions of peel specimen need not be rigidly defined but for many tests a total length of 100 mm and width of 20 mm proves to be quite satisfactory. An example of fixed arm peel test geometry is shown on Figure 2. Mirroring the fixed arm geometry, about the bond line, derives the T-peel test geometry. Symbols used for peel geometry are given below.

Experimental procedure

The choice of peel fixture is not unique but the jig should incorporate a number of facilities. Most important among them is that the fixture should be able to select the peel angle in the range up to 180 ºC. The peel specimen is fixed at the bottom of the supporting frame of the tensile testing machine (Instron), and attached to the load cell and the testing machine crosshead. A peel test speed (crosshead speed) of 10 mm/min can be used as a standard with a 90º peel angle. However, the peel speed will be influenced by the peel angle. For the fixed peel arm testing, the peel arm is clamped to a load cell and the specimen base is bolted to a linear bearing trolley, which moves in the horizontal direction as to keep the position of the crack front constant. For the T-peel specimens two clamps are used to grip the specimen in position, with one clamp attached to the testing machine load cell, the other to the base of the machine.

Analyses of the fixed arm peel test

In order to peel one laminate from another, or from a rigid support, requires energy in the form of external work to be applied to the laminate, Figure 3. Since the peel arm may exhibit plastic or viscoelastic behav-

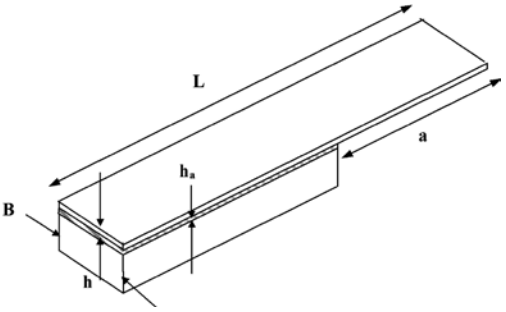

Figure 2. Fixed arm peel test specimen geometry. Where, *a* - crack length, distance between the load line and the tip of the crack, *B* - specimen width, *h* - arm thickness, h_a - adhesive layer thickness, *L* - specimen length.

Slika 2. Geometrija enostransko vpetega odluščnega preizkušanca. Oznake: *a* - dolžina razpoke, razdalja med linijo obremenitve in vrhom razpoke, *B* - širina preizkušanca, *h* - širina konzolnega nosilca, h_a - debelina adheziva, *L* - dolžina preizkušanca.

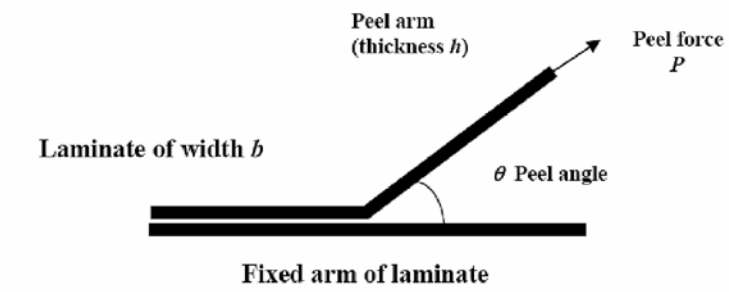

Figure 3. Fixed arm peel test specimen [5]
Slika 3. Enostransko vpet odluščni preizkušanec

iour, the historically used peel strength, which was the governing factor in the peel tests, was very geometry and material dependent. ESIS protocol was written by MOORE AND WILLIAMS [5] to transfer historically measured peel strength, which measures the strength of the adhesively bonded joint, to adhesive fracture energy, which is a measure of how well the two surfaces are bonded together. The protocol used was based on the work of KINLOCH et al. [10] and GEORGIOU et al. [11] where they used the energy balance argument and derived the adhesive fracture energy, which relates external work added to the system (U_{ext}), strain energy stored in the peel arm (U_s), energy dissipated during tensile deformation of the peel arm (U_{dt}) and the energy dissipated during the bending of the peeling arm near the peel front (U_{db}).

$$G_C = \frac{1}{B}\left(\frac{dU_{ext}}{da} - \frac{dU_s}{da} - \frac{dU_{dt}}{da} - \frac{dU_{db}}{da}\right) \quad (3.1)$$

Where G_C stands for a geometry independent property and is a characteristic value for a particular adhesive [1,10]. To convert peel strength (P/mm) to adhesive fracture energy, the following equation is used

$$G_C = G - G_P \quad (3.2)$$

where G is the peel strength-measured load, G_P is the plastic arm energy caused by bending the peel arm. When no tensile strain in the peel arm is assumed, input energy G may be written as

$$G = \frac{P}{B}(1-\cos\theta) \quad (3.3)$$

If zero bending stiffness is considered, this expression is also used as the adhesive fracture energy, where θ is the peel angle as shown in Figure 3.
This would be the case for a material of infinite stiffness and no bending stiffness. However, if there is an elastic-plastic deformation in the peeling arm, it is necessary to have knowledge of the tensile characteristics of the peel arm material and the full expression for G_C becomes

$$G_C = \frac{P}{B}(1+\varepsilon-\cos\theta) - h\int_0^{\varepsilon}\sigma d\varepsilon - G_{db} \quad (3.4)$$

where ε is the tensile strain, σ is the stress, h is the height of the peel arm and G_{db} accounts for plastic or viscoelastic bending of the peel arm given by

$$G_{db} = -\frac{1}{B}\frac{dU_{db}}{da} \quad (3.5)$$

Analysis of the T-peel test

In Figure 4, the specimen configuration of T-peel-test is shown. The analysis adopts the same steps as in the fixed peel arm, except that now two peel arms are considered instead of one. If one peel arm is stiffer than the other, as in the case of unbalanced peeling, two different peel angles are present rather then two 90° angles. Since the angles are correlated via $\Phi = \pi - \theta$, only one angle should be considered. The Equation (3.3) becomes:

$$G_1 = \frac{P}{B}(1+\cos\theta) \tag{3.6a}$$

$$G_2 = \frac{P}{B}(1-\cos\theta) \tag{3.6b}$$

where subscripts 1 and 2 stand for each peel arm. In a similar manner there will be two forms of plastic peel arm dissipative energy, which results in two forms of fracture toughness energy expressions:

$$G_{C1} = G_1 - G_{P1} \tag{3.7a}$$

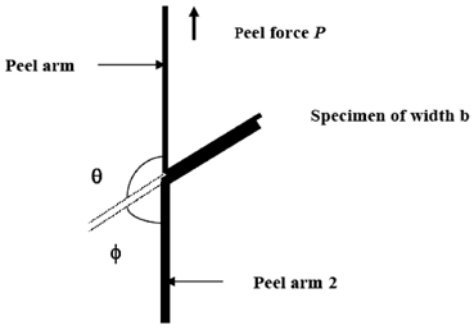

Figure 4. T-peel-test specimen [5]
Slika 4. Odluščni preizkušanec v obliki črke T ali T-odluščni preizkušanec

$$G_{C2} = G_2 - G_{P2} \tag{3.7b}$$

The adhesive fracture toughness is simply the sum of the last two equations:

$$G_C = G_{C1} + G_{C2} \tag{3.8}$$

When balanced T-peel test is assumed, $\Phi = \theta = 90^\circ$, $\cos\theta$ becomes equal to zero, and all the equations derived for fixed arm peel test at 90º may be multiplied by 2, hence describe the situation in T-peel test.

In order to determine G_C, from peel tests, elastic and plastic deformations are taken into account, and two tests must be conducted:
(1) Peel test
(2) Tensile test of the peel arm material
All the detailed calculations regarding peel tests are given in references [5, 10, 11] and while theoretical calculations can be very complex, software that may be used to conduct the calculation is available on the Imperial College web site [12].

RESULTS AND DISCUSSION

In DCB experiment mild steel beam arms (E = 207 GPa) and ESP110 (E = 4 GPa) adhesive were used. The geometry details of the DCB test specimen are given in Table 1.
All data analysis were preformed using the Microsoft Excel© spreadsheets, which were written at Imperial College and can be obtained freely from [9,12]. The spreadsheets automatically performed all the data reduction, plots and calculations of G_C, using the presented theory.

Table 1. DCB-test specimen data
Tabela 1. Geometrijski podatki za DCB-preizkušanec

	Label	[mm]
Specimen length	L	190
Arm thickness	H	20
Specimen width	B	25
Initial crack length	a_0	50
Adhesive layer thickness	h_a	0.4

In Figure 5 a typical load versus crosshead displacement curve is shown. Due to load take up effects, there was initial non-linear trace, which was removed by extrapolating the linear part and resetting the intercept to zero displacement. The first, linear part up until maximum load applied, depicts the elastic loading history before the crack growth. During the crack growth the compliance of the DCB is increasing and the load is dropping. Another way of presenting the results is via load versus crack growth, starting at the beginning of the crack growth, Figure 6.

When very stiff DCB specimens are tested, significant displacement errors could be introduced. For that reason a system compliance value was measured and a correction was made. Figure 7 shows the resistance curves corrected for the effect of system compliance via the three analyses methods previously presented. The resistance curves are constructed to show how the values of G_{IC} develop during crack growth. It may be seen that SBT is in disagreement with CBT and ECM, most likely due to incorrect assumptions made in SBT derivation. Neglecting the crack root rotation, as is the case in SBT derivation, may leads to substantial errors.

The initial and mean propagation values of G_{IC} were directly deduced from the spreadsheet, Table 2. The mean propagation was simply the mean of all the non-initiation G_{IC} values.

Table 2. Initiation and mean propagation values of G_{IC} for the DCB joints
Tabela 2. Začetna in srednja vrednost napredovanja G_{IC} pri DCB-spojih

	G_{IC}(SBT)/(J/m^2)	G_{IC}(CBT)/(J/m^2)	G_{IC}(ECM)/(J/m^2)
Initiation	345	434	458
Mean propagation	636	978	977

For the peel test experiment the substrate material was made of Aluminium-alloy 5754 (E = 69 GPa) and the adhesive used was ESP110 (E = 4 GPa). Details of the dimensions of the peel joints are given in Table 3.

Table 3. T-peel-test specimen data
Tabela 3. Geometrijski podatki za T-odluščni preizkušanec

	Label	[mm]
Specimen length	L	295
Arm thickness	H	1
Specimen width	B	20
Initial crack length	A	180
Adhesive layer thickness	h_a	0.4

An example of a typical load versus crosshead displacement for a T-peel specimen is shown in Figure 8. The load fluctuates significantly with displacement during the crack growth as the crack moves form one substrate interface to the other (load is expressed in N per mm width as peel force).

The load versus crosshead displacement trace for the 90° peel test differs considerably from the T-peel trace as is shown

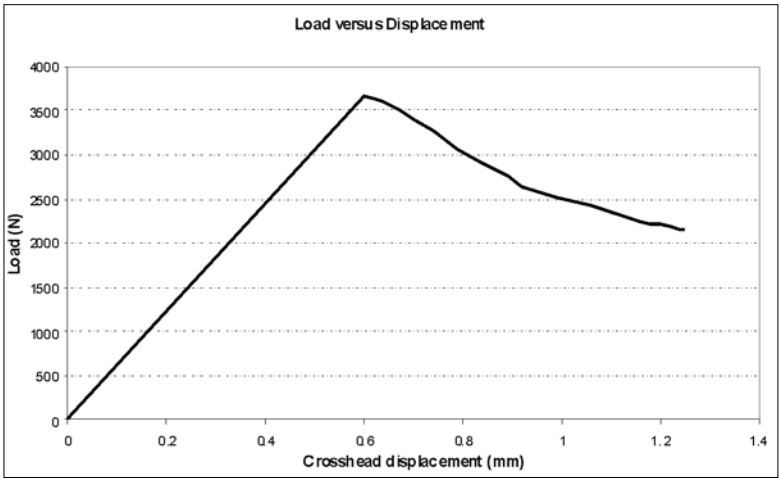

Figure 5. A typical load-displacement trace for a DCB joint [7]
Slika 5. Značilen potek krivulje obremenitev-pomik čeljusti, pri DCB-spojih

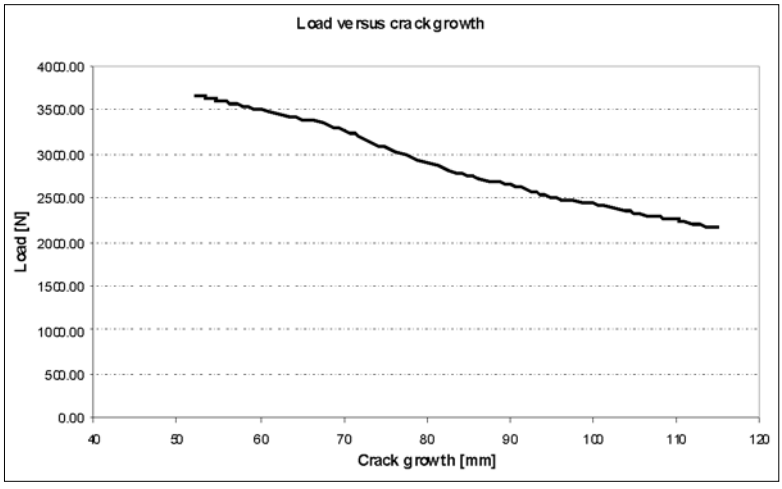

Figure 6. A typical load-crack growth trace for a DCB joint [7]
Slika 6. Značilen potek krivulje obremenitev-rast razpoke, pri DCB-spojih

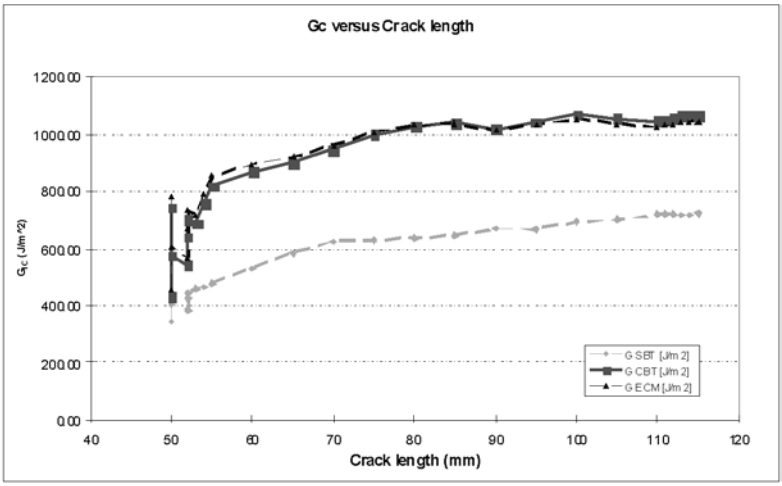

Figure 7. A typical set of resistance curves for a DCB joint [7]
Slika 7. Značilne krivulje raztržne žilavosti DCB-spojev

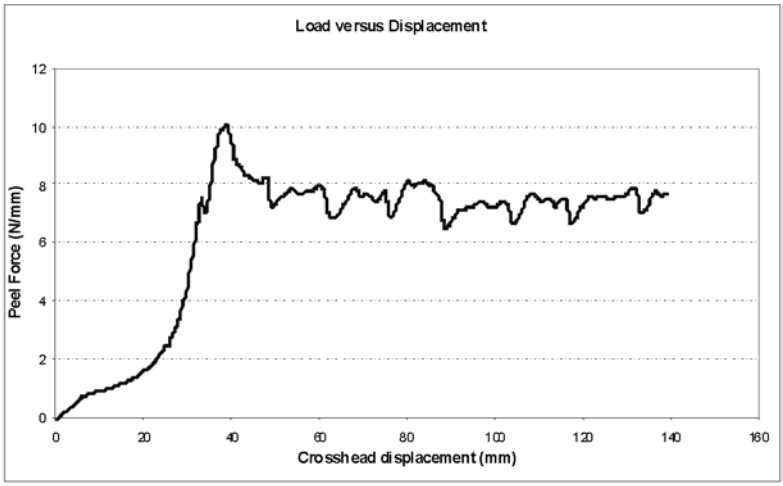

Figure 8. A typical load-displacement trace for a T-peel test
Slika 8. Značilen potek krivulje obremenitev-pomik čeljusti za T-odluščni preizkušanec

in Figure 9. Only minor load fluctuations with displacement during crack growth are observed. It can be said that the load reaches a steady state value after a certain amount of crack growth.

Using the spreadsheet for peel tests and the data obtained from the experiment the values of G_I can be easily obtained, although the calculations may look fairly complicated. Since the mean steady state peel force is used in the calculations, the G_I represents the propagation value. It is almost impossible to detect the beginning of the crack growth for these tests therefore the initiation value of G_I is not attainable.

Table 4. Propagation values of G_C for the peel tests
Tabela 4. Obremenitev in G_C odluščnih preizkusov

	P/(N/mm)	G_I/(J/m^2)
T-peel	7.43	1370
90° peel	5.00	922

From table 4 it may be seen that the adhesive fracture toughness between T-peel and 90 ° peel tests differ greatly, which is most likely due to an unsteady crack growth. There is a combination of adhesive and cohesive fracture, for which cohesive and adhesive fracture toughness should be determined.

CONCLUSIONS

Firstly, a LEFM-based approach was presented via DCB test geometry. To calculate G_{IC} (Mode I loading condition) from a DCB specimen, three methods were presented. Corrected beam theory and Experimental compliance method both yield accurate results, whereas Simple beam theory can only be applied under specific conditions.

Secondly, two types of elastic plastic peel tests were presented. Fixed arm peel test

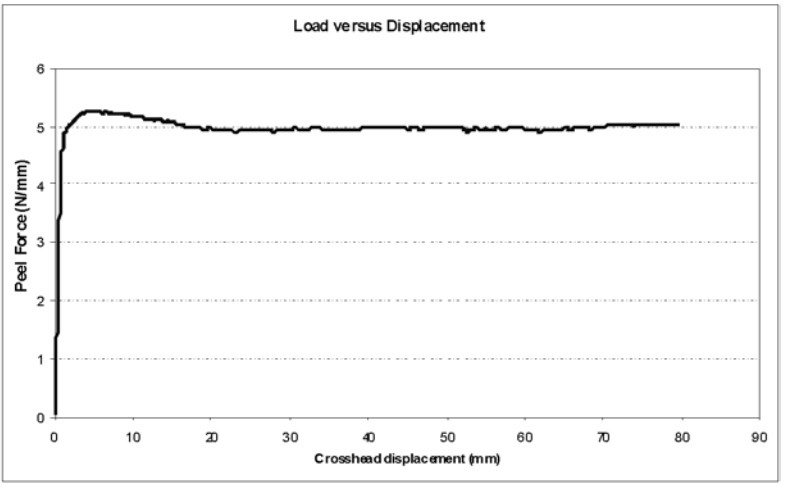

Figure 9. A typical load-displacement trace for a 90° peel test
Slika 9. Značilen potek krivulje obremenitev-pomik čeljusti za 90-stopinjski odluščni preizkušanec

(90° peel test) and the T-Peel test were introduced to show how the plastic deformation and root rotation of the beam arms is accounted for in determining the fracture toughness of adhesives. All the steps needed to transfer experimentally obtained data, peel strength to fracture toughness of the adhesive, were outlined. Additionally, the experimental results, the load versus crosshead displacement traces, were shown for DCB and Peel tests. All data manipulations were made using the Microsoft Excel© spreadsheets. It may be seen that the SBT gives inferior results comparing to CBT and EC methods.

The adhesive fracture toughness, G_C, from the DCB and 90° peel tests agreed well. On the other hand the value for the T-peel test is higher, which is in disagreement with the statement of characteristic adhesive property. In order to obtain an excellent agreement, further studies must be performed, where special care must be dedicated to the test specimen preparation and test procedure to ensure cohesive fracture through the adhesive layer.

Povzetek

Adhezivna sredstva so učinkovit način spajanja različnih strukturnih elementov, kot so kovine in polimeri. V primerjavi s tradicionalnimi metodami spajanja imajo adhezivni spoji številne prednosti, med katerimi so za letalsko in avtomobilsko industrijo najpomembnejša zmanjšanje mase. Obstaja veliko različnih geometrij preizkusov za določitev energije loma strukturnih adhezivov. V tem delu sta predstavljena dva osnovna tipa geometrije: elasto-plastični odluščni preizkus in preizkus z uporabo dvojnega konzolnega nosilca (DCB), ki je osnovan na linearni mehaniki loma. Natančna navodila in opis opravljanja različnih preizkusov so predstavljena v različnih standardih, npr. za DCB obstaja BS 7991 [2], za odluščne preizkuse imamo več ISO-standardov: ISO 8510-1 1990 [3], ISO 8510-2 1990 [4] in ISO 11339 1993. Za izračun energije loma iz izmerjene sile pri različnih preizkusih je bil na Imperial Collegeu razvit ICPeel [5] protokol.

Najbolj razširjen preizkus za izračun energije loma, GIC, pri načinu obremenjevanja I, je DCB-preizkus z uporabo dvojnega konzolnega nosilca (Slika 1), kjer sta konzoli navadno kovinski in razpoka poteka vzdolž adheziva ob obremenitvi na krajiščih konzol. S tem preizkusom lahko določimo odpornostno energijo pričetka rasti in energijo rasti razpoke ter izračunamo krivulje energije loma v odvisnosti od dolžine razpoke. Za izračun energije loma obstajajo tri teorijske metode:
(1) enostavna teorija konzolnega nosilca;
(2) popravljena teorija konzolnega nosilca;
(3) eksperimentalna metoda s podajnostjo (ang. compliance).

Odluščni preizkusi se uporabljajo za določanje odluščne energije pri fleksibilnih spojih, kjer je težko ločiti med energijo loma adheziva in deformacijsko energijo posameznih elementov spoja. Idealno je energija loma adhezivov neodvisna, karakteristična veličina adheziva. Med različnimi geometrijami odluščnih preizkusov sta v tem delu predstavljeni dve:

enostransko vpet odluščni preizkušanec (Slika 2) in odluščni preizkušanec v obliki črke T ali T-odluščni preizkušanec (Slika 4). Pri enostransko vpetem odluščnem preizkušancu obstaja več variacij, ki se razlikujejo v kotu med fiksiranim in obremenjenim delom preizkušanca, npr. 90-stopinjski odluščni preizkus (Slika 3). V primeru preslikanja enostransko vpetega odluščnega preizkušanca preko adhezivne plasti dobimo T-odluščni preizkušanec, kar olajša analizo odluščnih preizkušancev.

Pri DCB- preizkusih so bili uporabljeni jekleni konzolni nosilci (E = 207 GPa) in adheziv z oznako ESP110 (E = 4 GPa) Geometrijski podatki DCB-preizkušanca so podani v Tabeli 1.

Pri odluščnih preizkusih je bila kot podlaga uporabljena aluminijeva zlitina 5754 (E = 69 GPa) in enak adheziv kot v prejšnjem primeru ESP110 (E = 4 GPa). Vsi geometrijski podatki, uporabljeni pri odluščnih preizkusih, so zbrani v Tabeli 3.

Prikazane so značilne krivulje obremenitev-pomik čeljusti za vse obravnavane preizkuse (Slike 5, 8, 9). Na Sliki 6 je viden padec obremenitve med potekom rasti razpoke pri DCB- preizkusu. Za DCB-preizkus so prikazane krivulje energije loma (Slika 7), izračunane iz eksperimetalnih podatkov in z uporabo ICPeel-protokola, ki obsega predstavljeno teorijo.

Iz Tabel 2 in 4 je razvidno, da se energija loma adheziva med DCB in 90°-odluščnim preizkusom dobro ujema, medtem ko je vrednost pri T-odluščnem preizkusu višja in se ne ujema z načelom o karakteristični lastnosti energije loma adheziva.

References

[1] KINLOCH, A. J. (1987): Adhesion and Adhesives. 1st edition. *Chapman and Hall*, London.

[2] BSI. (2001). Determination of the mode I adhesive fracture energy, G, of structural adhesives using the double cantilever beam (DCB) and tapered-cantilever beam (TDCB) specimens. BS 7991.

[3] ISO: Adhesives – Peel test for a flexible-bonded-to-rigid test specimen assembly – Part 1. ISO 8510-1:1990.

[4] ISO: Adhesives – Peel test for a flexible-bonded-to-rigid test specimen assembly – Part 2. ISO 8510-2:1990.

[5] MOORE, D. R. & WILLIAMS, J. G.: A protocol for Determination of the Adhesive Fracture Toughness of Flexible Laminates by Peel Testing: Fixed Arm and T-peel Methods ESIS protocol, updated 2006 [cited 20. 12. 2006]. Accessible on Internet: <http://www3.imperial.ac.uk/meadhesion>.

[6] MOSTOVOY, S., CROSLEY, P. B. & RIPLING, E. J. (1967): Use of crack-line-load specimens for measuring plane strain fracture toughness. *J. Mat. 2*, pp. 661–681.

[7] BLACKMAN, B. R. K., KINLOCH, A. J., PARASCHI, M. & TEO, W. S. (2003): Measuring the mode I adhesive fracture energy, $G_{IC,}$ of structural adhesive joints: the results of an

international round-robin. *Int. J. Adhes. Adhes. 23*, pp. 293–305.

[8] Hashemi, B., Kinloch, A. J. and Williams, J. G. (1990): The analysis of interlaminar fracture in uniaxial fibre-polymer composites. *Proc. R. Soc. London A. 427*, pp. 173–199.

[9] Blackman, B. R. K.& Kinloch, A. J.: Protocol for Determination of the Mode I Adhesive Fracture Energy, $G_{IC,}$ of Structural Adhesives using the Double Cantilever Beam (DCB) and Tapered Double Cantilever Beam (TDCB) Specimens. Imperial College London, 2000, updated 2006 [cited 20.12. 2006]. Accessible on Internet: <http://www3.imperial.ac.uk/meadhesion>.

[10] Kinloch, A. J., Lau, C. C. & Williams, J. G. (1994): The peeling of flexible laminates. *Int. J. Frac. 66*, pp. 45–70.

[11] Georgiou, I., Hadavinia, H., Ivankovic, A., Kinloch, A. J., Tropsa, V. & Williams, J. G. (2003): Cohesive zone models and the plastically deforming peel test. *J. Adh. 79*, pp. 239–265

[12] Imperial College London Website [online]. Peel test protocols: ICPeel. updated 2006 [cited 20.12. 2006]. Accessible on Internet: <http://www.me.ic.ac.uk/AACgroup/>.

Characterization of black crusts of Robba´s fountain statues, Ljubljana (Slovenia)

Karakterizacija črnih oblog na kipih Robbovega vodnjaka, Ljubljana (Slovenia)

Sabina Kramar[1], Breda Mirtič[2]

[1]Institute for the Protection of Cultural Heritage of Slovenia, Restoration Centre, Poljanska 40, SI-1000 Ljubljana, Slovenia; E-mail: sabina.kramar@rescen.si
[2]University of Ljubljana, Faculty of Natural Sciences and Engineering, Department of Geology, Aškerčeva 12, SI-1000 Ljubljana, Slovenia;
E-mail: breda.mirtic@guest.arnes.si

Received: September 8, 2008 **Accepted:** November 17, 2008

Abstract: Black crusts are result of various chemical-physical reactions between stone surface and environmental factors. Detailed characterization is required to determine causes and mechanisms of black crusts formation, which enables us to chose appropriate cleaning method and prevent their further formation. Statutes of Robba fountain, made of Carrara marble, are encrustated by crusts which differ in composition, morphology and colour. Composition of black crusts and deterioration of the Carrara marble statuary has been investigated by means of optical, electron microscopy and X-ray powder diffraction. Results demonstrated that in sheltered areas of upper parts of the statues, gypsum crusts occur, while calcite crusts cover lower parts of the statues which are within range of the fountain water. In some samples, taken from the lower parts of the fountain, where moisture is constantly present, endolitic green algae and Cyanobacteria are present.

Izvleček: Črne obloge nastajajo kot posledica kemično-fizikalnih reakcij med površino naravnega kamna in različnimi okoljskimi dejavniki. Da bi jih lahko z najprimernejšo metodo odstranili in preprečili njihovo nadaljnje nastajanje, jih je treba natančno okarakterizirati ter ugotoviti mehanizem njihovega nastanka. Na treh kipih Robbovega vodnjaka, ki so izklesani iz carrarskega marmorja, so nastale obloge, ki se med seboj razlikujejo po sestavi, morfologiji in barvi. Vzorci so bili preiskani z optično in elektronsko mikroskopijo ter rtg-difrakcijo. Preiskave so pokazale, da so v zgornjih in zavetnejših delih spomenika, kjer jih deževnica ni izpirala, nastale sadrine, v spodnjem delu vodnjaka, ki je v dometu dotoka vode, pa so se odlagale kalcitne obloge. V nekaterih vzorcih, odvzetih na mestih, ki so bila v dometu vodnega curka, so bili opazni mikroorganizmi, predvsem gre za endolitske modrozelene cepljivke in zelene alge.

Review paper

Key words: black crusts, Carrara marble, Robba's fountain, deterioration
Ključne besede: črne obloge, carrarski marmor, Robbov vodnjak, propadanje

Introduction

Stones, used in the construction of buildings and monuments, eventually change due to interaction of the stone surface with various environmental factors to which it is subjected. The form and intensity that stone deterioration takes, depends on environmental factors and duration of exposure. On stone surfaces different patinas, efflorescence, soiling of particles from the atmosphere and crusts may occur. These encrustations are the results of either inorganic or organic factors or an interaction of both. They commonly occur as a synchronous activity of different processes, for example dissolution or oxidation of minerals, soiling from the atmosphere, etc. Nevertheless, several biological factors and consequences of some previous restoration interventions could be involved in the process [1]. Encrustations on stone surfaces may differ in morphology and composition, which influences the appearance of the colour.

The formation of black crusts on stone monuments is an important process in stone deterioration. Black crusts occur due to various chemical–physical reactions between stone surfaces and different environmental factors. The most important factors in crust formation are atmospheric pollution and the presence of moisture. Apart from the aesthetical appearance, which is normally unacceptable, such crusts may house various microorganisms that can contribute to the stone degradation [2–4]. Total carbon, present in crusts, has a carbonate and non-carbonate fraction. The non-carbonate fraction includes two different components, organic carbon of biogenic and anthropogenic origin and elemental carbon that could originate from biogenic or anthropogenic sources [5, 6]. The tendency in restoration practice is to remove these crusts by the appropriate cleaning method. For that reason, a detailed characterization is required to determine the causes and mechanisms of black crust formation, to enable the choice of an appropriate cleaning method and prevent their further formation [7–13]. Precise characterization is important especially in the case of laser cleaning [6, 14–19].

Robba's Fountain, the Fountain of the Three Carniolian Rivers, is one of the most important Baroque monuments in Ljubljana, constructed in 1751 (Figure 1). Elements of the monument consist of four different natural stones; the architectural part is made of two different Slovenian limestones and conglomerates, while the three statues are sculptured of Carrara marble. Owing to accelerated deterioration processes, affecting the monument especially in the last years, it has been decided by conservators that the fountain should be relocated into a museum.

The previous removal of black crusts was carried out in restoration interventions in 1983 [20]. Since then new crusts have formed, differing in composition, morphology and colour. As part of a broader conservation–restoration project, representative samples from Carrara marble statues were taken in

Figure 1. Marble statuary of Robba's Fountain with marked locations of taken samples; Photo: Valentin Benedik, fotodocumentation of Restoration Centre
Slika 1. Kipi Robbovega vodnjaka iz carrarskega marmorja z označenimi lokacijami odvzetih vzorcev; Foto: Valentin Benedik, fotodokumentacija Restavratorskega centra

2006 to characterize and study the marble deterioration.

Experimental

With permission from the current authorities, representative samples of black crusts from each of the three marble statues shown in Figure 1 were collected. Eleven samples were taken from different locations of the marble surfaces. Crusts were carefully detached from the stone surface. On some areas it was possible to take crusts with stone substrate.

Samples were studied with optical microscopy, using a standard petrographic microscope NIKON eclipse E600 pol and scanning electron microscopy (SEM JEOL 5600 LV with X-ray energy microanalysis).

Mineral composition of an average powdered sample was determined by X-ray powder diffraction, using X-ray diffractometer Philips PW3710 with Cu Kα radiation and graphite secondary monochromator. Data were collected at a voltage of 40 kV and current of 30 mA in the range of 2–70° (2θ), with a speed of 3 °/min. Mineral phases were determined using the computer program Philips X'Pert software.

Results and discussion

Macroscopical description

It is possible to distinguish four types of crust, by morphology and colour, on the sculptures: In the upper rough parts of the sculptures poorly adhesive deposits due to soiling by particles from the atmosphere (type 1: sample RO75) are present. Compact black crust, tracing (type 2: RO66, RO67, RO69, RO70 and RO71, RO73) and changing (type 3: sample RO65) the surface and white crusts (type 4: RO63), changing the surface, occur within reach of the fountain water, mostly on lower parts of the sculptures. Black crusts (type 2: samples RO68, RO76), tracing the surface, are also present on sheltered areas of upper parts of the sculptures.

Mineral composition

On the monument it is possible to distinguish two types of crusts by mineral composition. In general, one type of crust consists of gypsum, while the other consists of calcite (Table1). Both types are described in detail in the following text.

Table 1. Mineral composition of samples, determined by optical, electron microscopy and X-ray powder diffraction

Tabela 1. Mineralna sestava vzorcev, določena z optično in elektronsko mikroskopijo v presevni in odsevni svetlobi, s SEM in z rentgensko difrakcijo

Sample	Prevailing mineral
RO63	micritic calcite
RO65	micritic calcite
RO66	laminated calcite
RO67	laminated calcite
RO68	gypsum
RO69	laminated calcite
RO70	laminated calcite
RO71	micritic calcite
RO73	laminated calcite
RO75	gypsum and calcite crystals
RO76	gypsum

Calcite crust

On the lower parts of the monument, which are within range of the fountain water, crusts are predominately composed

of calcite (samples RO63, RO65, RO66, RO67, RO69, RO70, RO71, RO73). These crusts occur as well-known calc-sinters [21] with parallel-banded layers. The majority of crusts are laminated (type 2: samples RO66, RO67, RO69, RO70, RO71, RO73) probably due to seasonal precipitation of calcite from water during the summer period, when water circulates in the fountain. They are also known as microstromatholitic carbonate crusts [22]. Crusts consist of white laminas of calcite crystals, elongated perpendicular to the stone surface, which alternate with black laminas rich in silica (Figure 2). Silica-rich laminas equate to winter time, when water circulation in the fountain is absent and soiling of combustion particles occurs. Silica is probably derived from ash released by industrial sources, which is for the most part composed of silicates. Thus, laminas of crust alternate in colour and composition according to the season of the year. Under the laminated calcite layers a micritic zone is present, which represents the deteriorated stone surface (Figure 2a and 2b). Grains of marble are micritized and deeper decohesion of marble grains is present. An unreacted zone of marble is beneath this zone.

In some areas, lamination of calcite crusts is absent; crusts are less dense and respectively more porous (type 3 and type 4: samples RO65, RO63). They consist of fine-grained calcite – micrite. Several calcite and dolomite grains are entrapped and form in areas with inconstant water motion.

During calcite precipitation, soiling from the atmosphere occurs as well, i.e. soiling of anthropogenic particles, which are entrapped in crusts and also result in the black colour of the crust. Calcite crusts contain spherical aerosols, which are rich in iron and chromium (Figure 3). Lefevre and Ausset [23] reported that atmospheric particles could originate from anthropogenic sources (ash, dust rich in Fe and Si-Al, glass particles), sea (halite), terigene sources (calcite, gypsum, alumosilicates) and biogenic sources (spore, pollen). The black colour is the result of mainly ash particles and dust [24–26]. These particles often contain metal oxides, which catalyze the oxidation of SO_2 and consequently crust formation [24]. In fuel combustion various black carbonaceous particles such as ash and organic matter are emitted. Diesel engines especially are an enormous source of ash. The main component of ash, produced as waste material in burning coal is silica, while liquid fuels emit porous carbonaceous particles, i.e. ash [27]. As all combustion sources produce black carbon particles, this is the reason why the stone surfaces blacken.

Gypsum crust

Crust on the upper parts of the statues, above the range of the fountain water, consists of gypsum (samples RO68, RO75 and RO76). Gypsum crusts occur in sheltered areas of the statues that are not exposed to rain water. Crusts are present as compact black crusts, tracing the surface (type 2: samples RO75 and RO 76) or poorly adhesive deposits (type 1: sample RO75). Gypsum crystals fall in the range of 50 μm to 100 μm (Figure 4). Between crystals several aerosols are present. Since soiling of atmospheric particles rich in iron, nickel or chromium could catalyze SO_2 oxidation, which is present on stone surfaces, these aerosols contribute to enhanced stone deterioration when the process is followed by soluble salt crystallization, for example

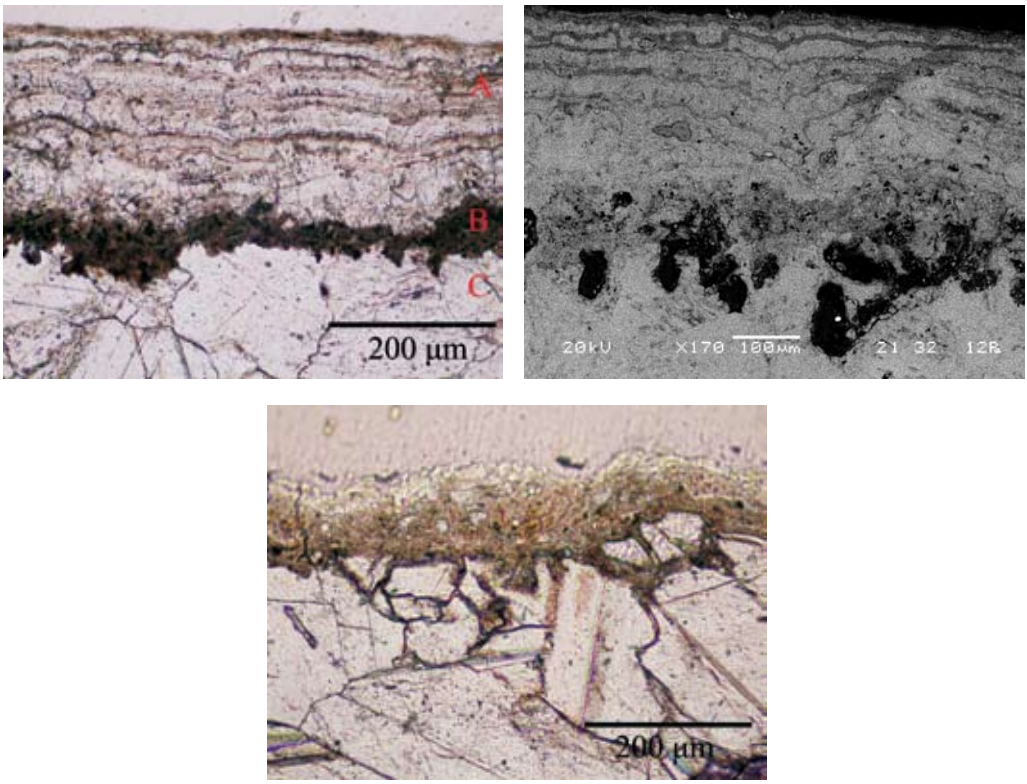

Figure 2. A transverse profile of weathered marble (sample RO 70), the laminated calcite crust, where white laminae of calcite crystals alternate with black siliceous laminae (zone A), as seen under transmitted light (a) and electron microscope (b). Crust is followed by micritized zone (zone B), underneath unaltered marble is present (zone C). Under the micritized zone etched calcite grains of marble are noticed. (c) Decohesion between calcite grains and etched calcite crystals. Transmitted light, crossed polars.

Slika 2. Profil preperele kamnine (vzorec RO70), cona A: laminirana kalcitna obloga. Izmenjujejo se svetle lamine kalcitnih kristalov ter temne lamine, bogate s silicijem. Cona B: mikritizirana površina marmorja, cona C: nespremenjen marmor; a) presevna svetloba, prekrižani nikoli, b) SEM, BSE. c) Dekohezija med kalcitnimi zrni in najedkani kalcitnimi kristali. Presevna svetloba, prekrižani nikoli.

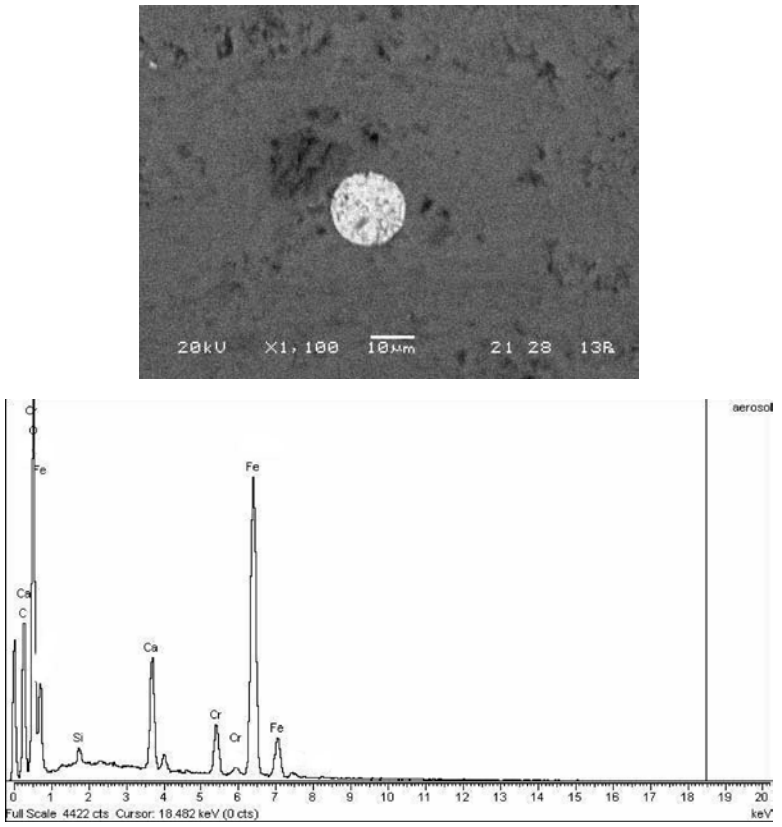

Figure 3. a) Aerosol, rich in Fe and Cr, SEM, BSE; b) chemical composition of aerosol, EDX
Slika 3. a) Aerosol, bogat z železom in kromom, SEM, SE; b) kemična sestava aerosola, EDS

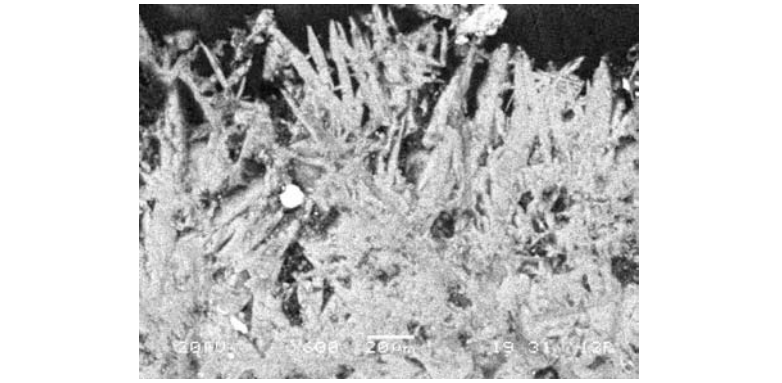

Figure 4. Crystals of gypsum in sample RO68; SEM, BSE.
Slika 4. Kristali sadre. Vzorec RO 68; SEM, BSE.

gypsum formation [9–10, 26].

The process of sulphation is one of the most important reactions and contributes to calcium carbonate deterioration [13] and is already a well-known phenomenon [7, 28–30]. A crust of gypsum is formed as a result of the reaction between water, calcite and sulphuric acid. As gypsum crust is more soluble compared to calcium carbonate substratum [31], it remains on sheltered zones of the monument, while on zones exposed to rain it is washed out. The process of sulphation continues under the crust. A higher solubility of gypsum compared to calcite enables water infiltration and processes of recrystallisation, but favours water retention under the crust as well [13, 32].

Presence of microorganisms

Investigation of samples with an optical microscope showed the presence of cyanobacteria, green algae and lichen (Table 2). Endolitic, unicellular or filamentous cyanobacteria, green algae and lichens colonize lower parts of the fountain, which are within range of the circulating water. Unicellular green algae are, in some places, already subjected to the process of fossilization. On some samples of calcite crusts, microorganisms and the consequences of their activity are observable. These microorganisms are present on the surface of calcite crusts, in calcite crusts or they penetrate into the marble substrate. Filamentous cyanobacteria and green algae in sample RO69 form crust coating under the laminated calcitic crust (Figure 5a). Filaments are perpendicular to the stone surface, penetrating into the marble. By penetrating between the marble grains and by etching crystals in the form of biopitting they contribute to the physical and chemical deterioration of marble (Figure 5b).

Sarro et al. [33] reported that filamentous green algae are frequently present in fountains. It was reported [34] that cyanobacteria and chlorophycea comprise the two of most common groups of algae found on building stones, as endolithic habitats provide good growth conditions in otherwise harsh environments. Cyanobacteria and algae are normally pioneers in colonizing stone surfaces because they are autothrophic organisms [22, 35]. Thus, organic matter, necessary for the growth of heterotrophic organism is ensured by dead cells of autotrophic organisms.

The presence of algae on stone surfaces favours carbonatization as a result of the process of respiration and fixation of CO_2. Although all taxonomic groups of algae and cyanobacteria are capable of contributing to carbonate precipitation, this is especially seen in the case of green algae and cyanobacteria [33, 36]. On the other hand, organic acids, which are produced in their metabolic processes, could dissolute minerals.

Table 2. Groups of microorganisms, present in crusts

Tabela 2. Skupine mikroorganizmov v oblogah

Sample	Microorganisms
RO63	lichen on calcite crust surface
RO65	-
RO66	cyanobacteria
RO67	cyanobacteria and green algae
RO68	-
RO69	cyanobacteria and green algae
RO70	-
RO71	cyanobacteria and green algae
RO73	cyanobacteria and green algae
RO75	-
RO76	-

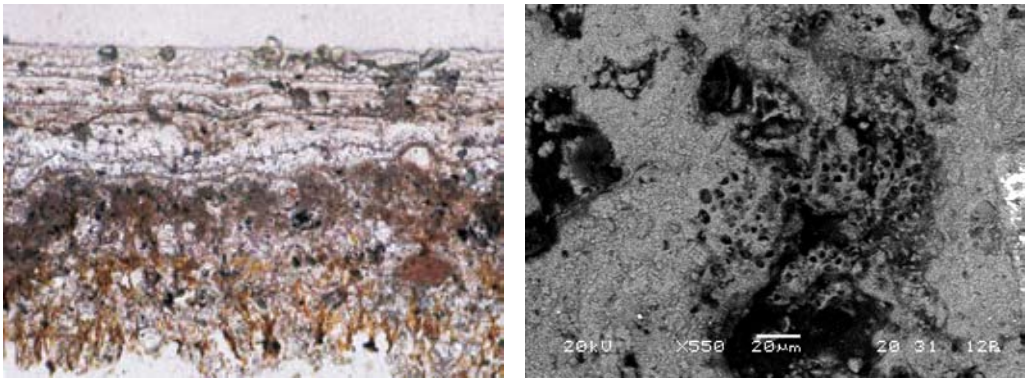

Figure 5. a) Filamentous algae and cyanobacteria under laminated calcite crust. Sample RO69, transmitted light, parallel polars; b) Effect of microbial activity in the form of biopitting, sample RO70, SEM, SE

Slika 5. a) V spodnjem delu slike pod laminirano kalcitno oblogo so vidne filamentne alge. Vzorec RO 69, presevna svetloba, vzporedni nikoli; b) posledice delovanja mikroorganizmov v obliki luknjičastega raztapljanja zrn kalcita – biopiting; vzorec RO 70, SEM, BSE

Deterioration of marble

The deterioration can be expressed in a simplified form as a function of the principal parameters only. Distinction can thus be made between parameters whose effect is decidedly predominant and those whose incidence is practically negligible. The surface of Carrara marble is subjected to various processes of deterioration. In some areas a micritized zone (Figure 2a) is present, which is a result of several factors, probably also due to activity of microorganisms. The role of microorganisms in micritizing processes is reported by Kabanov [37]. Mineral dissolution and decohesion between calcite crystals is easily observable (Figure 2c), while on the surfaces different crusts occur. Formation of different crusts and biofilms is caused by various mechanisms of marble deterioration [38]. Crusts have a different thermal expansion compared to marble substrate. In repeated heating–cooling cycles, tension between the stone and crust occurs, which leads to mechanical breakdown and disintegration of the stone. As can be seen, crusts can represent a habitat for various microorganisms, which with their metabolic products and growth affect and cause the structure of marble to deteriorate. Chemical weathering is induced due to excreted metabolic products, such as organic acids, proteins, pigments and sugars [39]. Fissures in the marble are enhanced due to swelling caused by water absorption and growth of the microorganisms present. It has been reported [22], that biodeterioration of fountains is mainly caused by the activity of microalgae, which are generally pioneers in the processes of biodeterioration. Their action is direct and also indirect, since they promote other mechanisms of deterioration and the growth of other communities.

Erosion of marble surfaces in areas where crusts are not present is enormous due to acid rain.

Conclusions

The statues of Robba's Fountain, made of Carrara marble, are covered by crusts which differ in composition, morphology and colour. Results have demonstrated that two different crusts can be distinguished by mineral composition. In sheltered areas of upper parts of the statues, gypsum crusts occur, while calcite crusts are present within the range of water in lower parts of the statues. The marble surface is subjected to process of micritization of crystals, which increases the specific surface of the grains and consequently the reactive surface. Above that zone, various crusts are formed.

The lower parts of the fountain, which is within water range, colonize endolitic, unicellular or filamentous green, cyanobacteria and lichens. These microorganisms are present in calcite crusts or they penetrate into the marble substrate. Continuous exposure to moisture enables the existence and growth of microorganisms on the marble, which contribute to its chemical and physical deterioration by micritization of the marble surface and calcite dissolution. On the other hand, they could contribute to the calcium carbonate precipitation from the fountain water and thus calcite crust formation.

Crust formation is cyclic with regard to season and as a consequence to a period of the marble being constantly wet from the fountain's water and to the quantity of atmospheric particle soiling (dust, ash), which blackens the marble surface. The main factors resulting in crust formation are atmospheric pollution and circulation of the fountain's water. Calcite crust could also function as a protection of the marble surface, since calcite precipitation prevents dissolution of marble and thus erosion of the statues.

Detailed characterization enables an appropriate cleaning method to be chosen for crust removal and to prevent further formation.

Acknowledgements

This research is part of the Slovenian conservation-restoration project 'Robba´s fountain – Fountain of three Carniloian Rivers'. This research was financially supported by Slovenian Research agency, contract number 3211-05-000545. The authors would like to thank Mr Alexandre François from LRMH in France for identification of microorganisms.

Povzetek

Površina kamnine, uporabljene pri gradnji spomenikov in stavb, se z leti spreminja zaradi interakcije kamnine z okolico, s katero je v neposrednem stiku. Vrsta in jakost spremembe sta odvisni od časa trajanja stika in od medija, s katerim je kamnina v stiku. Na površini kamnine nastajajo različne patine, oprhi in celo kompaktne skorje. S skupnim imenom jih označujemo kot obloge. Lahko so anorganskega ali organskega izvora ali kombinacija obeh. Obloge pogosto nastanejo zaradi hkratnega delovanja različnih procesov, kot npr. raztapljanja ali oksidacije kamnite podlage, usedanja delcev iz atmosfere itd. Po navadi so posledica kemično-fizikalnih procesov med površino kamnine in okoljskimi dejavniki. Nastanejo tudi zaradi številnih bioloških

dejavnikov ter kot posledica preteklih restavratorskih posegov (VAZQUES-CALVO et al., 2007). Med seboj se lahko ločijo tako po morfologiji kot po sestavi, ki vpliva tudi na njihovo barvo.

Črne obloge, ki jih najdemo na spomenikih iz naravnega kamna, so s stališča konservatorsko-restavratorske stroke estetsko moteče, škodljive za samo kamnino in jih je treba z najustreznejšo metodo odstraniti. V ta namen jih je treba natančno okarakterizirati ter ugotoviti mehanizem njihovega nastanka, da bi jih lahko primerno odstranili in preprečili njihovo nadaljnje nastajanje (VERGES-BELMIN, 1993, MORPOULOU et al., 1998, AUSSET&LEFEVRE, 2000, BUGINI et al., 2000, MARAVELAKI-KALAITZAKI, 2001, MARAVELAKI-KALAITZAKI, 2005, GIAVERINI et al., internet). Natančna karakterizacija je pomembna predvsem v primeru odstranjevanja oblog z laserskim čiščenjem (PINI et al., internet, CATALANO et al., internet, MARAVELAKI-KALAITZAKI et al., 1999, MARAKIS et al., 2000, BROBLET et al., 2003, MARAKIS et al., 2003, POTGIETER-VERMAAK et al., 2005).

Trije kipi Robbovega vodnjaka »Vodnjak treh kranjskih rek« so izklesani iz carrarskega marmorja. Črne obloge na njih so bile nazadnje odstranjene pri restavratorskih posegih leta 1983 z mikropeskanjem. V tem času so nastale nove obloge, ki se med seboj razlikujejo po sestavi, morfologiji in barvi. Kot del konservatorsko-restavratorskega projekta »Robbov vodnjak – Vodnjak treh kranjskih rek« smo v letu 2006 odvzeli značilne vzorce oblog na kipih iz carrarskega marmorja za njihovo karakterizacijo ter študij propadanja te kamnine v mestnem okolju.

Na kipih iz carrarskega marmorja po morfologiji lahko ločimo štiri tipe oblog. Gre za črne usedline atmosferskih delcev, ki so slabo vezane na kamnito površino in se pojavljajo v zgornjih delih kipa na hrapavih površinah. V spodnjem delu kipov, ki so bili v dosegu tekoče vode vodnjaka, so bile kompaktne temne obloge, ki sledijo reliefu kamnine, in temne ter svetle obloge, ki spreminjajo relief kamnine. Kompaktne temne obloge, ki sledijo reliefu kamnine, so bile tudi v zgornjih delih kipov v zavetnejših predelih.

Na spomeniku po sestavi ločimo dva tipa črnih oblog, po morfologiji pa vsaj štiri različne vrste oblog. Površina kamnine prepereva. Pojav označujemo kot mikritizacija kamnine. Pri tem se specifična površina zrn poveča in s tem reaktivna površina. Nad to mikritizirano cono pa nastajajo različne vrste oblog. V zgornjih predelih spomenika, kjer je marmor v stiku z atmosfero, nastajajo sadrine obloge, v spodnjem delu vodnjaka, ki je v dometu dotoka vode, pa se odlagajo kalcitne obloge. V nekaterih vzorcih, odvzetih z mest na vodnjaku, ki so bili v dometu vodnega curka, so bili opazni mikroorganizmi, predvsem gre za endolitske modrozelene cepljivke in zelene alge. Stalna izpostavljenost kamnine vlagi omogoča obstoj in rast organizmov v kamnini, ki povzročajo in pospešujejo propadanje – mikritizacijo in kasnejše raztapljanje kamnine. Rast oblog je ciklična glede na letni čas in/oz. glede na obdobja stalne omočenosti kamnine z vodo iz vodnjaka ter glede na količino atmosferskih delcev (prah, pepel), ki se vgrajujejo v obloge in jih pri tem obarvajo. Glavni dejavniki nastajanja oblog so onesnaženost ozračja ter voda. Kalcitne obloge lahko delujejo tudi kot zaščita površine, saj nalaganje kalcita iz vode preprečuje raztapljanje kamnine in s tem erozijo kipov.

Natančna analiza sestave oblog in vzrokov za njihovo nastajanje omogoča primeren izbor učinkovite metode čiščenja in odpravljanje vzrokov propadanja. Pri izbiri najučinkovitejše metode moramo upoštevati določena merila, ki bi pripomogla k izboljšanju stanja objekta. Metoda, ki jo izberemo, ne sme povzročiti neposredne ali posredne škode na kamniti površini.

References

[1] Vazquez-Calvo, C., Alvarez De Buergo, M., Fort, R. & Varas, M. J. (2007): Characterization of patinas by means of microscopic techniques. *Materials characterization*, pp. 119–1132.

[2] Diakumaku, E., Gorbushina, A. A., Krumbein, W. E., Panina, L. & Soukharjevski, S. (1995): Black fungi in marble and limestone - an aesthetical, chemical and physical problem for the conservation of monuments. *The Science of the Total Environment 167*, pp. 295–304.

[3] Potgieter-Vermaak, S., Godoi, R., Potgieter, J. H., Van Grieken, R. & Castillejo, M.: Chemical characterisation of the black crust and laser cleaned surfaces of limestone from a cathedral in Seville, Spain, with Micro-Raman spectroscopy. http://www.publish.csiro.au/?act=view_file&file_id=SA0402289.pdf.

[4] Turtura, G. C., Perfetto, A., Lorenzelli, P. (2000): Microbial investigation on black crusts from open-air stone monuments of Bologna (Italy). *New Microbiol. 23*, 2, pp. 207–28.

[5] Gavino, M., Hermosin, B., Verges-Belmin, V., Nowik, W. & Saiz-Jimenez, C. C. (2004): Composition of the black crusts from the Saint Denis Basilica, France, as revealed by gas chromatography-mass spectroscopy. *Journal of Separation Science*, 27, 7–8, pp. 513–523.

[6] Potgieter-Vermaak, S. S., Godoi, R. H. M., Van Grieken, R., Potgieter, J. H., Oujja, M. & Catillejo, M. (2005): Micro-structural characterization of black crusts and laser cleaning of building stones by micro-Raman and SEM techniques. *Spectrochimica Acta Part A,* 61, pp. 2460–2467.

[7] Verges-Belmin, V. (1994): Pseudomorphism of gypsum after calcite, a new textural feature accouting for the marble sulphation mechanism. *Atmospheric Environment*, 28, 2, pp. 295–394.

[8] Moropoulou, A., Bisbikou, K., Torfs, K., Van Grieken, R., Zezza, F. & Macri, F. (1998): Origin of weathering crusts on ancient marbles in industrial atmosphere. *Atmospheric Environment*, 32, 6, pp. 967–982.

[9] Ausset, P. & Lefevre, R. A. (2000): Early mechanisms of development of sulphated black crusts on carbonate stone. *9th International congress on deterioration and conservation of stone.* Venice, pp. 265–273.

[10] Bugini, R., Laurenzi Tabasso, M., Realini, M. (2000): Rate of for-

mation of black crusts on marble. A case study, *Journal of Cultural Heritage*, pp. 11–116.

[11] MARAVELAKI-KALAITZAKI, P., ANGLOS, D., KILIKOGLOU, V. & ZAFIROPULOS, V. (2001): Compositional characterization of encrustation on marble with laser induced breakdown spectroscopy, *Spectrochimica Acta Part B,* 56, pp. 887–903.

[12] MARAVELAKI-KALAITZAKI, P. (2005): Black crusts and patinas on Pentelic marble from the Parthenon and Erechtheum (Acropolis, Athens): charactarization and origin. *Analytica chimica acta*, 532, pp. 187–198.

[13] GIAVARINI, C., INCITTI, M., SANTARELLI, M. L., NATALINI, R. & FUROHOLT, V.: A nonlinear model of sulphation of calcium carbonate stones: numerical simulations and preliminary laboratory assessments. http://www.iac.rm.cnr.it/~natalini/abCIpre.pdf.

[14] PINI, R., SIANO, S., FABIANI, F., SALIMBENI, R., GIAMELLO, M., SABATINI, G.: Laser cleaning of stones: basic research and development of an optimised laser system. http://www.litosonlin.com/articles/47/art4703.html.

[15] CATALANO, I. M., ANDIRANI, S. E., LAVIANO, R., VONA, F., DAURELIO, G. & STEA, G. (2005): The influence and use of the SFR or LQS Nd:YAG laser beam on the cleaning and restoration of two diverse church facades. XV International Symposium on Gas Flow, Chemical Lasers, and High-Power Lasers. Edited by Kodymova, Jarmila. Proceedings of the SPIE, Vol. 57, pp. 940–945.

[16] MARAVELAKI-KALAITZAKI, P., ZAFIROPULOS, V. & FOTAKIS, C. (1999): Excimer laser cleaning of encrustation on Pentelic marble: procedure and evaluation of the effects. *Applied Surface Science*, 148, pp. 92–104.

[17] MARAKIS, G., MARAVELAKI, P., ZAFIROPULOS, V., KLEIN, S., HILDENHAGEN, J. & DICKMAN, K. (2000): Investigations on cleaning of black crusted sandstone using different UV-pulsed lasers. *Journal of Cultural Heritage*, 1, pp. 61–64.

[18] BROMBLET, P., LABOURE, F. & ORIAL, G. (2003): Diversity of the cleaning procedures including laser for the restoration of carved portals in France over the last 10 years, *Journal of Cultural Heritage*, 4 , pp. 17–26.

[19] MARAKIS, G., POULI, P. P, ZAFIROPULOS, V. & MARAVELAKI-KALAITZAKI, P. (2003): Comparative study on the application of the 1st and the 3rd harmonic of a Q-switched Nd:YAG laser system to clean black encrustation on marble. *Journal of Cultural Heritage*, 4, pp. 83–91.

[20] VUKOVIĆ, M. (1985): Conservation, restoration, reconstruction and realisation of the »Fountain of three Carniolian Rivers«, Ljubljana 1971–1985. *In* 5th *International congress on deterioration and conservtion of stone.* Lausanne, 1, pp. 1059–1062.

[21] ARNOLD, A. & KUENG, A. (1985): Crystalization and habits of salt efflorescences on walls I. *In 5th International congress on deterio-*

ration and conservation of stone, Lausane, 2, pp. 1059–1062.

[22] Peraza Zurita, Y., Cultrone, G., Sanchez Castillo, S., Sebastian, E. & Bolivar, F. C. (2005): Microalgae associated with deteriorated stonework of the fountain of Bibatauin in Granada, Spain. *International Biodeterioration & Biodegradation*, 55, pp. 55–60.

[23] Lefevre, R. A. & Ausset, P. (2004): Recent air pollution changes in Paris recorded on the Apollo statue in the Cour carree, Louvre Palace. In *6th International Symposium on the Conservation of Monuments in the Mediterranean Basin*, Lisbon, pp. 166–170.

[24] Price, C. A. (1996): Stone conservation: an overview of current research. USA: The J. Paul Getty Trust.

[25] Ausset, P. & Lefevre, R. A. (2000): Past air pollution recordings on stone monuments: the heads of the kings of Juda statues from Notre-Dame Cathedral (Paris). In *9th International congress on deterioration and conservation of stone*. Venice, pp. 265–273.

[26] Grossi, C. M., Esbert, R. M., Diaz-Pache, F. & Alonso, F. J. (2003): Soiling of building stones in urban environments. *Building and Environment*. pp. 147–159.

[27] Cachier, H. & Sarda-Esteve, R.: Atmospheric aerosols, black carbon particles and the soiling of European buildings. http://www.heritage.xtd.pl/pdf/full_cachier.pdf.

[28] Aberg, G., Stijfhoorn, D. E., Iden, K. & Lofvendahl, R. (1999): Carbon isotope exchange during calcite sulphation. *Atmospheric Environment,* 33, pp. 1399–1409.

[29] Lal Gauri, K. & Bandyopadhyay, J. K. (1999): Carbonate stone. Chemical behavior, durability and conservation. A Wiley interscience publication. p. 2845.

[30] Malaga-Starzec, K., Panas, I. & Lindquist, O. (2004): Model study of initial adsorption of SO_2 on calcite and dolomite, *Applied surface science*, pp. 82–88.

[31] Striegel, M. F., Bede Guin, E., Hallet, K., Sandoval, D., Single, R., Knox, K., Best, F., Fornea, S. (2003): Air pollution, coatings, and cultural resources. *Progress in Organic Coatings*. pp. 281–288.

[32] Thomachot, C. & Jeanette, D. (2000): Petrophysical properties modifications of Strassbourgs cathedral sandstone by black crusts, In 9th International congress on deterioration and conservation of stone. Venice, pp. 265–273.

[33] Sarro, M. I., Garcia, A. M., Rivalta, V. M., Moreno, D. A. & Arroyo, I. (2006): Biodeterioration of the Lions Fountain at the Alhambra Palace, Granada (Spain). *Building and Environment*, 41, pp. 1811–1820.

[34] Ortega-Calvo, J. J., Arino, X., Hernanderz-Marine, M. & Saiz-Jimenez, C. (1995): Factors affecting the weathering and colonization ofmonuments by phototrophic microorganisms. *The Science of Total Environment*, 167, pp. 329–341.

[35] Kumar, R. A. & Kumar, V. (1999): Biodeterioration of Stone in Trop-

ical Environments.

[36] GOLUBIČ, S. (1973): The relationship between lue-green algae and carbonate deposits. In: Carr, N. G., Whitten, B. A. (Eds.), The biology of Blue Green Algae. Blackwell, London, pp. 434–472.

[37] KABANOV, P., KABANOV, B. (2003): Products of micritization: evidences of microbial activity at and below the seafloor of the upper Moscovian epicontinental basin of central European Russia. In Proceedings of SPIE, Vol. 4939. Instruments, methods and missions fro Astrobiology V, Richard B. Hoover, Alexei Y. Rozanov, Jer H-Lipps, Editors, pp. 141–152.

[38] GU, J. D. (2003) Microbiological deterioration and degradation of synthetic polymeric materials: recent research advances. *International Biodeterioration and Biodegradation*, 52, pp. 69–91.

[39] ALLSOPP, D., SEAL, K. J. & GAYLORDE, C. C. (2004): Introduction to biodeterioration, Cambridge University Press, p. 252.

Author`s Index, Vol. 55, No. 4

Author`s Index, Vol. 55

RMZ Materials and geoenvironment
Contents
Volume 55, 2008/1, 2, 3, 4

55/1

55/2

55/3

55/4

INSTRUCTIONS TO AUTHORS

RMZ-MATERIALS & GEOENVIRONMENT (RMZ- Materiali in geookolje) is a periodical publication with four issues per year (established 1952 and renamed to RMZ-M&G in 1998). The main topics of contents are Mining and Geotechnology, Metallurgy and Materials, Geology and Geoenvironment.
RMZ-M&G publishes original Scientific articles, Review papers, Technical and Expert contributions (also as short papers or letters) **in English**. In addition, evaluations of other publications (books, monographs,...), short letters and comments are welcome. A short summary of the contents in Slovene will be included at the end of each paper. It can be included by the author(s) or will be provided by the referee or the Editorial Office.
**** Additional information and remarks for Slovenian authors:***
English version with extended »Povzetek«, and additional roles (in Template for Slovenian authors) ***can*** *be written. Only exceptionally the articles in the Slovenian language with summary in English will be published. The contributions in English will be considered with priority over those in the Slovenian language in the review process.*

Authorship and originality of the contributions. Authors are responsible for originality of presented data, ideas and conclusions as well as for correct citation of data adopted from other sources. The publication in RMZ-M&G obligate authors that the article will not be published anywhere else in the same form.

Specification of Contributions

Optimal number of pages of full papers is 7 to 15, longer articles should be discussed with Editor, but 20 pages is limit.
Scientific papers represent unpublished results of original research.
Review papers summarize previously published scientific, research and/or expertise articles on the new scientific level and can contain also other cited sources, which are not mainly result of author(s).
Technical and Expert papers are the result of technological research achievements, application research results and information about achievements in practice and industry.
Short papers (Letters) are the contributions that contain mostly very new short reports of advanced investigation. They should be approximately 2 pages long but should not exceed 4 pages.
Evaluations or critics contain author's opinion on new published books, monographs, textbooks, exhibitions...(up to 2 pages, figure of cover page is expected).
In memoriam (up to 2 pages, a photo is expected).

Professional remarks (Comments) cannot exceed 1 page, and only professional disagreements can be discussed. Normally the source author(s) reply the remarks in the same issue.

Supervision and review of manuscripts. All manuscripts will be supervised. The referees evaluate manuscripts and can ask authors to change particular segments, and propose to the Editor the acceptability of submitted articles. Authors can suggest the referee but Editor has a right to choose another. **The name of the referee remains anonymous.** The technical corrections will be done too and authors can be asked to correct missing items. The final decision whether the manuscript will be published is made by the Editor in Chief.

The Form of the Manuscript

The manuscript should be submitted as a complete hard copy including figures and tables. The figures should also be enclosed separately, both charts and photos in the original version. In addition, all material should also be provided in electronic form on a diskette or a CD. The necessary information can conveniently also be delivered by E-mail.

Composition of manuscript is defined in the attached Template

The original file of Template is temporarily available on E-mail addresses:
peter.fajfar@ntf.uni-lj.si,
barbara.bohar@ntf.uni-lj.si

References - can be arranged in two ways:
- first possibility: alphabetic arrangement of first authors - in text: (Borgne, 1955),
or
- second possibility: [1] numerated in the same order as cited in the text: example[1]

Format of papers in journals:

Le Borgne, E. (1955): Susceptibilite magnetic anomale du sol superficiel. *Annales de Geophysique*, 11, pp. 399-419.

Format of books:

Roberts, J. L. (1989): Geological structures, *MacMillan*, *London*, 250 p.

Text on the hard print copy can be prepared with any text-processor. The electronic version on the diskette, CD or E-mail transfer should be in MS Word or ASCII format. **Captions of figures and tables** should be enclosed separately. **Figures (graphs and photos)** and tables should be original and sent separately in addition to text. They can

be prepared on paper or computer designed (MSExcel, Corel, Acad).
Format. Electronic figures are recommended to be in CDR, Al, EPS, TIF or JPG formats. Resolution of bitmap graphics (TIF, JPG) should be at least 300 dpi. Text in vector graphics (CDR, Al, EPS) must be in MSWord Times typography or converted in curves.
Color prints. Authors will be charged for color prints of figures and photos.
Labeling of the additionally provided material for the manuscript should be very clear and must contain at least the lead author's name, address, the beginning of the title and the date of delivery of the manuscript. In case of an E-mail transfer the exact message with above asked data must accompany the attachment with the file containing the manuscript.
Information about RMZ-M&G:
Editor in Chief prof. dr. Peter Fajfar (tel. ++386 1 4250-316) or
Secretary Barbara Bohar Bobnar, un. dipl. ing. geol. (++386 1 4704-630),
Aškerčeva 12, Ljubljana, Slovenia

or at E-mail addresses:
peter.fajfar@ntf.uni-lj.si,
barbara.bohar@ntf.uni-lj.si

Sending of manuscripts. Manuscripts can be sent by mail to the **Editorial Office** address:

- RMZ-Materials & Geoenvironment
  Aškerčeva 12,
  1000 Ljubljana, Slovenia

or delivered to:

- **Reception** of the Faculty of Natural Science and Engineering (for RMZ-M&G)
  Aškerčeva 12,
  1000 Ljubljana, Slovenia
- E-mail - addresses of Editor and Secretary
- You can also contact them on their phone numbers.

TEMPLATE

The title of the manuscript should be written in bold letters (Times New Roman, 14, Center)

NAME SURNAME[1], …. , & NAME SURNAME[X]
(TIMES NEW ROMAN, 12, CENTER)

[x]Faculty of ... , University of ... , Address…, Country, e-mail: ...
(Times New Roman, 11, Center)

THE LENGTH OF FULL PAPER SHOULD NOT EXCEED TWENTY (20, INCLUDING FIGURES AND TABLES) PAGES (OPTIMAL 7 TO 15), SHORT PAPER FOUR (4) AND OTHER TWO (2) WITHOUT TEXT FLOWING BY GRAPHICS AND TABLES.

Abstract (Times New Roman, Normal, 11): The text of the abstract is placed here. The abstract should be concise and should present the aim of the work, essential results and conclusion. It should be typed in font size 11, single-spaced. Except for the first line, the text should be indented from the left margin by 10 mm. The length should not exceed fifteen (15) lines (10 are recommended).

Key words: a list of up to 5 key words (3 to 5) that will be useful for indexing or searching. Use the same styling as for abstract.

INTRODUCTION (TIMES NEW ROMAN, BOLD, 12)

Two lines below the keywords begin the introduction. Use Times New Roman, font size 12, Justify alignment.
There are two (2) admissible methods of citing references in text:

1. by stating the first author and the year of publication of the reference in the parenthesis at the appropriate place in the text and arranging the reference list in the alphabetic order of first authors; e.g.:
   "Detailed information about geohistorical development of this zone can be found in: Antonijević (1957), Grubić (1962), ..."
   "… the method was described previously (Hoefs, 1996)"

2. by consecutive Arabic numerals in square brackets, superscripted at the appropriate place in the text and arranging the reference list at the end of the text in the like manner; e.g.:
   "... while the portal was made in Zope[3] environment."

Materials and methods (Times New Roman, Bold, 12)

This section describes the available data and procedure of work and therefore provides enough information to allow the interpretation of the results, obtained by the used methods.

Results and discussion (Times New Roman, Bold, 12)

Tables, figures, pictures, and schemes should be incorporated in the text at the appropriate place and should fit on one page. Break larger schemes and tables into smaller parts to prevent extending over more than one page.

Conclusions (Times New Roman, Bold, 12)

This paragraph summarizes the results and draws conclusions.

Acknowledgements (Times New Roman, Bold, 12, Center - optional)

This work was supported by the ****.

References (Times New Roman, Bold, 12*)*

In regard to the method used in the text, the styling, punctuation and capitalization should conform to the following:

FIRST OPTION - in alphabetical order

Casati, P., Jadoul, F., Nicora, A., Marinelli, M., Fantini-Sestini, N. & Fois, E. (1981): Geologia della Valle del'Anisici e dei gruppi M. Popera - Tre

Cime di Lavaredo (Dolomiti Orientali). *Riv. Ital. Paleont.*; Vol. 87, No. 3, pp. 391-400, Milano.

Folk, R. L. (1959): Practical petrographic classification of limestones. *Amer. Ass. Petrol. Geol. Bull.;* Vol. 43, No. 1, pp. 1-38, Tulsa.

SECOND OPTION - in numerical order

[1] Trček, B. (2001): *Solute transport monitoring in the unsaturated zone of the karst aquifer by natural tracers.* Ph.D. Thesis. Ljubljana: University of Ljubljana 2001; 125 p.

[2] Higashitani, K., Iseri, H., Okuhara, K., Hatade, S. (1995): Magnetic Effects on Zeta Potential and Diffusivity of Nonmagnetic Particles. *Journal of Colloid and Interface Science 172*, pp. 383-388.

Citing the Internet site:

CASREACT-Chemical reactions database [online]. Chemical Abstracts Service, 2000, updated 2.2.2000 [cited 3.2.2000]. Accessible on Internet: http://www.cas.org/CASFILES/casreact.html.

Povzetek (Times New Roman, 12)

A short summary of the contents in Slovene (up to 400 characters) can be written by the author(s) or will be provided by the referee or by the Editorial Board.

TEMPLATE for Slovenian Authors

The title of the manuscript should be written in bold letters (Times New Roman, 14, Center)

Naslov članka (Times New Roman, 14, Center)

Name Surname[1],…. , & Name Surname[X] (Times New Roman, 12, Center)
Ime Priimek[1], …, Ime Priimek[X] (Times New Roman, 12, Center)

[X]Faculty of ... , University of ... , Address…, Country; e-mail: ...
(Times New Roman, 11, Center)
[X]Fakulteta…, Univerza…, Naslov…, Država; e-mail: …
(Times New Roman, 11, Center)

THE LENGTH OF ORIGINAL SCIENTIFIC PAPER SHOULD NOT EXCEED TWENTY (20, INCLUDING FIGURES AND TABLES) PAGES (OPTIMAL 7 TO 15), SHORT PAPER FOUR (4) AND OTHER TWO (2) WITHOUT TEXT FLOWING BY GRAPHICS AND TABLES.
DOLŽINA IZVIRNEGA ZNANSTVENEGA ČLANKA NE SME PRESEGATI DVAJSET (20, VKLJUČNO S SLIKAMI IN TABELAMI), KRATKEGA ČLANKA ŠTIRI (4) IN OSTALIH PRISPEVKOV DVE (2) STRANI.

Abstract (Times New Roman, Normal, 11): The text of the abstract is placed here. The abstract should be concise and should present the aim of the work, essential results and conclusion. It should be typed in font size 11, single-spaced. Except for the first line, the text should be indented from the left margin by 10 mm. The length should not exceed fifteen (15) lines (10 are recommended).

Izvleček (TNR, N, 11): Kratek izvleček namena članka ter ključnih rezultatov in ugotovitev. Razen prve vrstice naj bo tekst zamaknjen z levega roba za 10 mm. Dolžina naj ne presega petnajst (15) vrstic (10 je priporočeno).

Key words: a list of up to 5 key words (3 to 5) that will be useful for indexing or searching. Use the same styling as for abstract.

Ključne besede: seznam največ 5 ključnih besed (3-5) za pomoč pri indeksiranju ali iskanju. Uporabite enako obliko kot za izvleček.

Introduction – Uvod (Times New Roman, Bold, 12)

Two lines below the keywords begin the introduction. Use Times New Roman, font size 12, Justify alignment. All captions of text and tables as well as the text in graphics must be prepared in English and Slovenian language.
Dve vrstici pod ključnimi besedami se začne Uvod. Uporabite pisavo TNR, velikost črk 12, z obojestransko poravnavo. Naslovi slik in tabel (vključno z besedilom v slikah) morajo biti pripravljeni v slovenskem in angleškem jeziku.

Figure (Table) X. Text belonging to figure (table)
Slika (Tabela) X. Pripadajoče besedilo k sliki (tabeli)

There are two (2) admissible methods of citing references – obstajata dve sprejemljivi metodi navajanja referenc:

1. by stating the first author and the year of publication of the reference in the parenthesis at the appropriate place in the text and arranging the reference list in the alphabetic order of first authors; e.g.:
1. z navedbo prvega avtorja in letnice objave reference v oklepaju na ustreznem mestu v tekstu in z ureditvijo seznama referenc po abecednem zaporedju prvih avtorjev; npr.:
   "Detailed information about geohistorical development of this zone can be found in: Antonijević (1957), Grubić (1962), ..."
   "… the method was described previously (Hoefs, 1996)"

or/ali

2. by consecutive Arabic numerals in square brackets, superscripted at the appropriate place in the text and arranging the reference list at the end of the text in the like manner; e.g.:
2. z zaporednimi arabskimi številkami v oglatih oklepajih na ustreznem mestu v tekstu in z ureditvijo seznama referenc v številčnem zaporedju navajanja; npr.;
   "... while the portal was made in Zope[3] environment."

Materials and methods (Times New Roman, Bold, 12)

This section describes the available data and procedure of work and therefore provides enough information to allow the interpretation of the results, obtained by the used methods.
Ta del opisuje razpoložljive podatke, metode in način dela ter omogoča zadostno količino informacij, da lahko z opisanimi metodami delo ponovimo.

Results and discussion – Rezultati in razprava (Times New Roman, Bold, 12)

Tables, figures, pictures, and schemes should be incorporated (inserted, not pasted) in the text at the appropriate place and should fit on one page. Break larger schemes and tables into smaller parts to prevent extending over more than one page.
Tabele, sheme in slike je potrebno vnesti (z ukazom Insert, ne Paste) v tekst na ustreznem mestu. Večje sheme in tabele je potrebno ločiti na manjše dele, da ne presegajo ene strani.

Conclusions – Sklepi (Times New Roman, Bold, 12)

This paragraph summarizes the results and draws conclusions.
Povzetek rezultatov in zaključki.

Acknowledgements – Zahvale (Times New Roman, Bold, 12, Center - optional)

This work was supported by the ……..
Izvedbo tega dela je omogočilo ……

References - Viri (Times New Roman, Bold, 12)

With regard to the method used in the text, the styling, punctuation and capitalization should conform to the following:
Glede na uporabljeno metodo citiranja referenc v tekstu upoštevajte eno od naslednjih oblik:

FIRST OPTION (recommended) – PRVA MOŽNOST (priporočena) – in alphabetical order (v abecednem zaporedju)

Casati, P., Jadoul, F., Nicora, A., Marinelli, M., Fantini-Sestini, N. & Fois, E. (1981): Geologia della Valle del'Anisici e dei gruppi M. Popera – Tre Cime di Lavaredo (Dolomiti Orientali). *Riv. Ital. Paleont.*; Vol. 87, No. 3, pp. 391-400, Milano.

Folk, R. L. (1959): Practical petrographic classification of limestones. *Amer. Ass. Petrol. Geol. Bull.;* Vol. 43, No. 1, pp. 1-38, Tulsa.

SECOND OPTION – DRUGA MOŽNOST - in numerical order (v numeričnem zaporedju)

[1] Trček, B. (2001): *Solute transport monitoring in the unsaturated zone of the karst aquifer by natural tracers.* Ph.D. Thesis. Ljubljana: University of Ljubljana 2001; 125 p.

[2] Higashitani, K., Iseri, H., Okuhara, K., Hatade, S. (1995): Magnetic Effects on Zeta Potential and Diffusivity of Nonmagnetic Particles. *Journal of Colloid and Interface Science 172*, pp. 383-388.

Citing the Internet site:
CASREACT-Chemical reactions database [online]. Chemical Abstracts Service, 2000, updated 2.2.2000 [cited 3.2.2000]. Accessible on Internet: http://www.cas.org/CASFILES/casreact.html.

Citiranje Internetne strani:
CASREACT-Chemical reactions database [online]. Chemical Abstracts Service, 2000, obnovljeno 2.2.2000 [citirano 3.2.2000]. Dostopno na svetovnem spletu: http://www.cas.org/CASFILES/casreact.html.

Povzetek – Summary (Times New Roman, 12)

An extended summary of the contents in Slovene (from one page to approximately 1/3 of the original article length).
Razširjeni povzetek vsebine prispevka v Angleščini (od ene strani do približno 1/3 dolžine izvirnega članka).

Skupina HSE

PREMOGOVNIK VELENJE

PREMOGOVNIK VELENJE

je pomemben in zanesljiv člen
v oskrbi Slovenije
z električno energijo.

Zavedamo se odgovornosti do
lastnikov, zaposlenih in okolja.

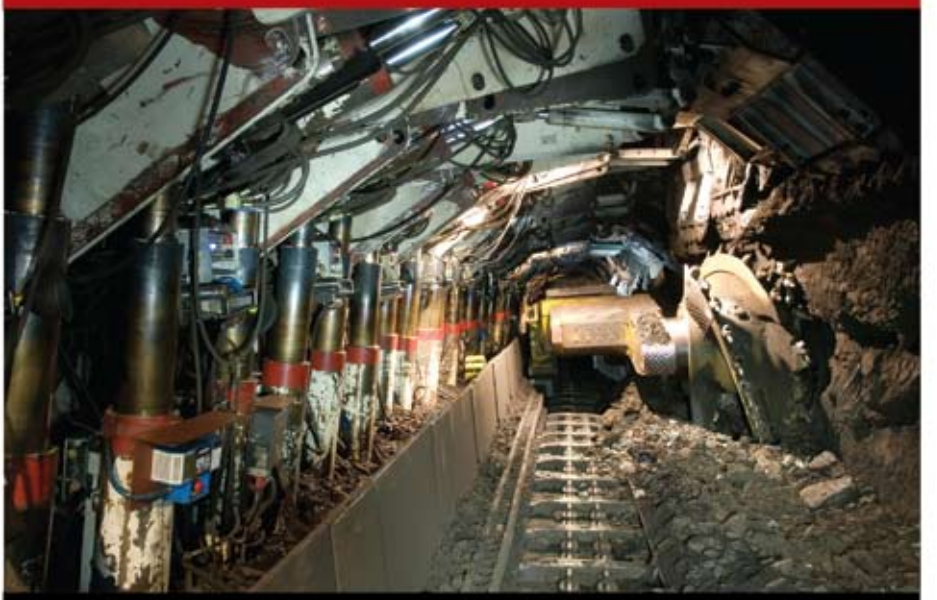

ČUT ZA PRIHODNOST


RTH

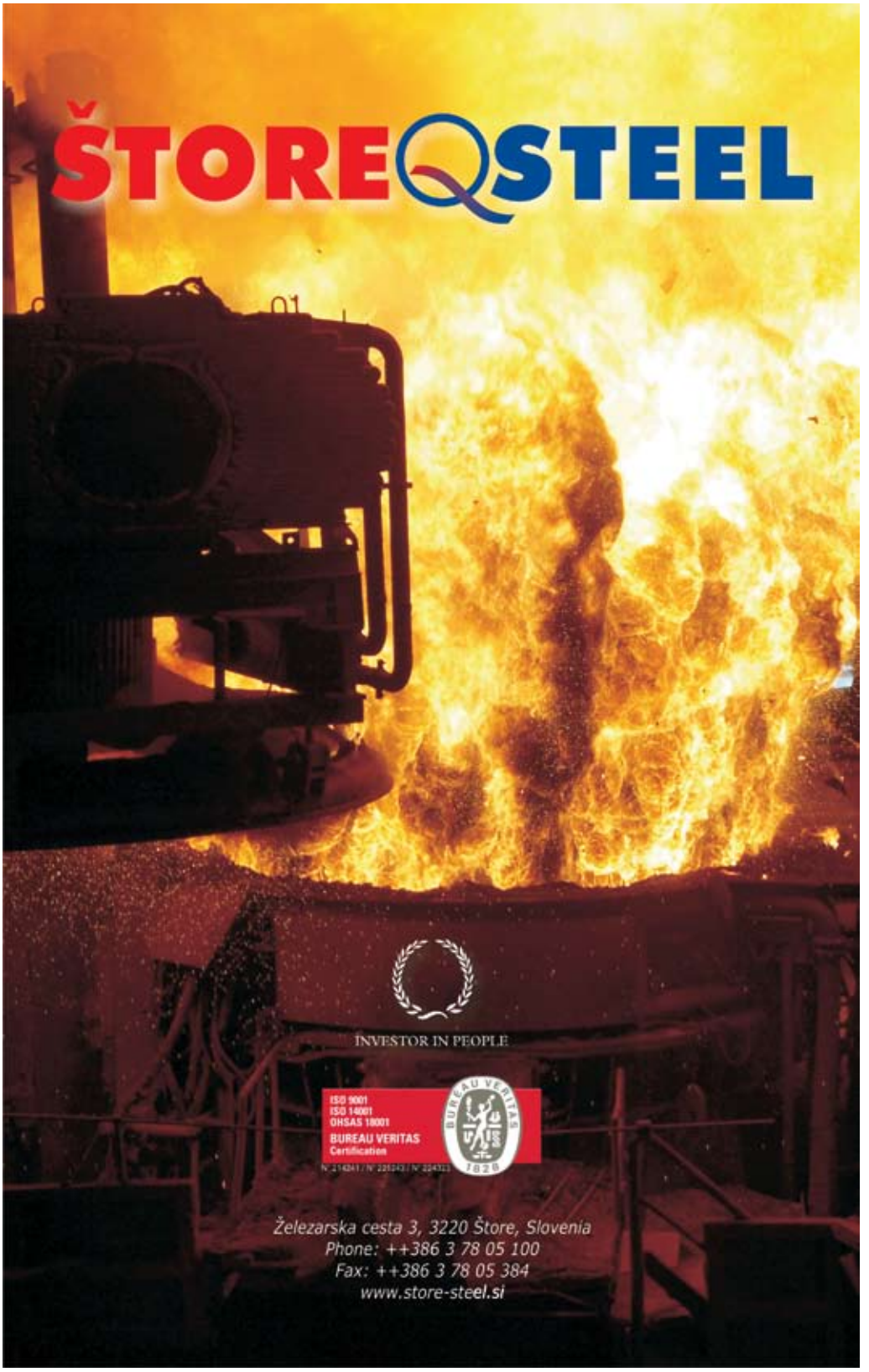
ŠTOREQSTEEL
INVESTOR IN PEOPLE
ISO 9001
ISO 14001
OHSAS 18001
BUREAU VERITAS
Certification
Železarska cesta 3, 3220 Štore, Slovenia
Phone: ++386 3 78 05 100
Fax: ++386 3 78 05 384
www.store-steel.si

prof. dr. Andrej Paulin

Tehniški metalurški slovar *(CD-ROM za WINDOWS)*

slovensko - angleško - nemški

Technical metallurgical dictionary *(CD-ROM for WINDOWS)*

Slovenian - English - German

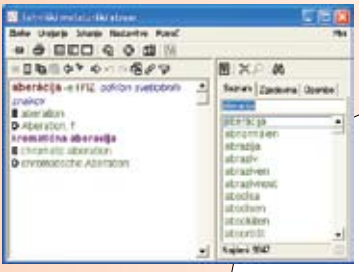

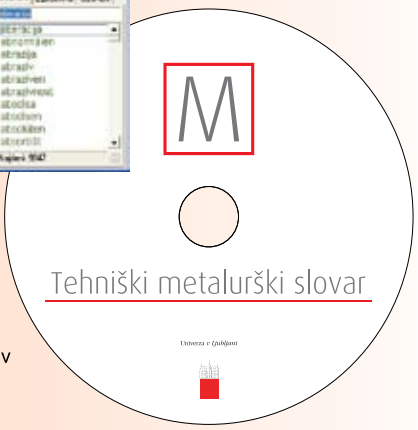

Več kot 10.000 gesel s področij:
- metalurgije,
- tehniških materialov,
- tehnike površin,
- analiznih metod,
- strojništva,
- kemije,
- elektrotehnike,
- ekologije,
- standardizacije,
- predpisov,
- ekonomike in
- uporabe računalništva pri tehnoloških postopkih.

Osnovne značilnosti oz. prednosti elektronske različice slovarja so preprost in izjemno hiter dostop do iskanega gesla, besede ali zveze, tudi pri zahtevnejših pogojih, ter velika prilagodljivost vmesnika uporabnikovim potrebam in željam. Slovar uporablja pregledovalnik ASP32 in je združljiv s številnimi drugimi slovarji v tem sistemu.

Cenik elektronskega slovarja:
Enouporabniška lokalna verzija - 58,00 EUR
5 licenc mrežna verzija - 390,00 EUR
10 licenc mrežna verzija - 535,00 EUR
20 licenc mrežna verzija - 680,00 EUR
30 licenc mrežna verzija - 825,00 EUR
40 licenc mrežna verzija - 970,00 EUR
50 licenc mrežna verzija - 1.115,00 EUR

Leto izdaje: 2007
Issued in 2007

Prices for the electronic dictionary:
Single user local version - 58,00 EUR
5 users network version - 390,00 EUR
10 users network version - 535,00 EUR
20 users network version - 680,00 EUR
30 users network version - 825,00 EUR
40 users network version - 970,00 EUR
50 users network version - 1.115,00 EUR

More than 10 000 technical terms on:
-metallurgy
-technical materials
-surface engineering
-analytical methods
-mechanical engineering
-chemical engineering
-electrical engineering
-environmental engineering
-standardization
-technical regulations
-economics, and
-computer engineering in technological processes

Basic characteristics or advantages, respectively, of electronic version of the dictionary is simple and very fast access to sought term, word or to complex term, also in more demanding conditions, and a great adaptability of the interface to user's needs and wishes. The dictionary uses ASP32 search system that is compatible to numerous other dictionaries in this system.

Za naročila in dodatne informacijenas kontaktirajte preko e-pošte:
For orders and additional information please contact us by e-mail: ***omm@ntf.uni-lj.si***

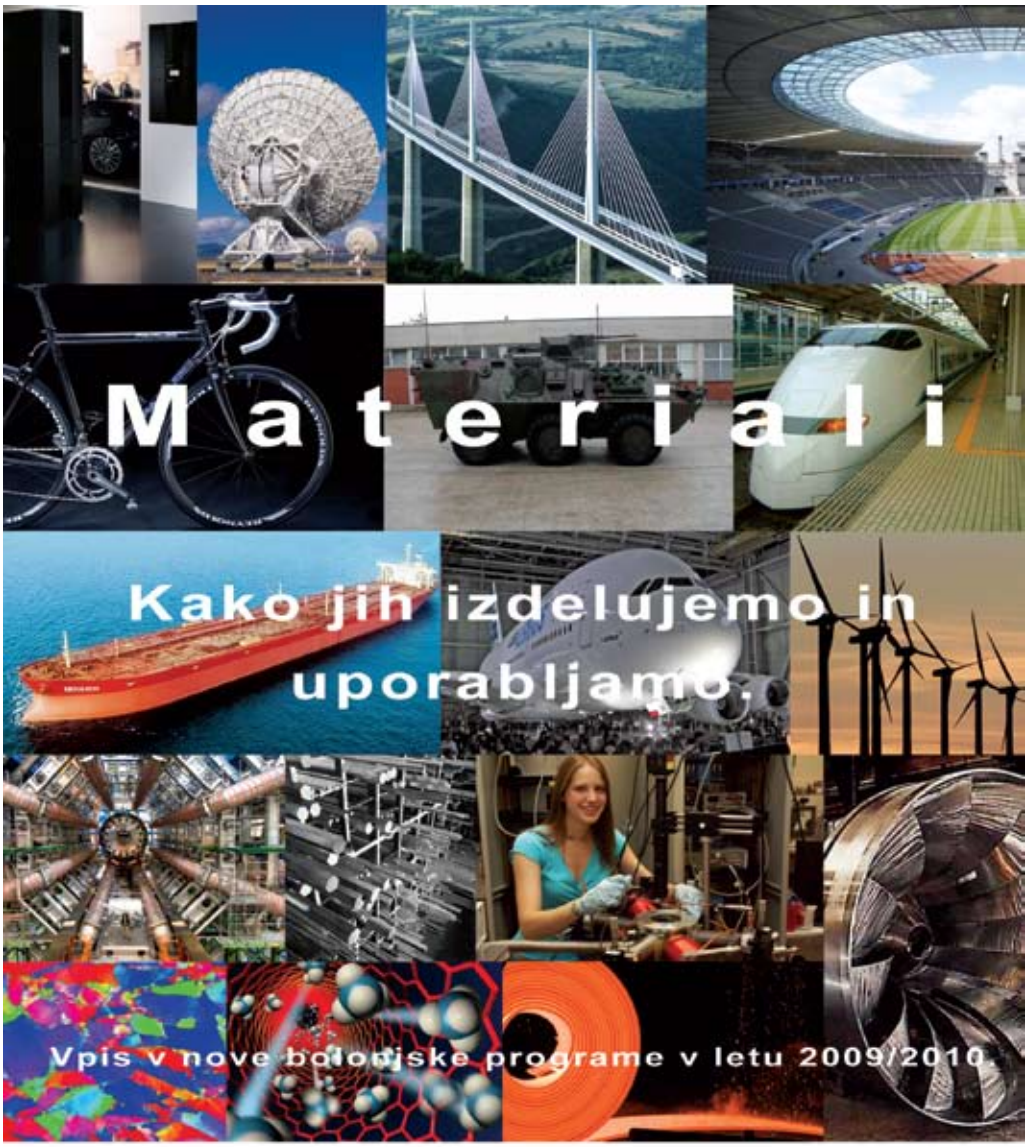

Univerza v Ljubljani, Naravoslovnotehniška fakulteta

Oddelek za materiale in metalurgijo

Aškerčeva cesta 12
1000 Ljubljana

Telefon: (01) 470 46 08,
E-pošta: omm@ntf.uni-lj.si

internetni naslov:
http://www.ntf.uni-lj.si/